

This report has been reproduced directly from the best available copy.

Available to DOE and DOE contractors from the Office Of Scientific and Technical Information, P.O. Box 62, Oak Ridge, TN 37831; prices available from (615)576-8401, FTS 626-8401.

Available to the public from the National Technical Information Service, U.S. Department of Commerce, 5285 Port Royal Rd., Springfield, VA 22161

Price: Printed A08
Microfiche A01

A SEMIANALYTICAL THERMAL MODEL
FOR LINEAR STEAM DRIVE

SUPRI TR 75

By
R. J. Gajdica
W. E. Brigham
K. Aziz

May 1990

Work Performed Under Contract No. FG19-87BC14126

Prepared for
U.S. Department of Energy
Assistant Secretary for Fossil Energy

Thomas B. Reid, Project Manager
Bartlesville Project Office
P. O. Box 1398
Bartlesville, OK 74005

Prepared by
Stanford University
Petroleum Research Institute
Stanford, CA 94305-4042

Contents

List of Tables	vii
List of Figures	ix
Acknowledgements	xiii
Abstract	xv
1 Introduction	1
2 Literature Survey	4
2.1 Frontal Advance Models	6
2.2 Bypass Models	10
2.3 Review of Analytical Models	16
2.4 Finite-Difference Models	16
3 One-Dimensional Model	19
3.1 Definition of One-Dimensional	21
3.2 Zone Definitions	22
3.3 Fractional Flow Calculations	23
3.4 Distance To Steam Front	26
3.5 Steam Zone Steam Saturation	30
3.6 Pressure Drop Calculations	30
3.7 Compressibility and Thermal Expansion	32
3.8 Concluding Remarks	33
4 One-Dimensional Model Results	34
4.1 One-Dimensional Simulator Runs	34

4.2	One-Dimensional Results	43
4.3	Concluding Remarks	71
5	Two-Dimensional Model	76
5.1	Definition of Two-Dimensional	77
5.2	Zone Definitions	77
5.3	Steam Zone Size and Shape	78
5.4	Hot Water Zone	81
5.5	Water Front	82
5.6	Comparison of Viscous to Gravity Ratios	94
5.7	Pressure Drops	95
5.8	Concluding Remarks	96
6	Two-Dimensional Model Results	97
6.1	Two-Dimensional Simulator Runs	97
6.2	Two-Dimensional Results	100
6.3	Concluding Remarks	119
7	Conclusions and Recommendations	120
7.1	Conclusions	120
7.2	Recommendations	121
8	Nomenclature	123
	Bibliography	127
A	Other Calculations Used in the Model	133
A.1	Three-Phase Relative Permeability	133
A.2	Corey Relative Permeability Curves	134
A.3	Porosity Calculation	135
A.4	Density Calculation	135
A.5	Liquid Viscosity	135
A.6	Wet Steam Property Correlations	136

A.7	Production Rate Calculations	137
B	SAM Assumptions	139
B.1	SAM General Assumptions	139
B.2	Phase Relationships	140
B.3	Energy Assumptions	141
B.4	Initial Conditions	141
B.5	Boundary Conditions	142
C	Program Structure	143
D	Model Application and Data Requirements	148
D.1	General Control Section	149
D.2	Reservoir Description Section	150
D.3	Initial Conditions Section	150
D.4	PVT Section	151
D.5	Relative Permeability Section	151
D.6	Thermal Data Section	151
D.7	Injection Well	152
D.8	Production Well	152
D.9	Program Files	152

List of Tables

4.1	Simulator One-Dimensional Data Set for Grid Study	38
4.2	Simulator PVT and Thermal Data for Grid Study	39
4.3	Simulator Well Data for Grid Study	40
4.4	Water/Oil Relative Permeability Data	41
4.5	Liquid/Gas Relative Permeability Data	41
4.6	Variable Ranges for One-Dimensional Analysis	42
4.7	Cases Displayed for One-Dimensional Analysis	44
5.1	Symbols and Data for Crossplot of $\mu_o = 10$ cp	92
5.2	Symbols and Data for Crossplot of $\mu_o = 1000$ cp	94
6.1	Ranges of Variables Used in Two-Dimensional Analysis	100
6.2	Two-Dimensional Results Displayed	103
A.1	Correlation Coefficients for Wet Steam Pressure and Density	136
A.2	Correlation Coefficients for Wet Steam Enthalpy Properties	137
B.1	Relationships Between Phases and Components	141

List of Figures

3.1	One-Dimensional Zone Definition	22
3.2	Fractional Flow Curve Tangent Construction	25
4.1	Oil-Water Relative Permeability	35
4.2	Gas-Liquid Relative Permeability	36
4.3	Variable Distribution at 3 years as a Function of Grid Density	37
4.4	Oil Production Rate as a Function of Grid Density	40
4.5	Oil Rate vs Time, Case 044	45
4.6	Water Rate vs Time, Case 044	46
4.7	Variable Distributions at 4 years, Case 044	47
4.8	Oil Rate vs Time, Case 083	49
4.9	Water Rate vs Time, Case 083	50
4.10	Variable Distributions at 2 years, Case 083	52
4.11	Oil Rate vs Time, Case 119	53
4.12	Water Rate vs Time, Case 119	53
4.13	Variable Distributions at 1 year, Case 119	54
4.14	Oil Rate vs Time, Case 062	55
4.15	Water Rate vs Time, Case 062	56
4.16	Variable Distributions at 4 years, Case 062	58
4.17	Oil Rate vs Time, Case 101	59
4.18	Water Rate vs Time, Case 101	59
4.19	Variable Distributions at 2 years, Case 101	60
4.20	Oil Rate vs Time, Case 137	61
4.21	Water Rate vs Time, Case 137	62

4.22	Variable Distributions at 1 year, Case 137	63
4.23	Oil Rate vs Time, Case 224	64
4.24	Water Rate vs Time, Case 224	65
4.25	Variable Distributions at 4 years, Case 224	66
4.26	Oil Rate vs Time, Case 263	67
4.27	Water Rate vs Time, Case 263	67
4.28	Variable Distributions at 2 years, Case 263	69
4.29	Oil Rate vs Time, Case 263d	70
4.30	Water Rate vs Time, Case 263d	70
4.31	Variable Distributions at 2 years, Case 263d	72
4.32	Oil Rate vs Time, Case 299	73
4.33	Water Rate vs Time, Case 299	73
4.34	Variable Distributions at 1 year, Case 299	74
5.1	Two-Dimensional Zone Definition	78
5.2	Effect of Viscous/Gravity Force Ratio on Steam Front Shape	81
5.3	Discretization of Steam Zone for a Four Layer Case	82
5.4	Effect of Pressure and Steam Quality on Heat Function, F	86
5.5	Sweep Efficiency at Water Breakthrough, $M=0.039$	87
5.6	Sweep Efficiency at Water Breakthrough, $M=0.319$	87
5.7	Sweep Efficiency at Water Breakthrough, $M=1.44$	88
5.8	Sweep Efficiency at Water Breakthrough, $M=3.25$	88
5.9	Sweep Efficiency at Water Breakthrough, $M=4.80$	89
5.10	Effect of Variables in the MCR on Volumetric Sweep, $\mu_o = 10$ cp	91
5.11	Effect of Variables in the MCR on Volumetric Sweep, $\mu_o = 1000$ cp	93
6.1	Oil Rate vs Time for 5- and 9-Point Difference Method	98
6.2	Oil Rate vs Time for 8 Layer Grid Systems	99
6.3	Oil Rate vs Time for 1 and 4 Layer Grid Systems	99
6.4	Oil Rate vs Time, Case 0122	103
6.5	Water Rate vs Time, Case 0122	101
6.6	Gas Saturation Distribution at 1000 Days, Case 0122	106

6.7	Oil Saturation Distribution at 1000 Days, Case 0122	106
6.8	Gas Saturation Distribution at 2000 Days, Case 0122	107
6.9	Oil Saturation Distribution at 2000 Days, Case 0122	107
6.10	Gas Saturation Distribution at 3000 Days, Case 0122	108
6.11	Oil Saturation Distribution at 3000 Days, Case 0122	108
6.12	Oil Rate vs Time, Case 0203	109
6.13	Water Rate vs Time, Case 0203	109
6.14	Oil Rate vs Time, Case 0287	110
6.15	Water Rate vs Time, Case 0287	111
6.16	Gas Saturation Distribution at 1000 Days, Case 0287	112
6.17	Oil Saturation Distribution at 1000 Days, Case 0287	112
6.18	Gas Saturation Distribution at 2000 Days, Case 0287	113
6.19	Oil Saturation Distribution at 2000 Days, Case 0287	113
6.20	Gas Saturation Distribution at 3000 Days, Case 0287	114
6.21	Oil Saturation Distribution at 3000 Days, Case 0287	114
6.22	Oil Rate vs Time, Case 1122	115
6.23	Water Rate vs Time, Case 1122	116
6.24	Oil Rate vs Time, Case 1203	116
6.25	Water Rate vs Time, Case 1203	117
6.26	Oil Rate vs Time, Case 1287	118
6.27	Water Rate vs Time, Case 1287	118
C.1	Fractional Flow Curve Tangent Construction, After Breakthrough . .	145
C.2	Flow Chart for Program	147

Acknowledgements

The authors are grateful for the financial support of the Petroleum Engineering Department of Stanford University, the Stanford University Petroleum Research Institute (SUPRI-A), U.S. DOE Contract DE-FG19-87BC14126, and Tenneco Oil Exploration and Production. Thanks is also expressed to AIME for granting the Henry Dewitt Smith Fellowship. The Computer Modelling Group is acknowledged for allowing their simulators to be installed on the Stanford computers.

2019年10月

2019年10月1日，星期一。秋高气爽，阳光明媚。今天是个好日子，我决定去郊外走走。清晨，薄雾还未散去，空气中弥漫着泥土的芬芳。我沿着乡间小路漫步，两旁是金黄的稻田，沉甸甸的稻穗在微风中摇曳。远处，几座青山若隐若现，构成了一幅美丽的画卷。不知不觉，太阳已经升起，金色的阳光洒满大地。我来到了一片果园，红彤彤的苹果挂满枝头，散发出诱人的香气。我忍不住摘下一个，咬了一口，汁水四溢，甜中带酸，真是美味极了。果园里传来阵阵欢声笑语，原来是几个孩子在这里嬉戏玩耍。他们追逐打闹，笑声在果园里回荡。时间过得真快，转眼间已经到了中午。我坐在果园的长椅上，享受着这难得的宁静与美好。看着眼前的一切，心中充满了喜悦和满足。这就是生活，简单而美好。在大自然的怀抱中，所有的烦恼都烟消云散，只剩下内心的平静与安宁。下午，我继续我的旅程，来到了一个清澈见底的小溪边。溪水潺潺，清澈见底，水底的鹅卵石清晰可见。几只小鱼在水中欢快地游来游去。我蹲下身来，用手捧起一捧水，清凉的感觉瞬间沁入心脾。溪边的野花竞相开放，散发出阵阵清香。我深吸一口气，感觉整个人都焕然一新。不知不觉，天色已晚。夕阳的余晖洒在溪面上，波光粼粼，美不胜收。我依依不舍地离开了小溪，踏上归途。回首望去，今天的旅程充满了美好的回忆。在大自然的怀抱中，我找回了久违的宁静与美好。生活就是这样，在平凡的日子里，处处都是风景。只要我们用心去感受，就能发现生活的美好。2019年10月2日，星期二。今天是个阴天，微风轻拂。我决定去图书馆看看书。图书馆里安静祥和，空气中弥漫着书香。我挑选了几本自己喜欢的书，坐在窗边的座位上，静静地阅读。阳光透过窗户洒在书页上，给人一种温暖的感觉。时间在不知不觉中流逝，不知不觉已经到了下午。我合上书，走出图书馆，来到一个公园。公园里绿树成荫，鸟语花香。孩子们在草地上奔跑嬉戏，大人们则在长椅上悠闲地散步。我漫步在小径上，感受着大自然的气息。公园的景色真美啊，让人流连忘返。不知不觉，天色已晚。我依依不舍地离开了公园，踏上归途。回首望去，今天的旅程充满了美好的回忆。在大自然的怀抱中，我找回了久违的宁静与美好。生活就是这样，在平凡的日子里，处处都是风景。只要我们用心去感受，就能发现生活的美好。

Abstract

Thermal recovery by steam injection has proven to be an effective means of recovering heavy oil. Forecasts of reservoir response to the application of steam are necessary before starting a steam drive project. Thermal numerical models are available to provide forecasts. However, these models are expensive and consume a great deal of computer time. An alternative to numerical modeling is to use an analytical model. Analytical models are fast, but the assumptions necessary to generate the solutions may lead to poor results. Common assumptions in analytical models are: (1) a horizontal reservoir, (2) incompressible oil, water, and formation, and (3) no thermal expansion of the oil, water, and formation. Furthermore, many analytical models require steam zone saturation as input, or do not consider the water front when calculating production rates. Finally, one-dimensional analytical models do not consider gravity override of steam.

A semianalytical model (SAM) has been developed for one-dimensional linear systems and two-dimensional linear cross-sectional systems. Wells are located at both ends of the reservoir. At the injection well, wet steam is injected at a constant rate and enthalpy. The production well produces at a constant flowing bottomhole pressure. The SAM includes formation dip, compressible formation, water, and oil, and thermal expansion of the formation, water, and oil. The model automatically calculates the steam zone steam saturation and includes the water front and overburden heat losses. The two-dimensional model also includes gravity override of steam.

The system of equations is solved by iterating on the injection well pressure. For each iteration, the lengths of the steam, water, and oil zones are determined. The pressure drop is calculated for each of these zones and at each well to compute the

production well pressure. This value is compared to the production well boundary condition, and iteration continues until convergence is achieved, usually in five iterations. In the process, front locations, temperatures, pressures, and phase saturations are determined for each of the zones. Since the temperatures and pressures are computed, the compressibility and thermal expansion of the rock, oil, and water can be considered. Oil and water production rates are calculated by material balance. In the two-dimensional model, a new empirical method is presented which determines the shape of the steam front, and an extension of an existing water flooding correlation is used to determine the volumetric sweep efficiency for the reservoir.

Many cases were run on both the SAM and a numerical model. The Computer Modelling Group's general purpose thermal simulator ISCOM was used for comparisons. The SAM runs were several orders of magnitude faster than the thermal simulator, yet matched thermal simulator results accurately in over 2,000 runs over a wide range of variables. The result is a computer program that can be run on a personal computer by a field engineer. The program is not intended to replace a thermal simulator. The simulator is more general and can handle more detailed problems than the SAM. However, the SAM is ideal for: (1) preliminary studies before running a numerical model, (2) running many cases for sensitivity analysis and optimization, (3) screening prospective field projects, and (4) providing guidance for operating decisions.

Chapter 1

Introduction

Thermal oil recovery projects are usually not started unless there is potential for economic gain. Economic risk is usually low because the projects are initiated on heavy oil reservoirs that have already been located, and have low primary oil recoveries. The important unknown is how a reservoir will respond to the application of heat. It is necessary to estimate the reservoir response before a thermal oil recovery project is started. The thermal response can be determined from finite-difference thermal simulators, from analytical and semianalytical solutions, and by analogy with field results. Many good finite-difference thermal models are in use today which provide engineers with reasonable forecasts of reservoir behavior. However, thermal simulators are expensive, require large computers, and often consume a great deal of expensive computer time before satisfactory results are obtained.

Empirical, analytical, and semianalytical models, on the other hand, may be used to forecast reservoir behavior with less time and expense, but do not provide the detail or the accuracy that can be obtained from a finite-difference model. Many analytical models have been published over the last three decades, with varying assumptions and accuracy. A model has value if the results obtained are reasonably accurate. Analytical models range from simple to complex, but most models reported in the petroleum literature have the common assumption of a horizontal reservoir and neglect gravity drainage. Existing analytical models also assume flow is incompressible. Where large pressure and temperature variations exist, however, compressibility and

thermal expansion of the oil, water and formation may have a significant effect on the results.

Existing analytical models also require that the steam zone steam saturation be specified. Steam saturation has a significant effect on the results, but usually is not known. Some analytical models consider only the shape and/or location of the steam front, and ignore the remainder of the reservoir. Thus, they do not provide a complete fluid recovery prediction. In reality, the condensed water front is important and must be considered if production rates are to be forecast.

The purpose of this work is to develop an analytical model that produces results close to thermal simulator results. Furthermore, this model should avoid restrictive assumptions of existing analytical models and run on a personal computer. This dissertation presents the development of two such models. Models were developed for both one-dimensional linear and two-dimensional cross-sectional systems in a Cartesian coordinate system. The definitions of one- and two-dimensional flow geometry are discussed in Sections 3.1 and 5.1, respectively. In the one-dimensional model, both updip and downdip steam injection were considered. However, the two-dimensional model considered updip steam injection only. The reason for this is discussed in Chapter 5. The models require a computer for solution because of the iterative method used, so they are called semianalytical models, and will be referred to as SAM, semi-analytical models.

Chapter 2 includes a literature survey of steam drive analytical models. Previous work in analytical modeling of steam injection is reviewed, and the assumptions associated with each of the models are discussed. Chapter 3 presents the development of the one-dimensional SAM. Results from the one-dimensional model are presented in Chapter 4. The one-dimensional model was modified to consider the effects of a two-dimensional system. These modifications are presented and discussed in Chapter 5. The results of the two-dimensional model are presented in Chapter 6. Finally, conclusions and recommendations for further work are presented in Chapter 7. A nomenclature chapter, bibliography, and several appendices complete the dissertation. The appendices include the calculations used by the SAM, the assumptions made by the SAM, program structure, and model application and data requirements. A

computer floppy disk is available that contains FORTRAN computer programs based on the model, and sample data files. Files containing listings of the cases run and the results obtained are also included on the disk. The disk is available through the Petroleum Engineering Department at Stanford University.

The next chapter is a literature survey which discusses steam drive analytical models.

Chapter 2

Literature Survey

This chapter reviews analytical models that are used to calculate oil production rates in steam injection projects. Assumptions general to models, as well as specific assumptions of each model, are discussed.

Oil recovery by steam injection may be classified into two major methods. The first is cyclic steam injection, also known as steam stimulation, steam soak, and “huff-n-puff,” in which steam is injected and oil is later recovered from the same wellbore. The second is steam drive or steamflooding, a process in which oil is displaced from injection wells toward production wells.

There are many analytical models for cyclic steam injection. One good recent model was presented by Gontijo and Aziz [22]. Two zones were considered, a heated steam zone and an oil zone. The shape of the steam zone was assumed conical. The flow rate of oil in this model is influenced by oil viscosity, effective permeability of the heated zone, porosity, mobile oil saturation and thermal diffusivity of the reservoir. The change in reservoir temperature with time was also considered, and results in a decline in oil production rate during a cycle. The model equations were kept simple and, correlations were incorporated to minimize data requirements.

The equations on which the model is based consider both potential and gravity as the driving forces. Pseudo-steady state flow is assumed inside the heated zone. As oil is produced, the steam zone slowly expands downward. Solution was performed by a

computer program which calculates fluid properties, heated zone geometry, and temperature and saturations at the start of a production cycle. Oil and water production rates were then calculated for time steps within a cycle. At the end of a cycle, the amounts of water and heat remaining in the reservoir were calculated. The process was then repeated for each cycle. Results from the model were compared with field data, another analytical model, and with a thermal simulator. The comparison was good.

There are many analytical models in the petroleum engineering literature that may be used to forecast reservoir response to steam drive. Steam drive models can be classified into one-dimensional frontal advance models and two-dimensional x - z cross-sectional bypass models. Frontal advance models assume vertical steam fronts, while bypass models consider gravity override of steam [37].

The analytical models discussed here are for two-component systems. The water component can exist in the water or gas phase, and the oil component can exist only in the oil phase. Thus, the oil is a dead oil with no solution gas and no distillation. These models also neglect the effects of compressibility and thermal expansion of the oil, water, and formation. They assume horizontal, homogeneous, isotropic reservoirs, and neglect capillary pressure.

While most of the analytical models, as published, make the assumptions stated above, there is a way to get around some of the assumptions. However, engineers can include some of these effects by making changes in the models. For example, the effects of thermal expansion can be easily included by using high temperature densities for the fluids in the steam zone. If the pressure in each zone is known, the effects of compressibility can be included. Capillary pressure and distillation of oil can be included by adjusting the relative permeability data. Thus, even though certain assumptions are made in the analytical models, there are often ways to include the neglected mechanisms indirectly.

One also can represent oil distillation even when using a two-component system like the one discussed above. Relative permeability data can be used that give the correct residual oil saturation to steam drive [40]. These data would not be the relative permeability curves derived from laboratory coreflood experiments, but adjusted data

that consider oil distillation. This adjustment does not affect the basic equations upon which the model is based. However, the correction can be used on analytical models, thermal simulators, or any type of model in which relative permeability data are used.

2.1 Frontal Advance Models

In frontal advance models, the steam front is assumed to be normal to the bedding planes and to extend through the full thickness of the reservoir. Similar assumptions are made about the saturation and temperature profiles. Isosurfaces are considered to be normal to the bedding planes and to extend through the full thickness of the reservoir.

The earliest analytical model for continuous steam injection that gained wide acceptance was that of Marx and Langenheim [32]. A horizontal, homogeneous, isotropic, constant thickness porous medium was considered. A steam zone and an oil zone were defined, and a step function was used to describe the temperature profile in the reservoir. The steam zone was at the injection temperature, and the unheated region was at initial reservoir temperature. The steam front was assumed to be vertical. Laplace transformation was used to solve the one-dimensional heat balance, generating an error function equation for heat losses to the adjacent formation. The heat balance considered the rate of heat injection, the rate of heat loss, and the rate of heat stored in the reservoir. Oil production and economic limits were also discussed. The method assumes: (1) all heat reaching the condensation front is used to heat the matrix and residual oil from original reservoir temperature to steam temperature, (2) local thermal equilibrium, (3) the temperature and oil saturation in the steam zone are constant and independent of position and time, and (4) heat losses occur in the vertical direction only. The assumption of constant temperature in the invaded zone at a location has been called the "Lauwerier assumption" [29, 36].

Ramey [38] indicated that the Marx and Langenheim model was not restricted to specific geometries. He showed that superposition could be applied to the Marx and Langenheim equation for cases of variable injection rates.

The Marx and Langenheim method neglects gravity effects and the flow of heat

from the steam zone into the liquid zone ahead of the condensation front, so it fails to consider the growth of a hot liquid zone ahead of the front. No hot water was considered to be produced ahead of the steam. Furthermore, the solution does not consider radial heat conduction either within or outside the reservoir. Distillation of the oil is also neglected.

The Marx and Langenheim model does not work well at late times, at low steam quality, and at low injection rates. The reasons for this are discussed below when modifications to this work are considered. The Marx-Langenheim model does not include a water zone or gravity override of the steam, and the steam saturation in the steam zone must be provided as input data.

Hearn [23] presented a modification of the Marx and Langenheim solution that considered both the latent heat and the sensible heat in saturated steam. He argued that, for a step temperature profile, heat losses are supplied by latent heat only. At late time, the latent heat injection rate will not be sufficient to supply the heat losses. The result is a smaller steam zone and a larger heated zone than calculated by Marx and Langenheim. Hearn presented equations for calculating the area of the steam zone as a function of time. The ratio of latent to total heat injected was used in a table to determine a time function, which in turn was used to calculate the steam zone area.

Mandl and Volek [31] improved the early work of Marx and Langenheim [32]. They retained most of the earlier assumptions. The steam quality and injection rate, however, were allowed to be arbitrary and vary with time. They assumed that the specific heat of the water and the formation were constant, but treated the specific heat of oil and phase densities as functions of temperature.

They showed that after a critical time, t_c , heat transfer ahead of the steam zone becomes important and could not be neglected as in the Marx and Langenheim model. At times earlier than t_c , the heat flow across the condensation front is purely conductive, but at the critical time the heat flow becomes predominantly convective. Therefore, at times later than the critical time, the equation which governed the expansion of the steam zone changes. After the critical time, the steam zone growth still depends upon heat and mass flow in the liquid zone, but only via the preheating

of the rock layers which surround the liquid zone.

Equations were derived by considering a heat balance for a control volume that includes the steam front. Fluxes through a fixed cross-section and through the moving steam front were considered. Upper and lower bounds were presented for steam zone volume after the critical time. The upper bound is simply the Marx and Langenheim solution for the case of no heat flow through the steam front. The lower bound considers heat transfer across the steam front by convection, but neglects the preheating of the adjacent formations by the hot water zone. The steam zone volume is calculated by taking the arithmetic average of the upper and lower bounds. The model predicts nonzero steam zone growth when the injected steam quality is zero. Thus, it may not be good for low injection rate and low steam quality. The model does not consider the water front or gravity override of the steam, and the steam saturation in the steam zone must be provided.

The work of Mandl and Volek [31] was improved by Myhill and Stegemeier [33]. They presented a method for computing the ultimate oil-steam ratio for field steam injection projects. The method used a slightly modified version of the Mandl and Volek equations. They invoked similar assumptions, including heat transfer across the steam front only after the critical time defined by Mandl and Volek. Steam is assumed to be injected at constant pressure, quality, and rate. Instead of using the arithmetic average for interpolating between the upper and lower bounds as suggested by Mandl and Volek, Myhill and Stegemeier used the sensible heat fraction of the wet steam as the interpolating factor. The oil produced was equal to the product of the steam zone pore volume and the change in oil saturation in that zone. They compared the ultimate oil-steam ratios predicted by such calculations to those that were measured in seven laboratory model studies and eleven field steam drives, and good agreement was observed. The delay resulting from oil bank formation and the effects of allowing steam injection rates to vary were not included in this model. The model does not consider the water front or gravity override of the steam, and the steam saturation in the steam zone must be provided.

Integral equations for the steam drive process were presented by Yortsos and Gavalas [54, 55]. They presented a mass-energy balance for computing the growth

of the steam zone for steam injection processes. They presented upper bounds for steam zone growth based on integral balances by introducing lower bounds for heat loss to the surrounding area and to the hot liquid zone. The two upper bounds for steam zone size were based on a total energy balance similar to the one used in earlier models, and a latent heat balance. Because of the latent heat balance, this method gave a better approximation to the steam zone growth rate for intermediate and late times than did the approximate expressions developed by Marx and Langenheim, Mandl and Volek, and Myhill and Stegemeier. The method also worked well for low steam quality and low injection rate. However, like the other models, this model does not consider the water front or gravity override of the steam. Again, the steam zone steam saturation must be provided. This model is discussed in detail in Section 3.4.

A study of heat losses in steam injection was conducted by Wang and Brigham [48]. Existing analytical solutions were examined to test the applicability of these solutions to laboratory steam injection. They found that for times greater than the critical time, the rate of heat loss from the steam swept zone must equal the rate of latent heat injection. This is the Hearn theory [23]. This theory neglects the latent heat used to heat additional reservoir to steam temperature. Although models by Myhill and Stegemeier [33] and Yortsos and Gavalas [54] give steam zone volumes smaller than the Hearn solution when time is greater than the critical time, in their calculations a decrease of the heat loss rate from the steam swept zone occurs during most of the time of interest. In reality, the rate of heat loss from the steam zone must continuously increase with time since the area for heat loss increases with time. Wang and Brigham presented a new method of determining the steam zone volume after the critical time. The method is to change the time scale using the fraction of latent heat injected raised to an empirical factor. The empirical factor was determined by the physical constraints of the steam injection process. The new method predicted lower values of steam zone volume than the previous methods. Laboratory experiments were used to confirm the validity of the new model.

The thermal efficiency of a process was considered by Ramey [39]. He showed that the fraction of heat lost to the adjacent formation given by the methods of Lauwerier [29] and Marx and Langenheim [32] is the same, for constant heat injection rate.

Prats [36] showed that this was a result of the "Lauwerier assumption" concerning vertical heat losses. Ramey also observed that the distribution of heat between the reservoir and the adjacent formations is independent of the heat injection rate and is a function only of the dimensionless time for a constant heat injection rate.

Shutler and Boberg [43] used Buckley-Leverett isothermal two-phase flow theory in conjunction with the Marx and Langenheim energy balance to determine fluid flow in a one-dimensional, horizontal reservoir. They assumed injection of 100 percent quality steam at a constant rate, assumed the steam to be incompressible, and neglected distillation. Two zones were considered, a hot zone containing steam and hot water, and a cold zone. They tracked the movement of a series of isothermal planes through the linear system. These planes were separated by discontinuities or "shocks" in temperature. The Buckley-Leverett relationship, which describes the velocity of surfaces of constant saturation, was used to calculate the steam zone saturation profile. This profile was represented by a series of shocks. Since the steam saturation and pressure changes across each shock, the temperature must also change, so a temperature distribution is also calculated. The model does not consider gravity override of the steam, nor does it work well with low steam quality because it uses the Marx and Langenheim heat loss method.

The one-dimensional frontal advance models are summarized along with the bypass models at the end of the next section.

2.2 Bypass Models

Bypass models are more realistic than frontal advance models because they consider gravity override of the steam, but they are also more complicated to describe, both physically and mathematically. These models are two-dimensional cross-sectional models. In the bypass models, the fronts are not vertical. The main causes of bypassing are gravity override and/or reservoir layering.

van Lookeren [46] presented a method for determining the shape of the steam front in a steam-oil system by employing segregated flow principles, but did not develop a predictive model. However, this work was used by many others in developing models.

This method gave analytical solutions in both linear and radial systems to the problem of steam zone shape in two-dimensions. Updip steam injection was assumed. The theory was based on segregated flow principles such as those used by Dupuit [15] and Deitz [13]. In segregated flow models, the flow potentials of each phase were taken as constant in any plane perpendicular to the bedding plane of the reservoir. Flow potentials in two successive planes are expressed in terms of pressure at the steam/oil interface to derive the differential equation

$$\frac{\partial z_{st}}{\partial x} = -A_{LD} \left(\frac{1 - M^*}{\cos \theta} \right) + \tan \theta \quad (2.1)$$

where z_{st} is the steam zone thickness, x is the distance from the injection well, and θ is the angle of formation dip. A_{LD} is a dimensionless ratio of viscous to gravity forces. The ratio is derived from segregated flow theory, quantifies the tendency for gravity override to occur, and is defined as

$$A_{LD} = \frac{\mu_{st} w_{st}(x_b)}{(\rho_o - \rho_{st}) g H k_{st} \rho_{st} W} \quad (2.2)$$

where μ_{st} is the steam viscosity, $w_{st}(x_b)$ is the mass flow rate of steam at the base of the steam zone, ρ is density, g is the acceleration due to gravity, H is the reservoir thickness, k is permeability, and W is the width of the reservoir. M^* is the pseudomobility ratio, and is defined as

$$M^* = \frac{\mu_o^* k_{st} \rho_{st} w_o(x_e)}{\mu_{st} k_o \rho_o w_{st}(x_b)} \quad (2.3)$$

In this relationship, μ_o^* is the oil viscosity at steam zone temperature, k is permeability, and $w_o(x_e)$ is the mass flow rate of oil at the end of the steam zone. The pseudomobility ratio consists of two parts. The first part is the mobility ratio evaluated at steam temperature. The second part is the ratio of the volumetric flow rate of oil at the most advanced end of the steam zone to that of steam at the least advanced end.

As the oil viscosity increases, the pseudomobility ratio approaches unity and then takes on values greater than unity. When this value is inserted into Eq. 2.1, the term in parentheses can be zero or even negative. This results in a solution that violates physical considerations. The calculated shape of the steam front has a negative slope.

i.e., gravity override of the steam is calculated when the pseudomobility ratio has a value greater than one. Furthermore, many thermal simulator results indicate that the steam zone does not always occupy the entire height of the reservoir as assumed by van Lookeren's model. Gravity override is often so severe that the steam zone tends to rise to the top of the reservoir, occupying only a portion of the total height of the reservoir. van Lookeren's method works for low and medium-viscosity oils, but problems are encountered for high-viscosity oils. This limitation was recognized by the van Lookeren and discussed in the paper. Furthermore, the work is based on segregated flow principles which assume constant potentials in any plane normal to the bedding plane. This assumption is not good for thick reservoirs [54], so van Lookeren's model may not give good results for thick reservoirs.

Three models based on van Lookeren's work are discussed next. These models are expected to have the same limitations discussed in the previous paragraph because the differential equation presented by van Lookeren is used to determine the shape of the steam front.

Rhee and Doscher [41] published a semianalytical method for calculating oil recovery by steamflooding. The method considered steam distillation and gravity override of steam. First, the equations for the heat balance and the shape of the steam front are solved simultaneously to predict the volume of the overall heated zone and the volume and shape of the steam zone. van Lookeren's work was used for the steam front shape. Second, the enthalpy and mass balances are combined with vaporization correlations to calculate the volume and composition of steam-distilled hydrocarbons. Finally, the results are combined with a fluid flow model, similar to Higgins and Leighton's [24] cell model for waterflood analysis to calculate oil recovery. Iterative techniques were used to solve the equations. Results from the semianalytical model were compared to experimental data and good agreement was obtained.

A model described by Jones [28] was based on works by van Lookeren and Myhill and Stegemeier to calculate an optimum steam injection rate and oil recovery. van Lookeren's equation can be used to optimize the steam injection rate if pressure vs. rate data are available. These data can be obtained from nearby injection wells or from extrapolation of data from the well of interest. The optimization is based

on maximizing the vertical sweep efficiency of the steam zone by injecting at the highest possible rate without violating pressure constraints. The Myhill and Stegemeier model, discussed earlier, is used to calculate steam zone size and oil production rates. An correction factor was used to fine tune the model so that it matched field performance. This factor varies from one field to another.

Palmgren *et al.* [35] described a semianalytical model for determining the shape and location of the steam front in a slightly dipping reservoir. However, oil and water production rates are not calculated. Fluid properties are assumed constant, and incompressibility is assumed. The shape of the steam front is determined by van Lookeren's equation. Heat losses are calculated in a manner similar to the other models discussed. A two-dimensional stream function equation for the oil/steam system was derived and solved by a finite element method. A correlation based on this solution was used by the model. Simplified relative permeability functions were used. Capillary forces were considered and the model showed that these forces are important under laboratory conditions; they tend to reduce gravity override and thereby stabilize the steam front. However, the model showed that capillary forces are not significant under field conditions. The details of how the equations were solved were not discussed.

A model that used the frustrum of a cone for the steam zone shape was presented by Aydelotte and Pope [1]. They presented a steam drive model that had six different regions and included a cash flow analysis. The six regions are the undisturbed zone, cold liquid zone, hot liquid zone, steam zone, hot water drive, and cold water drive. The size, saturation, and movement of each zone is calculated from a fractional-flow equation and the growth of the steam zone. Vertical and areal sweeps of the steam zone are estimated from empirical relationships, and the sweeps of the other banks are related to their mobilities. Heat losses from the reservoir to adjacent strata are calculated from a simple heat balance. Finite time steps are used to progress through the algorithm, solving for production and injection rates and zone sizes at the end of each step. Initially, the reservoir was assumed horizontal, homogeneous, isotropic, incompressible, in thermal equilibrium with the adjacent strata, and uniformly saturated with oil, water, and gas. They assumed radial flow, but made a modification

for a five-spot pattern by using an empirical correlation for areal sweep efficiency.

Another analytical solution in two dimensions was presented by Yortsos and Gavalas [54]. They presented a solution for steam zone volume in two-dimensional systems. However, the solution is for steam zone volume only, and can not be used to determine the time to steam breakthrough nor the shape of the steam front. Yortsos presented still another analytical solution to the two-dimensional problem [53]. The assumptions required to obtain the solution included using the lower bound expression for cumulative heat losses, a quasi-steady state approximation for cumulative net heat flux to the hot liquid zone, negligible horizontal conduction, and negligible conductive heat flux to the hot liquid zone. The results obtained from the solution do not match finite-difference results. The differences are probably caused by the simplifying assumptions that were used to obtain the analytical solution.

Dake [10] gave a derivation for unstable displacement of oil by water in a horizontal reservoir. Although this work was not for a steam drive, similar concepts could be used in steam drive work. Darcy's law was used to express the flow rates of the oil and the water phases. The density of the fluids was used to define the pressure changes due to gravity in the vertical direction. The derivation assumes that the pressure in the phases on each side of the oil-water interface must be equal. An analytical expression was derived for the fractional flow of water and was used in an oil recovery formula. The resulting equation is

$$N_{pD} = \frac{2\sqrt{W_{iD}M} - W_{iD} - 1}{M - 1} \quad (2.4)$$

where N_{pD} is the dimensionless oil produced and W_{iD} is the dimensionless water injected. This equation is applicable only for horizontal displacement under segregated conditions and for unstable flow ($M > 1$). The oil produced and the water injected are made dimensionless by dividing by the movable oil volume, MOV , which is

$$MOV = L W H \phi (1 - S_{wc} - S_{or}) \quad (2.5)$$

M is the mobility ratio and is defined for an oil-water system as

$$M = \frac{k_{rw}\mu_o}{k_{ro}\mu_w} \quad (2.6)$$

At the time of water breakthrough, the volume of oil produced is equal to the volume of water injected. Setting this condition into Eq. 2.4, the water injected at water breakthrough is

$$W_{iD} = \frac{1}{M} \quad (2.7)$$

This method does not involve the rate of water injection or the geometry of the system. The rate and the geometry are known to have a significant effect on the volumetric sweep efficiency of a system, so there is reason to believe that this method may not be generally useful. For systems with high mobility ratios, the predicted water breakthrough is early, and does not agree with the water breakthrough time found by simulators, even for very fine grid systems.

One extreme of analytical steam models is a vertical steam front like the one that exists in the frontal advance models. The other extreme is a horizontal steam front, in which steam overlays rapidly. This second type of model is called a descending steam chest model. Steam migrates upward because of gravity effects. When the steam zone reaches an impermeable barrier preventing further upward migration, continued injection of steam appears to result in a vertically expanding steam zone. Crude oil production occurs as a result of steam flowing above and across the oil column. Such models were presented by Doscher and Ghassemi [14], Vogel [47] and Neuman [34].

A constant-steam injection rate was assumed in all of these models. Heat flow from the steam chest into the underlying formation was by conduction only. The horizontal pressure gradient in the steam chest was assumed to be much less than the vertical pressure gradient. Both oil and water saturations were assumed constant in the steam zone. Horizontal flow below the steam/oil interface was neglected. Oil saturation in the heated reservoir beneath the steam zone was assumed to be the residual oil saturation to hot-waterflooding. The assumption of a horizontal steam front can be just as bad as the vertical steam front assumption that was used in the frontal advance models. The degree to which steam overrides due to gravity depends upon the ratio of viscous to gravity forces in the steam zone. For the cases where viscous forces dominate, the descending steam chest models have serious problems.

2.3 Review of Analytical Models

Review of the analytical models for steam drive shows that a generally useful model has not been developed. In all analytical models, an assumption must be made concerning the shape of the steam front. The one-dimensional frontal advance models assume a vertical steam front and do not consider gravity override of the steam. The descending steam chest models go to the other extreme and assume that gravity override of the steam is immediate and total. All of the models that fall between these two extremes have problems of one kind or another as discussed above. Furthermore, all of the models assume a horizontal reservoir, and neglect thermal expansion and compressibility of the oil, water, and formation. Thus, there is a need for a model that relaxes these assumptions. A generally useful semianalytical model (SAM) is presented in the next chapter.

2.4 Finite-Difference Models

The SAM that will be presented will be correlated against and compared to a thermal simulator, so some discussion about simulation will follow. The SAM was tested by comparing the results of identical cases run on both the SAM and a thermal simulator. The results from the thermal simulator were the "yardstick" by which SAM results were correlated and measured. Thermal simulators have been compared to field data, experimental data, analytical models, and other simulators. Good agreement has been obtained in most cases. History matching of field data and forecasting future performance is the primary commercial application of simulators.

Finite-difference thermal models (thermal simulators) require a high-speed computer to provide a solution. The current thermal simulators are capable of solving complex systems of non-linear equations. The models consider relative permeabilities, the effect of temperature and hysteresis on relative permeabilities, capillary pressure, overburden heat losses, phase changes, and reservoir heterogeneities. These models use more data than analytical models because fewer assumptions need to be made and more detail can be used. The simulators calculate pressures, temperatures, phase

saturations, and phase compositions for each grid block as a function of time. The results can be as detailed as the gridding system used. However, the amount of computing time required to provide answers increases rapidly with the number of grid blocks used.

A thermal simulator was used to correlate results for, and compare results from, the SAM. The ISCOM model [20, 42] written by the Computer Modelling Group was chosen for these comparisons because it is available on the Stanford computers, and it displayed good agreement with other thermal simulators in a comparison study, as discussed next.

A comparison of six steam injection simulators was carried out by Aziz, *et al.* [3]. ISCOM was one of the models considered. Three related but independent problems were selected for the comparison of steam injection models: (1) cyclic steam injection in a reservoir with non-distillable oil with a two-dimensional radial cross-sectional grid, (2) non-distillable oil displacement by steam in an inverted nine-spot pattern by considering one-eighth of the full pattern, and (3) displacement of an oil consisting of two volatile components and one non-volatile component in the same pattern as in Problem 2. Comparison of results from the different models showed that, from a practical standpoint, ISCOM gives approximately the same results as the other simulators included in the study. At the time of this comparison, ISCOM did not have a nine-point method to reduce the grid orientation effect. The Computer Modelling Group introduced high capillary pressure values to reduce grid orientation effects. Since then, a nine-point method has been introduced.

Since ISCOM was used in this work, a brief description of this model is included. ISCOM is a fully implicit, four-phase (oil, water, gas, solid) multi-component finite-difference thermal simulator for simulating hot water injection, steam injection, dry combustion, and wet combustion. Model equations are formed from component mass and energy balances that account for accumulation, fluid vaporization and condensation, injection and production of fluids, chemical reactions, heat conduction, heat loss and the flow of mass and energy. Interblock flow is calculated using single-point upstream mobility and enthalpy for Cartesian, radial, variable thickness and curvilinear grids. To advance one time step, Newton's iterative method is applied to residuals

of the coupled non-linear balance equations. Derivatives are obtained by numerical differentiation. The matrix equations are solved using either direct D4 Gaussian elimination or one of a suite of powerful incomplete LU factorization iterative methods. Each well generates a fully implicit equation which is coupled directly to, and is solved simultaneously with, the reservoir balance equations. Layer allocation in production wells takes into account phase mobilities, phase densities, layer thicknesses and fluid head in both the reservoir and wellbore.

Model features include the accommodation of an arbitrary number of oil, gas or solid components, and automatic time step selection that reduces time truncation error. Steam injection well heat loss and pressure drop calculations may be included. Phase behavior is calculated from a rigorous three-phase flash fluid property package.

The need for a generally useful analytical model has been established. A SAM for steam drive has been developed and is discussed in the next chapter.

Chapter 3

One-Dimensional Model

This chapter deals with the development of the one-dimensional semianalytical model (SAM). A one-dimensional model was addressed first because the complicating factors of multi-dimensional systems. Non-vertical front shapes are not present in a one-dimensional system. The one-dimensional model considers heat losses, gravity effects, and other important mechanisms, but it is the simplest model to solve. A short summary of the thought process that led to the creation of the one-dimensional model is presented. This is followed by sections on the definition of a one-dimensional system, zone definitions, fractional flow calculations, the method of determining the distance to the steam front, the method of determining the steam zone steam saturation, pressure drop calculations, how compressibility and thermal expansion are considered, and concluding remarks.

The semianalytical model development began with an inspectional analysis in order to determine the dimensionless groups that were relevant in the steam drive process. The development of general type curves based on inspectional analysis concepts for the steam drive process is not feasible because the number of dimensionless groups obtained was large. Many one-dimensional simulation runs were then made to see what simulation results looked like. This step resulted in the definition of steam and water fronts, and steam, water and oil zones. The purpose of the SAM is to provide, at any time, the location of the steam and water fronts, and the average phase saturations in each of the three zones. If this information can be provided,

then it is a simple matter to calculate pressure drops by Darcy's law and production rates by material balance.

A method of calculating the location of a water front for a waterflood problem was already available in the Buckley-Leverett fractional flow theory. This method uses the number of pore volumes of fluid injected into the reservoir and the fractional flow curve to determine the location of the water front. The same type of calculation can be applied to the steamflood problem if the volume of the steam zone is included. However, in order to make the necessary volumetric adjustment, the location of the steam front and saturation of the steam zone must first be known.

Several analytical models are available for calculating the location of the steam front, and the method of Marx and Langenheim was used initially. Later, the method of Yortsos and Gavalas was used because it makes fewer assumptions and matched the simulation results better. The analytical models that were used to determine the location of the steam front require that the steam saturation be known in the steam zone. This value is calculated automatically by a thermal simulator but must be estimated for an analytical model. Fractional flow theory can be used to determine the gas saturation if an adjustment is made for the condensation of the steam. However, to consider steam condensation the pressure in the steam zone must be known.

In order to calculate the pressure in the steam zone, the front locations and zone saturations must be known. Thus, one answer is required before another answer can be determined. A way around this problem is to use iterative techniques where an initial estimate is made and the answers are successively improved until convergence is achieved. In the SAM, an iterative technique is used that continuously updates the front locations, zone saturations, temperature, and pressure. The pressure at the injection well is estimated, and the pressure drops through the system are calculated. The front locations and zone saturations are determined in the process. The calculated pressure drops through the system are subtracted from the injection well pressure estimate so that a pressure at the production well is calculated. The calculated pressure is compared to the prescribed production well boundary condition. If the two values do not match within a convergence tolerance, the injection well pressure guess is revised. The amount of revision in the pressure estimate is equal to the

difference between the calculated and boundary condition pressures at the production well. Details about the computer program that is used to solve the model equations are given in Appendix C.

The remainder of this chapter will give information about the simulation runs, the modification of the fractional flow theory to calculate the location of the water front, the analytical model used to determine the location of the steam front, the method used to calculate the steam saturation in the steam zone, the way in which pressure drop calculations are made, and how compressibility and thermal expansion effects are included.

3.1 Definition of One-Dimensional

This work uses a Cartesian coordinate system. Dimensions are expressed in length, width, and height. For this work, the length is the x -direction, the width is the y -direction, and the height is the z -direction. The system is one-dimensional in the sense that all variables that are a function of position are a function of x only. Consider a plane that intersects the reservoir at right angles to the x -coordinate. The pressures, temperatures, and saturations in this plane are uniform.

When this definition is used, wells that penetrate the reservoir need not be points. Since the reservoir has finite height, the well can be a line. Since the reservoir has width, the well can also be a plane that intersects the reservoir at right angles. The otherwise linear stream lines converge at a wellbore resulting in radial flow at the well. The result is an additional pressure drop at the well compared to the pressure drop that would occur if flow were linear. This additional pressure drop is used by both the thermal simulator ISCOM and the SAM to model the convergence of stream lines at wells.

In reservoir simulators, injection and production wells act as sources or sinks over the entire grid block in which the well is completed. The pressure difference from the injection well to the injection grid block is described by an injectivity index. At the production well, the pressure drop from the grid block to the well is computed from a radial flow equation (see Eq. 3.21). The radial flow equation includes, among other

parameters, the width and height of the reservoir, so the geometry of the system is reflected in the pressure drop at the production well.

3.2 Zone Definitions

The simulation runs made in conjunction with this program indicated that three distinct zones develop in a one-dimensional system, as shown in Figure 3.1. Nearest

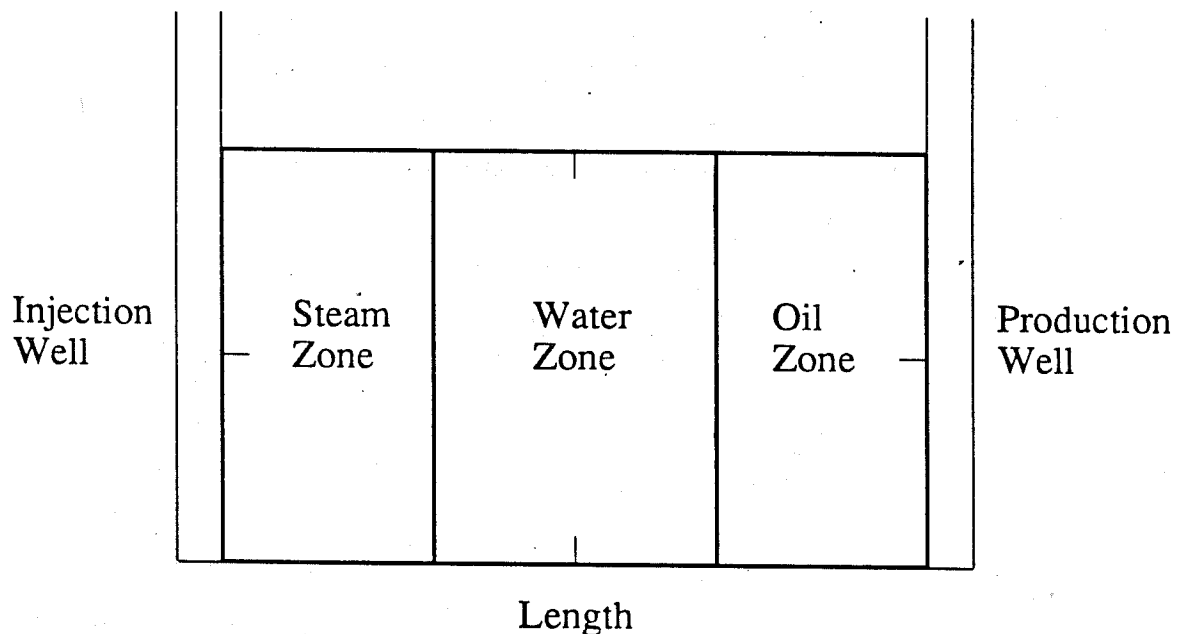


Figure 3.1: One-Dimensional Zone Definition

the injection well is the steam zone. In this zone the temperature is that of the wet steam, and this is the only zone where a gas phase exists. The oil, water and gas phases are all mobile in the steam zone.

The middle zone is the water zone, and the boundary between the steam and water zones is the steam front. As steam moves away from the injection well, it condenses. The point at which all steam has condensed is the steam front. The water zone has no gas saturation, but the water supplied by the condensation of steam flows

freely in this zone. The mobile water displaces the mobile oil in this zone, and the temperature is the original reservoir temperature.

The zone closest to the production well is the oil zone, and the boundary between the water zone and the oil zone is the water front. The oil zone is at initial reservoir temperature and initial saturation. Oil is mobile in this zone and in some cases, the water is also mobile. The water front acts like a cold waterflood and, depending on the oil viscosity, can displace a significant amount of the oil in place. No significant hot water zone was ever seen ahead of the steam front in any of the one-dimensional runs with the numerical reservoir simulator. An analytical solution that supports this finding is given by Wingard [52]. The one-dimensional flow sequence defined here was seen to be valid for either updip or downdip steam injection.

The boundary conditions at the wells are an injection well which injects wet steam at a constant rate and enthalpy, and a production well that produces at a constant flowing bottomhole pressure. The only mass flow to and from the system occurs at the wells. Heat flow is allowed to the adjacent formations in the z -direction only. A more detailed discussion of the assumptions made in the SAM is given in Appendix B.

3.3 Fractional Flow Calculations

Fractional flow theory is used to determine the location of the water front and to calculate the water zone water saturation and the unadjusted gas (steam) saturation in the steam zone. In this theory, a displacing fluid is injected into a porous medium containing both the displacing fluid and a fluid to be displaced. For this discussion, the displacing fluid will be water and the displaced fluid will be oil. The method is based on the relative permeability concept for two phases and the idea that there is a considerable amount of oil bypassed by the water front. A flood front exists with only oil moving ahead of the front but with both oil and water moving behind the front. Assumptions include linear, incompressible flow that is modeled by Darcy's law. The fluids are immiscible and isothermal conditions exist. The reservoir is a single homogeneous layer with a constant cross-sectional area.

The equations for fractional flow calculations employ the fractional flow of water. The equation for fractional flow of water, f_w , is [30]

$$f_w = \frac{1 + \frac{0.001127k_x k_{ro} A}{\mu_o q_t} [\partial p_c / \partial x - ((\rho_w - \rho_o) \sin \theta) / 144]}{1 + \mu_w k_{ro} / \mu_o k_{rw}} \quad (3.1)$$

where k_x is permeability in the x -direction, k_r is relative permeability, A is cross-sectional area, μ is viscosity, q_t is total flow rate, p_c is capillary pressure, ρ is density and θ is the formation dip. The relative permeability data for the oil-water system is used here. If capillary pressure is neglected, the equation becomes

$$f_w = \frac{1 - [7.8264 \times 10^{-6} k_x k_{ro} A (\rho_w - \rho_o) \sin \theta] / (\mu_o q_t)}{1 + \mu_w k_{ro} / \mu_o k_{rw}} \quad (3.2)$$

The frontal advance equation for one-dimensional immiscible displacement of oil by water in a porous medium was presented by Buckley and Leverett [5] as

$$\left(\frac{\partial x}{\partial t}\right)_{S_w} = \frac{5.6146 q_t}{\phi A} \left(\frac{\partial f_w}{\partial S_w}\right)_{S_w} \quad (3.3)$$

S_w is water saturation, t is time, q_t is the total flow rate at reservoir conditions, ϕ is porosity, A is cross-sectional area, and f_w is the fractional flow of water. Velocities of zones of equal fluid saturation, the location of the water front, and the average water saturation behind the water front can be determined by construction of a fractional flow curve as demonstrated by Buckley and Leverett and by Welge [49]. Integration of Eq. 3.3 gives

$$\Delta x = \frac{5.6146 q_t}{\phi A} \frac{\partial f_w}{\partial S_w} \Delta t \quad (3.4)$$

The distance to the water front in the SAM is calculated from

$$L_{s+w} = \frac{Q_{res}}{A\phi(\bar{S}_w - S_{wi})} \quad (3.5)$$

where L_{s+w} is the sum of the lengths of the steam and water zones and Q_{res} is the reservoir volume of the injected fluid. Calculation of this reservoir volume is discussed below. \bar{S}_w comes from the tangent construction to the fractional flow curve as shown in Figure 3.2.

The location of the water front, the water saturation in the water zone, and the steam saturation in the steam zone are derived from the fractional flow calculation.

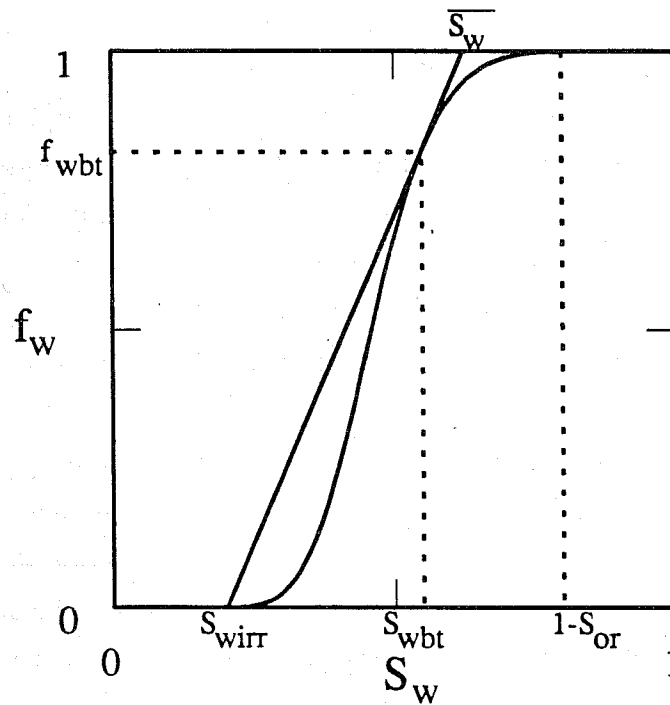


Figure 3.2: Fractional Flow Curve Tangent Construction

A tangent line is constructed from the point of irreducible water saturation and zero fractional flow of water to the fractional flow curve, as shown in Figure 3.2. The point where the tangent line intersects a water fractional flow value of unity is noted. The water saturation at this point is \bar{S}_w , the average water saturation behind the front. The point of tangency gives information about the water saturation and the fraction of water flowing at the front, but this information is not used in the program. The tangent line is determined numerically by the computer program which is discussed in Appendix C.

The distance from the injection well to the water front is determined from the fractional flow calculation and the slope of the tangent line. The reservoir volume of fluid injected is calculated, making an adjustment for the extra volume of the steam phase in the steam zone. This adjustment allows the fractional flow calculation to be used in the steamflood problem. However, calculation of the reservoir volume of the injected fluid requires that the volume of the steam zone be known. The method of determining this volume is presented in the next section.

3.4 Distance To Steam Front

The analytical methods for prediction of the steam front location can be divided into frontal advance models and bypass models. For the one-dimensional problem, only frontal advance models can be used. The Marx and Langenheim model [32] was initially used, and good results were obtained at early times and at high injection rates. However, at late time and low steam quality, oil and water production rates did not agree well with the thermal simulator results, so frontal advance models that involved fewer assumptions were considered.

The total heat injected can be divided into latent heat and sensible heat. Since the steam zone is at steam temperature, heat losses to the adjacent formations must be supplied entirely by latent heat. Initially, the rate of heat loss will be less than the latent heat injection rate. This means that some latent heat will be available at the condensation front to heat additional reservoir. In this case the entire heated zone will contain steam and the Marx-Langenheim method is adequate to calculate the swept area. At later times, however, the total rate of heat loss will become greater than the latent heat injection rate. All latent heat content of injected steam will be depleted in supplying the overburden heat losses. The steam will completely condense before it reaches the hot liquid front, and the steam zone will be smaller than the heated area. Because of the remaining sensible heat in the condensed steam, a hot water bank that grows with time will form ahead of the steam zone. The Marx-Langenheim method does not include this behavior.

The mass-energy balance presented by Yortsos and Gavalas [54] included these effects and was selected to determine the location of the steam front in the SAM. Since the Yortsos and Gavalas work is a significant part of the SAM, a description of their work is included here. Yortsos and Gavalas integrated the differential heat balance equation and the mass balance equation for each component (water and oil) over both the steam zone and the liquid zone volumes. The heat balance was considered for both total heat and latent heat in the system. The energy and mass differential equations representing the moving boundary relationship between the steam and liquid zone were also integrated over the area of the boundary. The temperature across the steam

front was considered continuous, unlike Marx and Langenheim [32] and Shutler and Boberg [43]. Heat losses to the overburden were in the vertical direction only, and were calculated using Laplace transformation, similar to the method used in other models. Heat losses were calculated as a function of time. As in most other analytical models, the Yortsos and Gavalas method assumes a constant temperature in the steam zone, thereby simplifying the heat loss calculations. In the SAM, the temperature changes in the steam zone are small, so this method can be used with little error.

Bounds on the heat losses to the overburden were derived by Yortsos and Gavalas. The lower bound was based on a temperature difference between the reservoir and overburden that must be at least zero. This means that heat can not flow from the overburden into the reservoir. The lower bound on heat losses was for a convection dominated liquid zone in which the temperature of the overburden was raised immediately to the temperature of the injected steam. The upper bound on heat losses was for a conduction dominated liquid zone with the instantaneous heat losses of a step temperature profile (Marx-Langenheim). This bound on heat losses is based on a temperature difference between the reservoir and overburden that is the difference between the temperature of the injected steam and the original formation temperature.

The steam zone advances only when latent heat is available to expand the steam zone. As the steam front propagates, heat losses to the adjacent formations increase. There comes a time where the latent heat injection rate is not sufficient to sustain these heat losses, and, as a result, the advance of the steam front slows down. The total heat balance is used to monitor heat losses, and the latent heat balance is used to monitor the growth of the steam zone.

The total and latent heat balances were each solved using the two bounds on heat losses to the overburden. From these equations, upper bounds were derived for the volume, and therefore length, of the steam zone. The growth rate of the one-dimensional steam zone is subject to two upper bounds resulting from heat balances on the total heat and on the latent heat. Each of the bounds controls the rate of growth of the steam zone in a different time interval, depending on the dominant mode of heat transfer in the liquid zone. At constant injection rates, the steam zone

growth at early time is controlled by the bound based on the total heat balance, and at late time is controlled by the bound based on the latent heat balance. The equation for one upper bound is based on the total heat balance and is

$$L_{sD} = \sqrt{t_D} - 1 + \exp(-\sqrt{t_D}) \quad (3.6)$$

The other upper bound is based on the latent heat balance and is

$$L_{sD} = F \left[\sqrt{t_D} - \frac{M_2}{M_1} + \frac{M_2}{M_1} \exp\left(-\frac{M_1}{M_2} \sqrt{t_D}\right) \right] \quad (3.7)$$

where M is a volumetric heat capacity. M_1 is for the entire reservoir and M_2 is for the steam phase only. The expressions are

$$M_1 = \phi(C_w \rho_w S_w + C_o \rho_o S_o + C_g \rho_g S_g) + (1 - \phi) \rho_R C_R + \phi \frac{L_v \rho_g S_g}{\Delta T} \quad (3.8)$$

$$M_2 = \phi \frac{L_v \rho_g S_g}{\Delta T} \quad (3.9)$$

and F is a heat function that is the ratio of the latent heat to the total heat injected. The expression for F is

$$F = \frac{f_s}{f_s + \frac{C_w \Delta T}{L_v}} = \frac{w_s L_v}{w_s L_v + (w_s + w_w) C_w \Delta T} \quad (3.10)$$

In these equations, C is the specific heat capacity, L_v is the latent heat of vaporization of water at steam zone temperature, ΔT is the difference between the steam zone temperature and the original system temperature, and f_s is injected steam quality. The saturations used in the preceding calculation are taken as constant over the entire length of the steam zone. An analytical argument for the constant saturation case is presented by Yortsos [56]. Also, the simulator results for the one-dimensional cases exhibited nearly constant steam zone saturations.

At early time, the upper bound based on the total heat balance is more restrictive than the upper bound based on the latent heat balance. The upper bound based on the latent heat balance is more restrictive at late time. There is a point in time, t_{Da} , where the two upper bounds are equal. Setting the equations for these two upper bounds equal to each other and solving for time determines which upper bound should be used. The result is the following equation which is solved for t_{Da}

$$\sqrt{t_{Da}}(1 - F) = 1 - \exp(-\sqrt{t_{Da}}) \quad (3.11)$$

If t_D is less than t_{Da} then the upper bound based on the total heat balance is used, otherwise the upper bound based on the latent heat balance is used. Yortsos and Gavalas used dimensionless variables in order to generalize the equations. The variables used to transform the dimensional equations to dimensionless ones were chosen so that the total number of variables would be reduced to a minimum. Dimensionless time is calculated from

$$t_D = t \left(\frac{2a}{M_1 \Delta T} \right)^2 \quad (3.12)$$

where a is expressed as

$$a = \frac{2\lambda_{ob}\Delta T}{H\sqrt{\pi\alpha_{ob}}} \quad (3.13)$$

λ_{ob} is the thermal conductivity of the overburden, π is 3.14159 and α_{ob} is the thermal diffusivity of the overburden. The dimensionless length is defined as

$$L_D = \frac{2La^2}{[(w_s + w_w)C_w\Delta T + w_sL_V]M_1\Delta T} \quad (3.14)$$

Yortsos and Gavalas used their work to define when the Marx and Langenheim model is valid. The steam zone length calculated from the Marx and Langenheim method is smaller than the length calculated from the total heat balance at all times and at all values of F . Similarly, the length from the Marx and Langenheim method is smaller than the length calculated from the latent heat balance for high values of F . For values of F below a critical value, however, a critical time exists when the Marx and Langenheim solution crosses above the upper bound from the latent heat balance. Yortsos and Gavalas showed that this situation exists if $F \leq \frac{2}{\pi}$. For low steam quality and high injection temperature, the Marx and Langenheim solution can give over optimistic results regarding the progress of the steam zone and the oil recovery rates, sometimes having an error of 30 percent or more.

The Yortsos and Gavalas method was used for the heat balance in the SAM. This heat balance provided the amount of heat given up to the overburden, the amount of heat needed to raise the temperature of the reservoir, and the volume of the steam zone. However, the method requires that the steam zone steam saturation be known. The next section presents a method of determining steam zone steam saturation.

3.5 Steam Zone Steam Saturation

The steam zone steam saturation is calculated from fractional flow theory and then corrected for condensation effects. If steam were a non-condensable gas, the gas saturation could be calculated from fractional flow theory of a gas-liquid system in a manner similar to the water saturation for a water-oil system. This type of calculation is made as an initial estimate during every iteration, however, the steam will condense, thereby reducing the steam saturation. The heat balance calculation discussed in the previous section provides information on the amount of heat lost to the overburden and the amount of heat used to heat the reservoir. Since the pressure of the steam zone is updated during each iteration, the latent heat, enthalpy, and density of the steam can be calculated. Section A.6 of Appendix A gives the details. The amount of heat lost, Q_{loss} , can be converted to mass of steam condensed by dividing the heat lost by the latent heat of vaporization, L_v . The mass of steam condensed can be converted to a volume of steam condensed, $V_{s,con}$, using the known steam density, ρ_s , as follows

$$V_{s,con} = \frac{Q_{loss}}{L_v \rho_s} \quad (3.15)$$

Since saturation is a volumetric term, the gas saturation determined from the fractional flow calculation is simply reduced by the volume of steam condensed to obtain the correct steam saturation. The calculation is a function of pressure. Since calculated steam zone pressure changes with each iteration, the calculation must be repeated each iteration. To determine the steam zone pressure, pressure drop calculations must be made. These calculations are discussed in the next section.

3.6 Pressure Drop Calculations

After making an estimate of pressure at the injection well, the pressure is determined at the production well by making five pressure drop calculations in series. The pressure drop is calculated through the injection well, across the steam zone, the water zone, the oil zone, and to the production well.

Injection Well

The pressure drop through the injection well is a simple water injectivity index calculation. The injection rate is measured in equivalent barrels of water, so the water injectivity index is used. The density of the water at standard conditions may not be the density of water at bottomhole conditions, so a density correction may be necessary. The pressure drop, Δp , is

$$\Delta p = \frac{q_{inj} \rho_{wsc}}{I_w \rho_w} \quad (3.16)$$

where I_w is the injectivity index, ρ_{wsc} is water density at standard conditions, and ρ_w is water density at bottomhole conditions. This equation is also used by the thermal simulator.

Steam Zone

The potential drop through each of the three reservoir zones is due to the sum of the pressure drop because of flow plus the pressure change due to hydrostatic head. In the steam zone, the temperature of the entire zone is elevated to the temperature of the wet steam. The oil, water and gas phases are all mobile. The pressure drop due to flow is calculated from Darcy's law [11, 25, 50, 51] for multiphase flow where the flow rate, q_t , is the total flow rate of the reservoir fluids taken at steam zone conditions. Gravity effects are also included in the equation. The pressure drop is

$$\Delta p = \frac{q_t L_s}{0.001127 k_r A \left(\frac{k_{rg}}{\mu_g} + \frac{k_{rw}}{\mu_w} + \frac{k_{ro}}{\mu_o} \right)} + \frac{\rho_{av} L_s \sin \theta}{144} \quad (3.17)$$

ρ_{av} is the saturation weighted average density of the fluids in the steam zone and is expressed as

$$\rho_{av} = \rho_g S_g + \rho_o S_o + \rho_w S_w \quad (3.18)$$

The hydrostatic head of the fluids in the reservoir is a function of the density and saturation of the fluids. Capillary pressure is neglected, so some expression for the average fluid density is required. The saturation weighted density makes sense so it was used in the SAM.

Water Zone

The pressure change through the water zone is similar to that of the steam zone. In the water zone, the temperature is the initial temperature, and no gas phase is present. Both the water and the oil phases are mobile, so the pressure drop is

$$\Delta p = \frac{q_t L_w}{0.001127 k_x A \left(\frac{k_{ro}}{\mu_o} + \frac{k_{rw}}{\mu_w} \right)} + \frac{\rho_{av} L_w \sin \theta}{144} \quad (3.19)$$

Oil Zone

No gas phase is present in this zone, and the temperature is the initial temperature. The oil phase is mobile in this zone, and in some cases the water can also be mobile. The pressure drop is calculated from Darcy's law for multiphase flow and is

$$\Delta p = \frac{q_t L_o}{0.001127 k_x A \left(\frac{k_{ro}}{\mu_o} + \frac{k_{rw}}{\mu_w} \right)} + \frac{\rho_{av} L_o \sin \theta}{144} \quad (3.20)$$

Production Well

The pressure drop into the production well is calculated using the same equation employed by the thermal simulator. The entire productive horizon is perforated. The pressure drop is

$$\Delta p = \frac{q_t \left[\ln \left(\frac{cc}{r_w} \sqrt{\frac{(\Delta x)^2 + (\Delta y)^2}{\pi}} \right) + s \right]}{0.007081 k_x H \left(\frac{k_{ro}}{\mu_o} + \frac{k_{rw}}{\mu_w} \right)} \quad (3.21)$$

where cc is a shape factor for the production well grid block, r_w is the wellbore radius, s is the skin factor, and Δx and Δz are the dimensions of the production well grid block. The relative permeabilities are evaluated at oil zone saturations. A well fraction of unity was used in this calculation.

3.7 Compressibility and Thermal Expansion

As the program iterates, the temperature and pressure of each zone is updated. The compressibility and thermal expansion of the oil, water, and rock are considered by adjusting the pore volume and the oil and water densities. Changes in temperature

and pressure cause the pore volume of the reservoir to change. The density of the oil and water phases that occupy the pore volume are also functions of temperature and pressure. The mass balance on each component determines the mass of oil and water in the reservoir. The calculated densities are used to determine the volume of oil and water in the reservoir. Front locations are functions of both pore volume and fluid volume. Thus, the locations of the water and steam fronts reflect the effects of compressibility and thermal expansion.

3.8 Concluding Remarks

The one-dimensional model consists of the equations presented in this chapter. A fractional flow calculation, adjusted for the volume of the steam zone, is used to determine the location of the water front. The Yortsos and Gavalas heat balance is used to determine the overburden heat losses and the location of the steam front. A fractional flow calculation corrected for condensation is used to determine the steam zone steam saturation. Pressure drops across the three reservoir zones are calculated using Darcy's law for three-phase flow. Assumptions that are required to use these analytical methods are included in Appendix B. The equations are solved on a computer by an iterative method. The computer program that is used to solve the equations is discussed in detail in Appendix C and is included on a floppy disk that is available through the Stanford University Petroleum Engineering Department. Auxiliary equations that are used to provide relative permeabilities, porosity, phase densities, viscosities, wet steam properties, and production rate calculations are included in Appendix A.

The one-dimensional SAM has been defined. In the next chapter, results from the one-dimensional SAM will be compared to results from the thermal simulator ISCOM.

Chapter 4

One-Dimensional Model Results

In this chapter, the one-dimensional semianalytical model (SAM) was compared with results from a thermal simulator. The simulator used for comparison was ISCOM [42], a general purpose thermal simulator written by the Computer Modeling Group. The simulator runs are described in the first section, followed by many comparisons of results in the second section. The second section also includes discussion of the differences between the SAM and ISCOM and the reasons for them.

4.1 One-Dimensional Simulator Runs

A Cartesian coordinate system with uniform gridding was used in all simulator runs. The reservoir was considered homogeneous in porosity and permeability. Two components were used. One component was a dead oil that existed only in the oil phase, the other was water that could exist in either the liquid water phase or in the gas phase as steam. The oil component was not soluble in the water or gas phases, nor was the water component soluble in the oil phase. The initial condition was assumed to be oil at an irreducible water saturation and a uniform temperature.

Of the many variables used in the thermal simulator, only the ones that have a significant effect on the results were varied. A one dimensional data set was assembled. Data used are shown in Tables 4.1 to 4.5. The relative permeability curves for the oil-water system are shown in Figure 4.1, and the curves for the gas-liquid system

are shown in Figure 4.2. These relative permeability data were taken from a paper dealing with a typical heavy oil reservoir [6] and smoothed by the Corey method using the exponents that gave the best fit of the data. The smoothed data were used as input to the simulator. While the SAM uses the Corey type equation directly, the simulator uses linear interpolation between data points. The one-dimensional case was run with differing numbers of grid blocks in order to determine how many grid blocks should be used on subsequent runs.

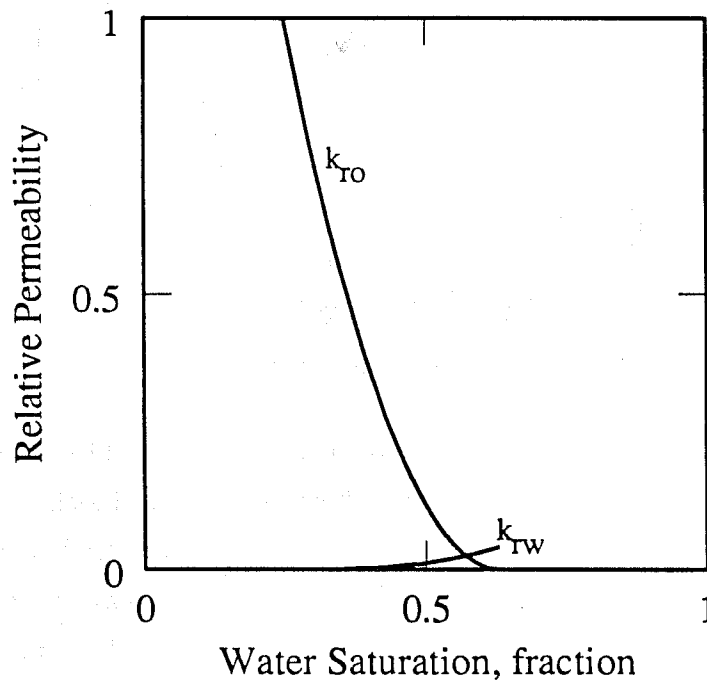


Figure 4.1: Oil-Water Relative Permeability

The one-dimensional case was run using 20, 100, and 500 grid blocks. Figure 4.3 compares the distribution in the reservoir of temperature, pressure, and oil, water and gas saturations after three years of injection for these three cases. Figure 4.4 compares the oil production rates for each of the cases. Figure 4.3 is a graph of the one-dimensional system results, graphing several variable results as a function of distance. The injection well is on the left at a distance of zero, and the production well is on the right at a distance of 2000 feet. The water and steam fronts can be seen clearly, separating the steam, water, and oil zones. The phase saturations in each

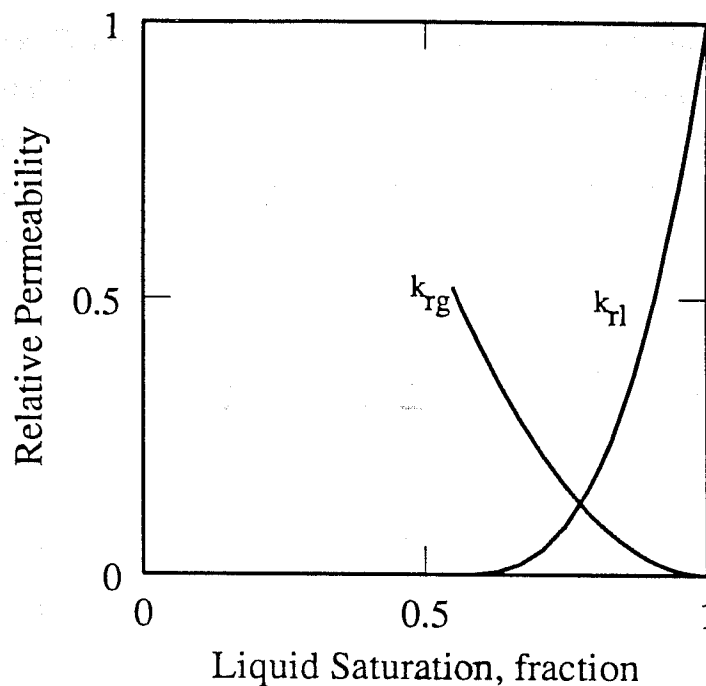


Figure 4.2: Gas-Liquid Relative Permeability

of the zones are practically constant, except near the fronts. The case with 500 grid blocks gives the smallest discretization error because the grid blocks are the smallest. The results show that the 100 grid block case gives an apparently better match to the 500 grid block case than does the 20 grid block case. The steam zone in the 20 grid block case was much smaller than in the other two cases. The temperature profile shows that, for the 20 grid block case, much less of the injected heat is retained in the reservoir. This difference is due to increased heat losses to the adjacent formations. However, using 500 grid blocks gives only a slight improvement over the 100 grid block case while significantly increasing the computer time required to generate a solution. The rest of the one-dimensional runs were made using 100 grid blocks.

Figure 4.4 shows oscillations for all three finite difference cases. The number of oscillations corresponds exactly to the number of grid blocks encountered by the steam zone. The oscillations do not represent a convergence problem or a problem with the simulator. Changing the time step size or the convergence tolerance does not change the nature of these oscillations. The oscillations occur whenever the steam zone

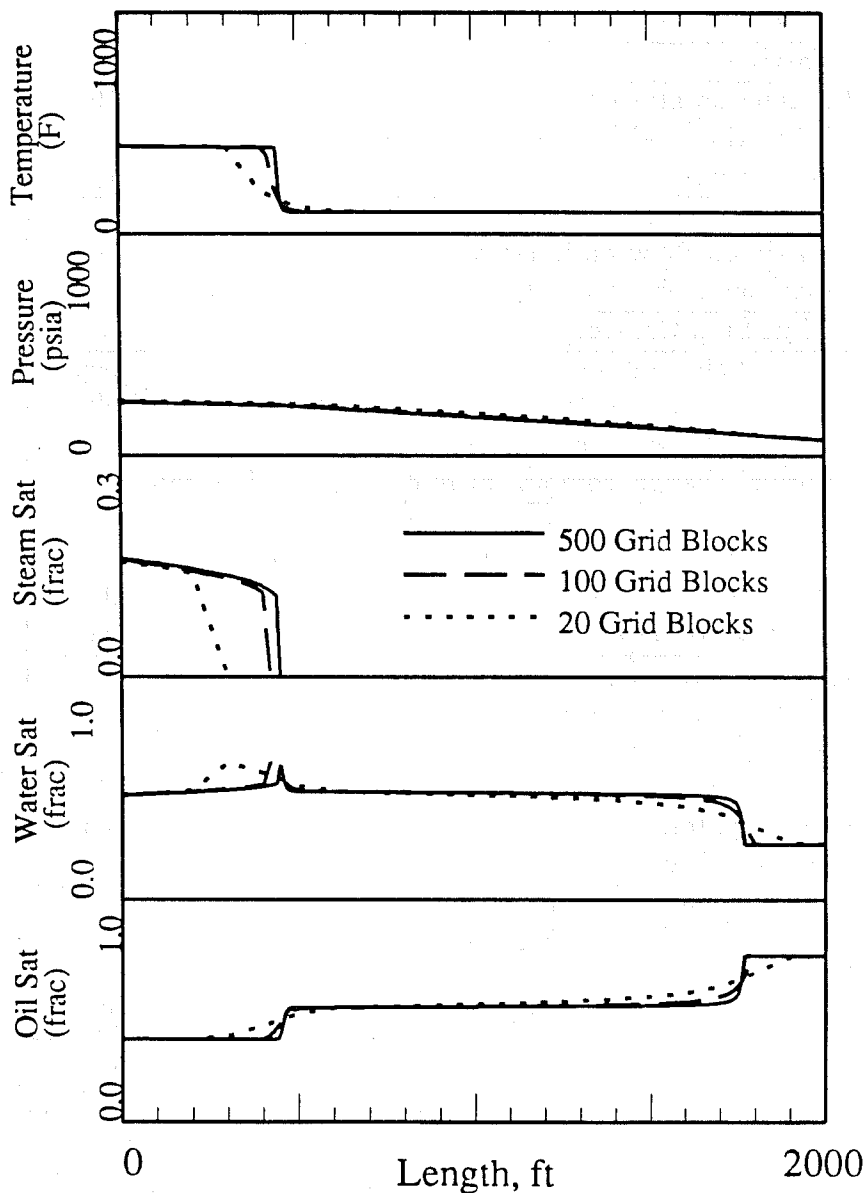


Figure 4.3: Variable Distribution at 3 years as a Function of Grid Density

Variable	Value
i-direction grid blocks	100
j-direction grid blocks	1
k-direction grid blocks	1
number of components	2
maximum Newton iterations	10
maximum time step, days	100
Time Step Control	
normal change, pressure, psi	200
normal change, saturation, fraction	0.2
normal change, temperature, degrees F	40
normal change, component mole fraction, fraction	0.2
convergence tolerance, pressure, psi	0.8
convergence tolerance, saturation, fraction	0.015
convergence tolerance, temperature, degrees F	0.08
convergence tolerance, mole fraction, fraction	0.2
reservoir dip, degrees	0
block size, i-direction, ft	20
block size, j-direction, ft	1000
block size, k-direction, ft	100
porosity, fraction	0.3
permeability, Darcy	2
initial pressure at top of reservoir, psia	70
initial temperature, degrees F	100
initial water saturation, fraction	0.25
initial oil saturation, fraction	0.75

Table 4.1: Simulator One-Dimensional Data Set for Grid Study

Variable	Value
molecular mass of water, lbm/mole	18.02
molecular mass of oil, lbm/mole	600
reference pressure for porosity, psia	14.7
reference pressure for density, psia	14.7
reference temperature for density, degrees F	60
standard pressure, psia	14.7
standard temperature, degrees F	60
molar density of water at STP, mole/cu ft	3.4628
compressibility of water, 1/psi	4.0e-06
thermal expansion of water, coefficient one, 1/F	3.8e-04
thermal expansion of water, coefficient two, 1/F/F	0.0
molar density of oil, at STP mole/cu ft	0.1
compressibility of oil, 1/psi	5.0e-06
thermal expansion of oil, coefficient one, 1/F	4.0e-04
thermal expansion of oil, coefficient two, 1/F/F	0.0
critical pressure of water, psia	3206.2
critical temperature of water, degrees F	705.4
gas viscosity coefficient, cp	4.8e-04
gas viscosity exponent	0.593
oil viscosity at initial temperature, cp	100
water viscosity at initial temperature, cp	1
molar heat capacity of oil, btu/mol-F	300
volumetric heat capacity of rock, btu/cu ft-F	35
volumetric heat capacity of overburden, btu/cu ft-F	35
formation compressibility, 1/psi	5.0e-06
formation thermal expansion, 1/F	0.0e-06
thermal conductivity of rock, btu/ft-day-F	38.0
thermal conductivity of water, btu/ft-day-F	9.0
thermal conductivity of oil, btu/ft-day-F	2.0
thermal conductivity of gas, btu/ft-day-F	0.5
thermal conductivity of overburden, btu/ft-day-F	24.0

Table 4.2: Simulator PVT and Thermal Data for Grid Study

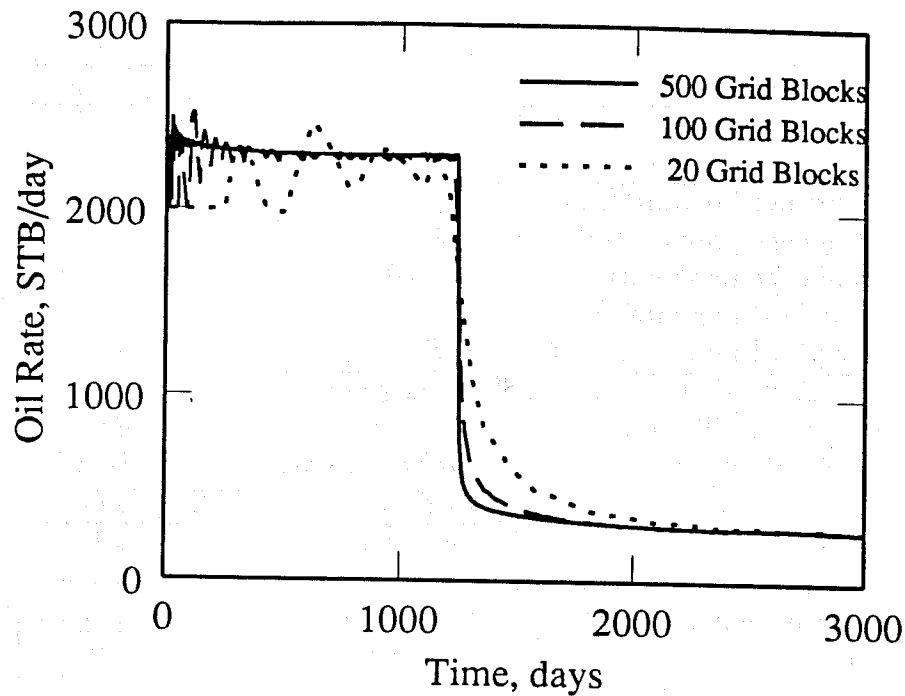


Figure 4.4: Oil Production Rate as a Function of Grid Density

Variable	Value
Injection Well	
water injection rate, bbl/day	2000
maximum pressure constraint, psia	1000
injection temperature, degrees F	450
steam quality, fraction	0.7
injectivity index, bbl/day/psi	9999
Production Well	
Bottomhole pressure, psia	70
maximum rate constraint, bbl/day	3000
wellbore radius, ft	0.4
shape factor	0.0008
skin factor	0.0

Table 4.3: Simulator Well Data for Grid Study

S_w	k_{rw}	k_{ro}	S_w	k_{rw}	k_{ro}
0.25	0.00000	1.00000	0.45	0.00588	0.22438
0.27	0.00001	0.89751	0.47	0.00782	0.17729
0.29	0.00005	0.80055	0.49	0.01015	0.13573
0.31	0.00016	0.70914	0.51	0.01291	0.09972
0.33	0.00038	0.62327	0.53	0.01612	0.06925
0.35	0.00073	0.54294	0.55	0.01983	0.04432
0.37	0.00127	0.46814	0.57	0.02407	0.02493
0.39	0.00202	0.39889	0.59	0.02887	0.01108
0.41	0.00301	0.33518	0.61	0.03427	0.00277
0.43	0.00428	0.27701	0.63	0.04030	0.00000

Table 4.4: Water/Oil Relative Permeability Data

S_l	k_{rl}	k_{rg}	S_l	k_{rl}	k_{rg}
0.55	0.52000	0.00000	0.83	0.07421	0.24090
0.57	0.47480	0.00009	0.85	0.05778	0.29630
0.59	0.43166	0.00070	0.87	0.04340	0.35959
0.61	0.39058	0.00237	0.89	0.03107	0.43132
0.63	0.35155	0.00562	0.91	0.02080	0.51200
0.67	0.27964	0.01896	0.93	0.01258	0.60216
0.71	0.21596	0.04495	0.95	0.00642	0.70233
0.75	0.16049	0.08779	0.97	0.00231	0.81304
0.79	0.11324	0.15170	0.99	0.00026	0.93480
0.81	0.09270	0.19288	1.00	0.00000	1.00000

Table 4.5: Liquid/Gas Relative Permeability Data

crosses into a cool grid block. Because of the assumption of instantaneous thermal equilibrium, the steam in a cool grid block condenses immediately, volume drops and as a result, the oil rate decreases. As the block heats, the steam zone once again propagates, and the oil rate increases. The amplitude of the oscillations decreases as the size of a grid blocks decreases. In the case in which 500 grid blocks were used, the oscillations are barely noticeable.

Throughout this dissertation, production rate curves will be displayed instead of cumulative production curves. Production rate curves tend to magnify variations and often show detail not discernible in cumulative production curves.

Many cases were run in one dimension. Table 4.6 shows the variable ranges used to compare the numerical model with the SAM. The values used were chosen to cover the range of values usually found in the field. The number of values examined per variable was limited because the number of cases required increased exponentially with the number of values included. Covering all of the combinations of variables in the table required 360 simulation runs.

μ_o (cp)	1, 10, 100, 1000, 10,000
k (Darcy)	2, 20
L (ft)	500, 1000, 2000
q_w (bbl/day)	500, 1000, 2000
c_f (1/psi)	0, 5e-4
θ (degrees)	0, 60

Table 4.6: Variable Ranges for One-Dimensional Analysis

In some cases, a combination of high oil viscosity, a long reservoir, and a high injection rate would cause the pressure constraint at the injection well to be violated. When the pressure constraint was encountered, the injection rate would decrease to accommodate the constraint. These injection rate declines do not coincide with the constant injection rate assumed by the SAM. Therefore, cases used for comparison were ones that did not violate the injection well pressure constraint.

When running a case in which the reservoir dip was severe, care was taken to prevent negative pressure values. If the hydrostatic head across the reservoir was

greater than the flowing bottomhole pressure specified at the production well, the pressure at the top of the reservoir could decrease until a vacuum was calculated. The simulator did not allow such unusual pressure behavior, and the run would terminate. In order to get a case to run, the pressure at the production well had to be high enough to prevent this problem. Likewise, the SAM could not handle a combination of geometry, fluid densities, and boundary conditions that generated a vacuum. When such a combination of variables did exist, an error message was printed. Data sets that avoided this problem were used in this work.

4.2 One-Dimensional Results

360 cases were run on both the thermal simulator and the SAM so that results could be compared. The table in the file 1DCASE included on a floppy disk that is available through the Stanford University Petroleum Engineering Department shows the data used and essential results from the 360 one-dimensional cases that were run in this study. Each entry shows a case number, reservoir dip, oil viscosity, formation compressibility, length, permeability, and injection rate. Also included in the table are the water breakthrough times given by the SAM and the numerical simulator. Determining water breakthrough time for the simulator results is an ambiguous task. The time used for comparison was the time at which water production was first noticeable on the production plots with the scales used in this work. The relative error in breakthrough time, using the numerical results as the correct value, was calculated for each case. The relative error value for each of the cases was less than five per cent, indicating that the one-dimensional SAM consistently gave comparable results. In some of the cases, the injection well pressure exceeded the constraint, so the boundary condition was violated. These cases are indicated by "pres" in the water breakthrough column and were not used for comparison.

Table 4.7 lists the ten one-dimensional cases for which results are displayed. Results consist of graphs of oil and water production rates as functions of time, and graphs of temperature, pressure, and oil, water and gas saturation as functions of distance at a given time. This last graph will be called a variable distribution graph.

Case	Dip (deg)	c_f (1/psi)	μ_o (cp)	Figure Numbers
044	0	0	10	4.5-4.7
083	0	0	100	4.8-4.10
119	0	0	1000	4.11-4.13
062	0	5e-4	10	4.14-4.16
101	0	5e-4	100	4.17-4.19
137	0	5e-4	1000	4.20-4.22
224	60	0	10	4.23-4.25
263	60	0	100	4.26-4.28
263d	-60	0	100	4.29-4.31
299	60	0	1000	4.32-4.34

Table 4.7: Cases Displayed for One-Dimensional Analysis

The oil and water production graphs compare the production rates from the SAM to the production rates calculated by the thermal simulator. The variable distribution graphs compare the temperature, pressure, and the oil, water, and gas phase saturation distributions from the SAM with the distributions calculated by the numerical model.

The independent variables that change in the ten cases are formation dip, formation compressibility, and oil viscosity. Horizontal cases and cases with a formation dip of 60 degrees are shown. One case with a dip of -60 degrees (down dip steam injection) is also shown. Formation compressibility has values of zero or 0.0005 inverse psi in these cases. Initial oil viscosities of 10, 100, and 1000 cp are used. Oil and water production graphs and variable distribution graphs are displayed in Figures 4.5-4.34. In all of these graphs, the numerical model results are represented with a solid curve, and the SAM results are represented with a dashed curve.

In general, good matches were obtained in all cases. The times of water breakthrough, and the oil rates both before and after water breakthrough, matched well. Water production rates also matched well. The SAM uses an average saturation for each of the three zones, so the saturation graphs consist of square waves. However,

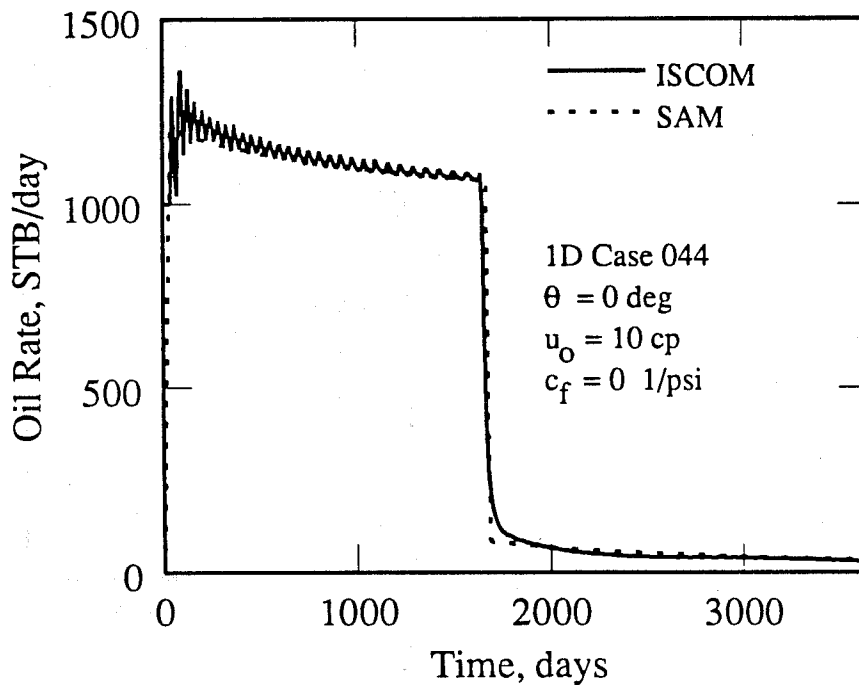


Figure 4.5: Oil Rate vs Time, Case 044

comparison of the results showed that the average saturation assumption gave a reasonably good match with the numerical model. The locations of the water fronts matched well. The steam front locations were slightly advanced in the SAM compared to the numerical results. The method used for calculating the location of the steam front gave an upper bound for this location, so the SAM steam front location should always be slightly ahead of the numerical location. The graphs of temperature, pressure, and phase saturations showed that good matches were obtained. Each of the ten cases will be discussed in detail in the following.

The first case displayed is Case 044 in Figure 4.5. In this case, the reservoir is horizontal and the formation compressibility is zero. An oil viscosity of 10 cp was used. The oil production rate graph is shown in Figure 4.5. The SAM matches the numerical model well. The match of water breakthrough time (see Figure 4.6) and the oil production rate after water breakthrough are almost exact. The oil production rate at early time is lower than ISCOM but still within the range of the oscillations. The lower production rate is caused by a pressure calculation in the SAM that is

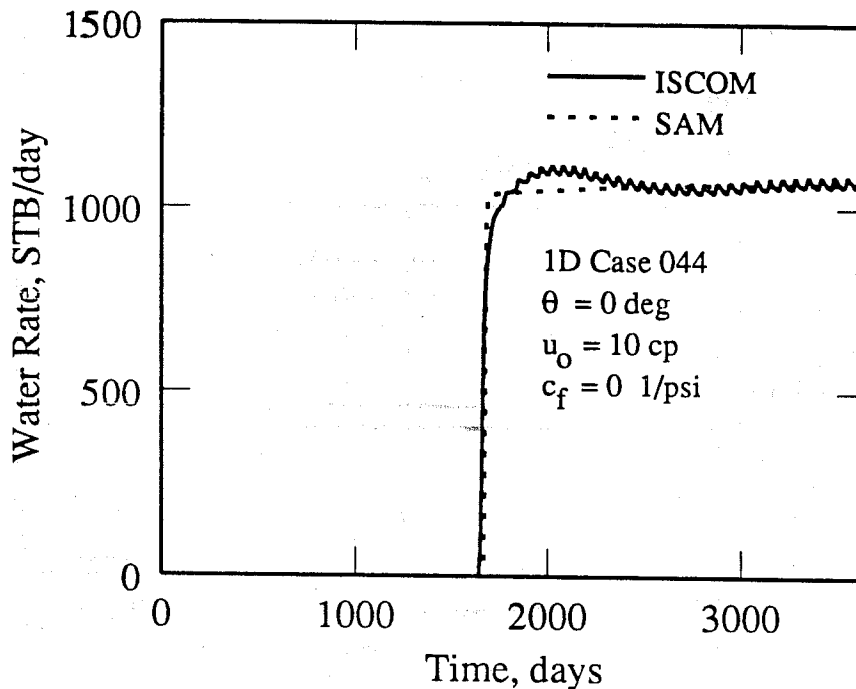


Figure 4.6: Water Rate vs Time, Case 044

higher, causing the volume of the steam zone and thus the oil production rate to be lower.

The water production rate graph is shown in Figure 4.6. The match for water breakthrough time is good, and there is some difference in the water production rates immediately after water breakthrough. This difference is caused by the method used to calculate saturations at the water front. The SAM uses average saturations for each of the zones, so there is a sharp increase in water saturation at the water front. The thermal simulator computes a different saturation for each grid block, resulting in a smooth saturation distribution at the water front.

Figure 4.7 shows the variable distribution graph for Case 044 at four years. These graphs show temperature, pressure, and gas, water and oil saturations as functions of distance. The injection well is located at $x=0$, and the production well is at $x=1000$ ft. On this type of presentation, fluids move from left to right. Five dependent variables are shown on this figure. Oil and water saturations are shown on a scale of zero to one. Gas saturation is graphed on an expanded scale of zero to 0.3 so that

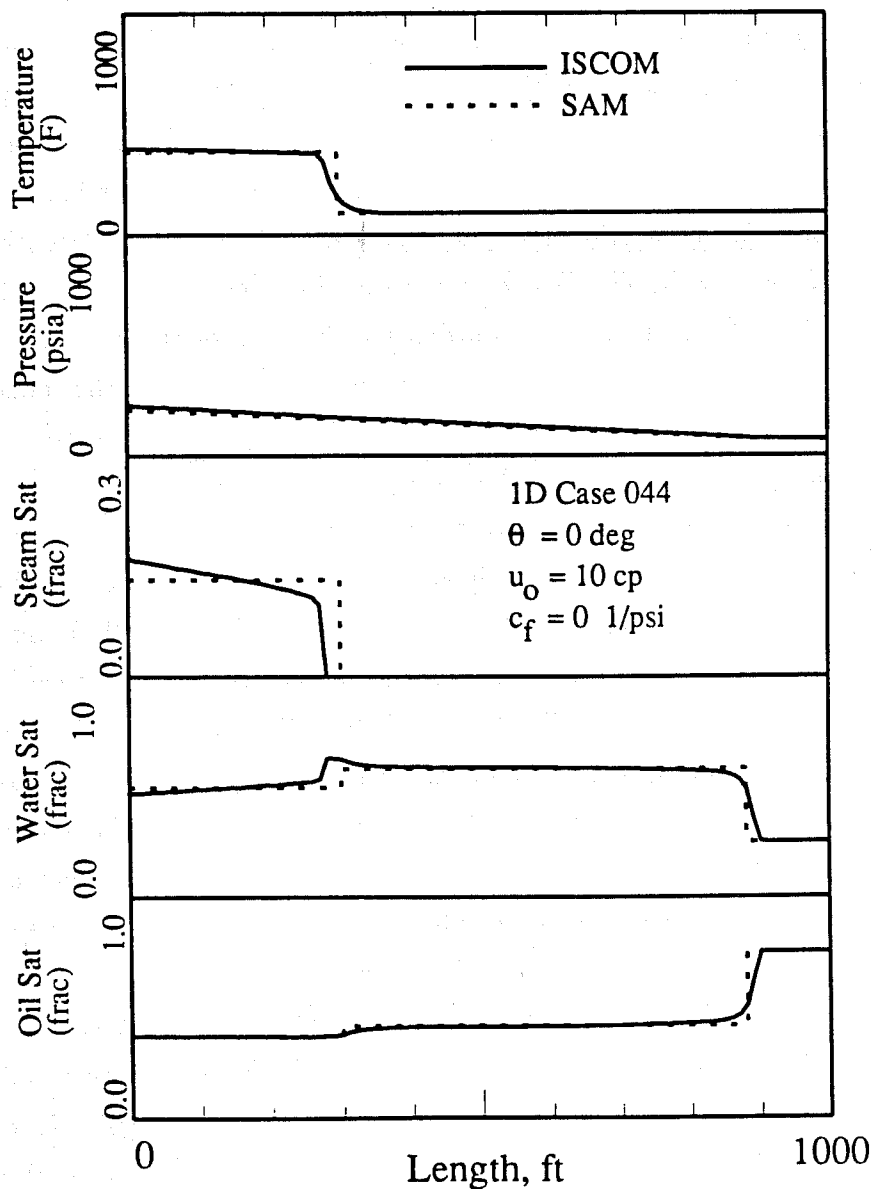


Figure 4.7: Variable Distributions at 4 years, Case 044

the steam zone may be clearly defined. Pressure is graphed from zero to 1000 psia, and temperature is graphed from zero to 1000 degrees F.

Figure 4.7 is for a time of four years. At this time, the pressure and temperature distributions in the reservoir match well, as they did for all times. The major differences in the models occur in the steam zone. The steam front for the SAM is more advanced than the steam front for the thermal simulator. The heat balance gives upper bounds for the volume of the steam zone so this result is not surprising. The steam saturation in the steam zone is constant for the SAM because an average value is used for the entire zone. The thermal simulator, on the other hand, calculates a steam saturation at each grid block. The steam saturation calculated by the simulator decreases with distance into the reservoir. The decline in steam saturation is a result of the heat losses to the overburden and heating of the reservoir. The steam saturation at the steam front must be zero because, at the front, the remaining latent heat is used to heat the cold reservoir encountered by the steam zone. There is a sharp drop in steam saturation at this point.

The declining steam saturation is explained by the overburden heat losses. The overburden nearest the injection well is exposed to the steam zone for a longer period of time than the overburden farther away from the injection well. Long exposure to the hot steam zone results in an overburden with a high temperature. As a result, the temperature of the overburden decreases with distance until, at the steam front, the temperature is the initial temperature. High overburden temperatures result in low heat loss rates. Consequently, the amount and rate of heat lost to the overburden increases with distance. The heat losses are supplied by latent heat as the steam condenses, so the steam condensation rate increases with distance. The higher steam condensation rate results in a lower steam saturation.

For the numerical model, there is a peak in water saturation at the steam front. At the steam front, cold reservoir is heated and steam condenses to supply this heat. As the steam condenses, water is added, resulting in an accumulation of hot water near the steam front. Because of negligible compressibility effects, each phase move through the system at a fixed rate. Therefore, the ratio of the water mobility to the oil mobility must be constant. The steep temperature decrease at the steam front

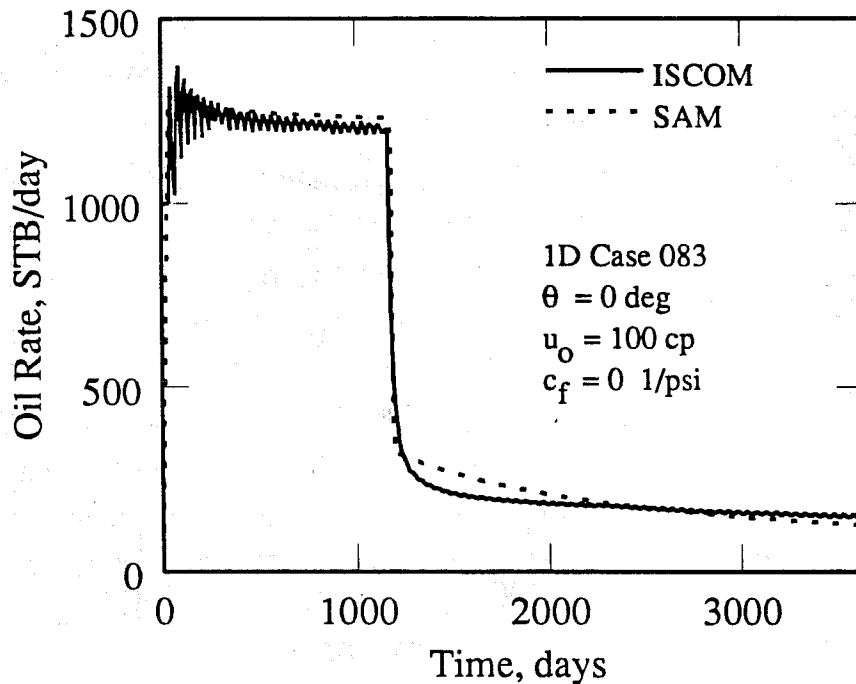


Figure 4.8: Oil Rate vs Time, Case 083

causes an increase in the oil viscosity. To keep the ratio of the mobilities constant, the relative permeability to water must increase and the relative permeability to oil must decrease. Therefore, the water saturation must increase, as is seen in the results. This effect is a function of the size of the grid blocks, and diminishes when smaller grid blocks are used (see Figure 4.3). The graph of oil saturation shows that the advancing water front displaced much of the oil, as is expected with a low viscosity oil and low mobility ratio. Since so much oil was displaced by the water zone, the change in oil saturation is small at the steam front.

The second case displayed is Case 083. In this case, the reservoir is horizontal and the formation compressibility is zero, but an oil viscosity of 100 cp was used instead of 10 cp. The numerical and SAM oil production rates for Case 083 are compared in Figure 4.8. A good match was obtained for water breakthrough time and oil rate both before and after water breakthrough. The oil production rate from the SAM before water breakthrough was higher than the ISCOM rate. The higher rate was caused by a slight error in the average water saturation in the water zone. Figure 4.10.

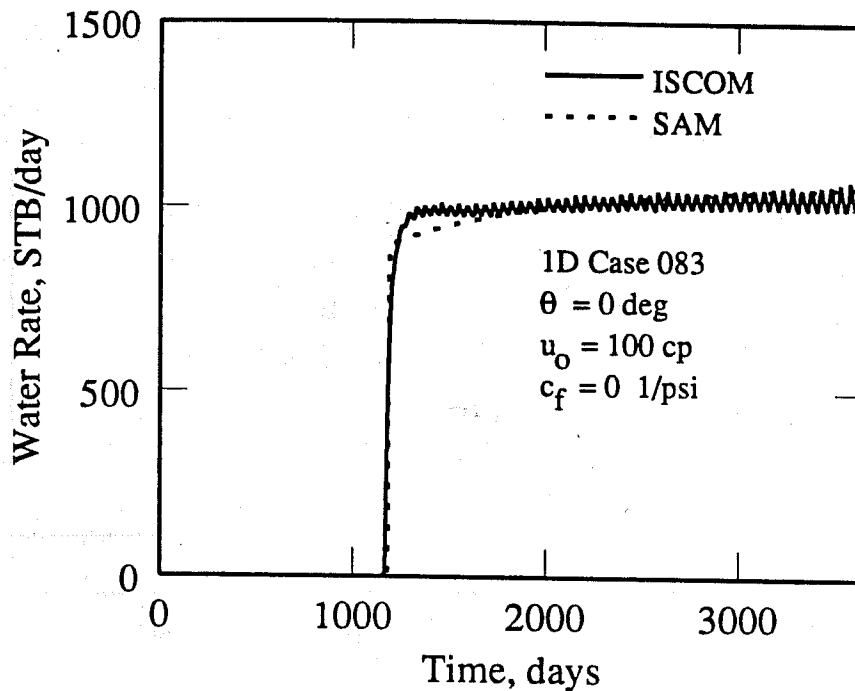


Figure 4.9: Water Rate vs Time, Case 083

discussed later, shows that the SAM gives a higher water saturation in the water zone. This higher water saturation causes more oil to be displaced and results in a higher oil production rate. Comparison of Figure 4.8 with Figure 4.5 from Case 044 shows the effect of an increase in oil viscosity. The two cases are identical in all other respects. The higher oil viscosity case has earlier water breakthrough caused by a higher residual oil saturation, which in turn is caused by a higher mobility ratio. The oil production rate after water breakthrough is higher for the higher oil viscosity case because of the poorer displacement efficiency associated with an unfavorable mobility ratio.

The water production rate comparison for Case 083 is shown in Figure 4.9. Good agreement was obtained, both in terms of water breakthrough time and water production rate after breakthrough. The water production rate immediately after water breakthrough is lower, and at late time it is higher compared to ISCOM. The water production rate is controlled by the growth of the steam zone and the change in average water saturation behind the water front. In this case, the water saturation

was increasing too fast shortly after breakthrough time, and too slowly at later times. This is to be expected since the SAM uses a sharp saturation front.

The comparison of temperature, pressure, and phase saturation distributions at two years for Case 083 is shown in Figure 4.10. Good agreement is obtained for all parameters. As in Case 044, the steam saturation in the steam zone from the ISCOM calculation decreases with distance. This steam saturation decline is observed in all of the simulation cases run, and will not be discussed further. The same is true of the accumulation of hot water and high water saturation at the steam front. The water saturation in the water zone is higher, resulting in a higher oil production rate.

The third case displayed is Case 119. In this case, as before, the reservoir is horizontal and the formation compressibility is zero; but the oil viscosity was increased to 1000 cp. The oil production rate comparison for Case 119 is shown in Figure 4.11. The match of water breakthrough time is good, as is the match of oil production rate before water breakthrough. The oil production rate increases with time up to water breakthrough. This increase is caused by pressure changes in the system. At early time, the pressure in the steam zone is high because viscous oil occupies most of the reservoir. As time passes, the water zone displaces some of the oil, and the system pressure decreases because the water is more mobile than the oil. This lower pressure results in a corresponding increase in the volume of the steam zone and an increase in the oil production rate. In the SAM, the oil production rate immediately after water breakthrough is too high. This is because the water saturation in the water zone increases too fast in the SAM. This error is corrected at later time when the oil rate is too low. The reason for the gentle oscillations in the ISCOM oil rate after water breakthrough is unknown.

The water production rate comparison for Case 119 is shown in Figure 4.12. The match for water breakthrough time is good, and the same differences that were evident in the graph of oil production rate are seen in the graph of water production rate. The error in water zone water saturation after water breakthrough causes the difference.

The variable distribution graph for Case 119 at one year is shown in Figure 4.13. A good match was obtained for all variables. The steam zone steam saturation is too low near the injection well, but too high at the steam front. However, the average

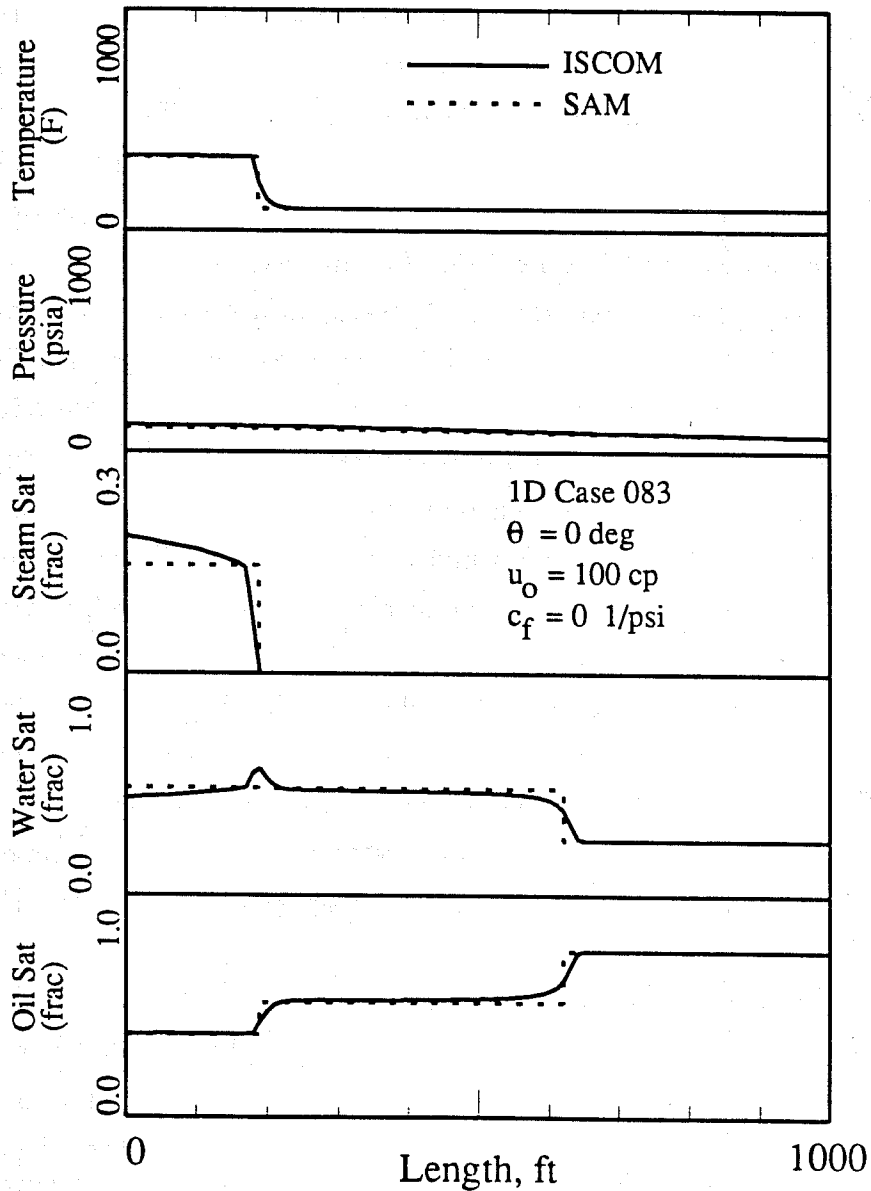


Figure 4.10: Variable Distributions at 2 years, Case 083

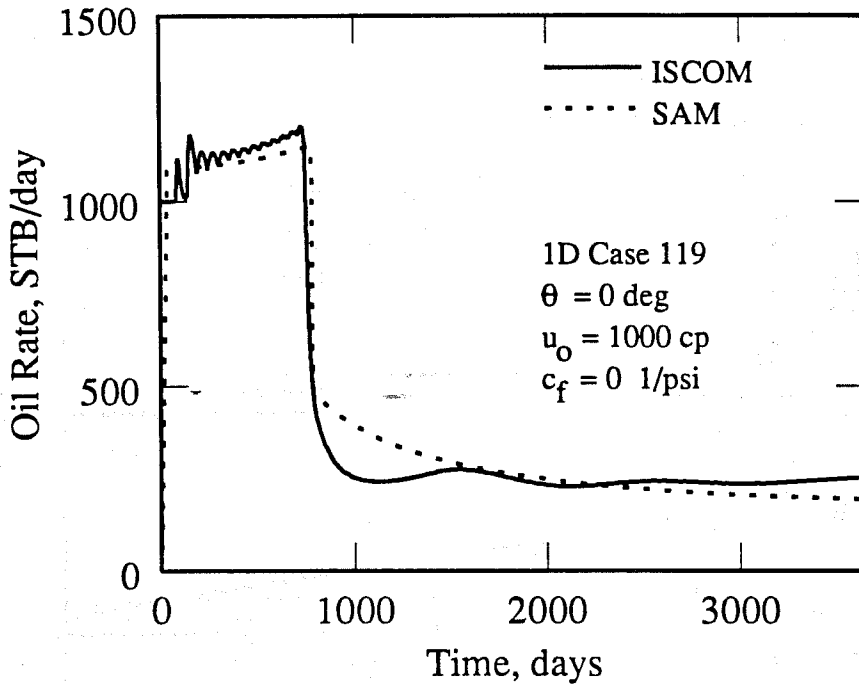


Figure 4.11: Oil Rate vs Time, Case 119

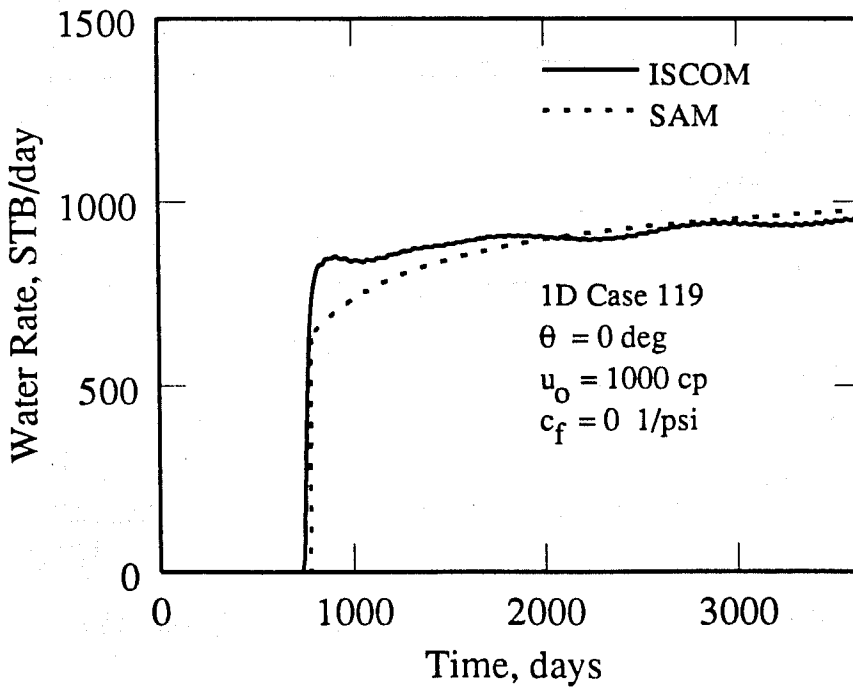


Figure 4.12: Water Rate vs Time, Case 119

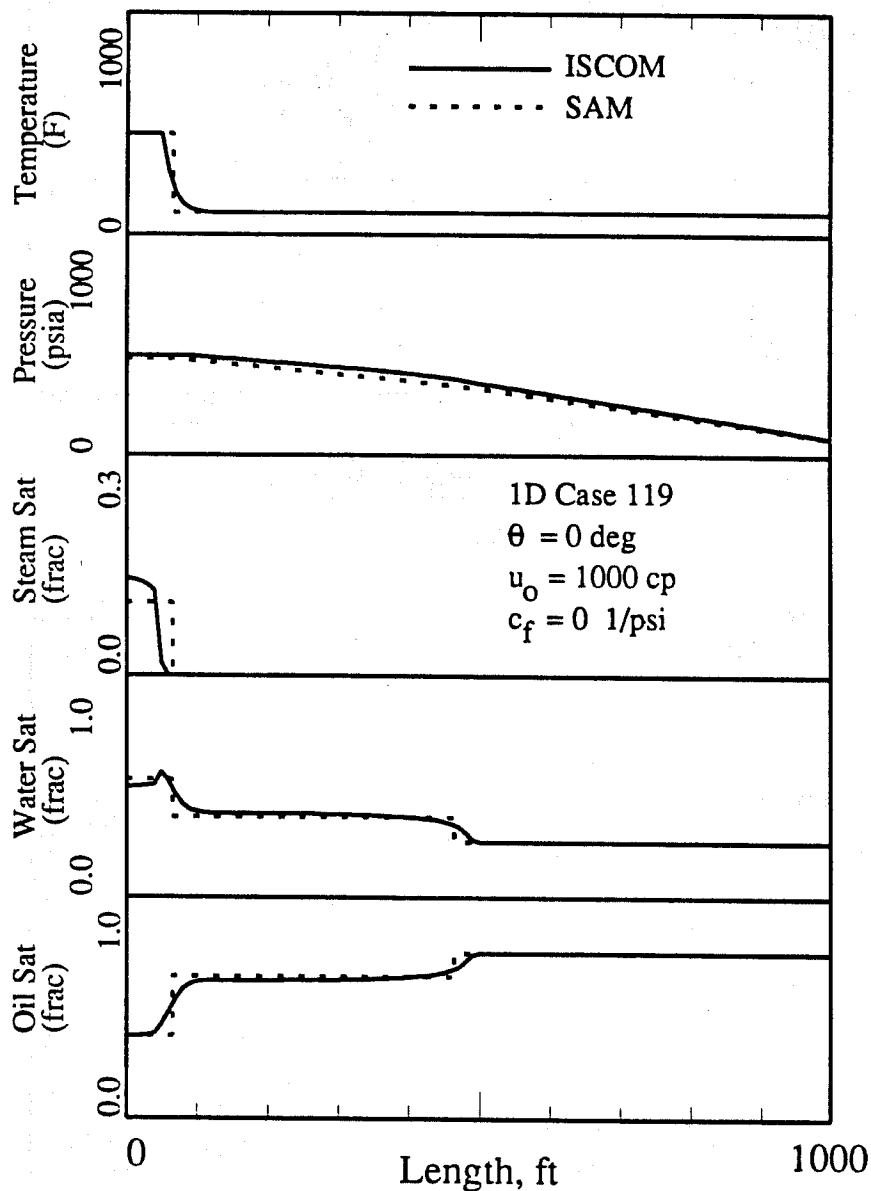


Figure 4.13: Variable Distributions at 1 year, Case 119

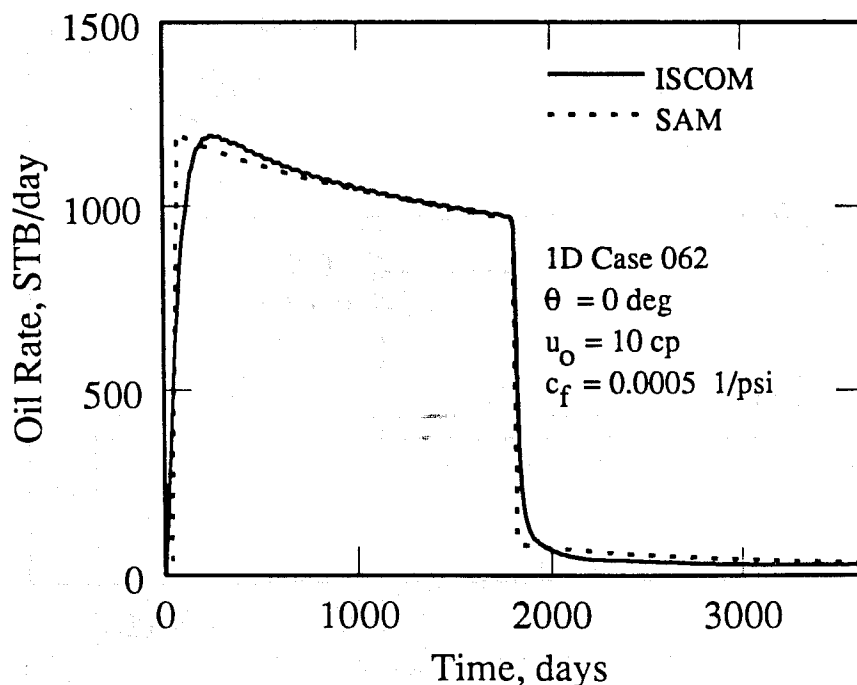


Figure 4.14: Oil Rate vs Time, Case 062

steam zone steam saturation used by the SAM appears to give the correct steam zone volume, because the areas beneath the two curves are equal. The graph of oil saturation shows that only a small portion of the high viscosity oil was displaced by the water zone. Therefore, the steam zone displaces a large amount of oil.

The next three cases are the same as the previous three cases except for the formation compressibility. The previous cases had zero formation compressibility, while the next three cases have a value of 0.0005 1/psi. This is much higher than normal formation compressibility values. It was used so that the model could be tested under an extreme condition in order to amplify and evaluate formation compressibility effects. Furthermore, a high compressibility is sometimes used to simulate the presence of an initial trapped gas saturation, using the “spongy rock” concept.

The fourth case displayed is Case 062. In this case, the reservoir is horizontal and the formation compressibility is 0.0005 1/psi and the oil viscosity is 10 cp. The oil production rate comparison for this case is shown in Figure 4.14. Good agreement was obtained at most points. However, at early time there is some difference. The

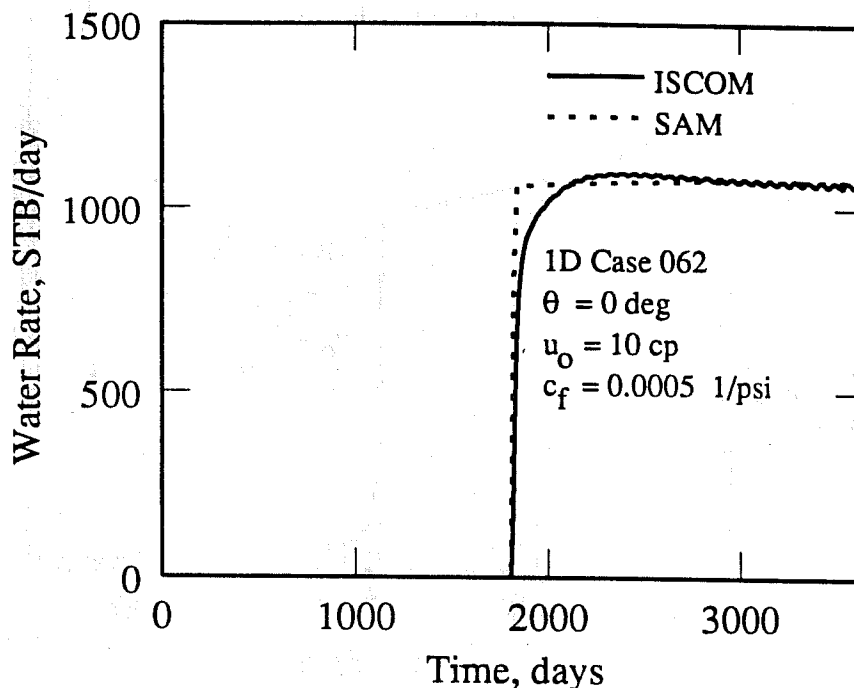


Figure 4.15: Water Rate vs Time, Case 062

difference is small in Case 062, but is more noticeable for Cases 101 and 137 which have higher viscosity oils. The differences are caused by the way that pressures are calculated in the SAM compared to the simulator. The simulator is able to calculate a pressure transient, so the presence of the injection well is not immediately observed at the production well. Of course, the injection well would be felt immediately if the system were incompressible. The SAM, on the other hand, uses a series of Darcy's law calculations to compute pressure drops, causing the injection well to have an immediate effect at the production well. The SAM considers formation compressibility in terms of a pore volume adjustment, but no attempt was made to employ a transient solution. The water breakthrough time and the oil production rate after water breakthrough match well, because by this time the transients have died.

The water production rate graph for Case 062 is shown in Figure 4.15. The water breakthrough time matches well, as does the water production rate. The difference in the water production rates is similar to that seen for Case 044. The difference is caused by the different methods used to calculate the water saturation profile.

The variable distribution graph for Case 062 at four years is shown in Figure 4.16. Good agreement is observed. The steam front is advanced too far but the steam zone volume matches well. The match of saturations in the water zone is almost perfect, and the residual oil saturation difference is barely noticeable on this graph. Temperature and pressure profiles also match well. Comparison of this figure with Figure 4.7 from Case 044 shows the influence of formation compressibility. Case 044 and 062 are identical except for the difference in formation compressibility. The high formation compressibility of Case 062 is reflected in the less advanced water front. The pressure increase in the system causes an increase in porosity, and therefore pore volume, for the compressible system. The increased pore volume results in more fluid required to sweep the system, so the water front is less advanced.

The fifth case displayed is Case 101. In this case, the reservoir is horizontal and the formation compressibility is 0.0005 1/psi and the oil viscosity is 100 cp. The oil production rate graph for Case 101 is shown in Figure 4.17. The transient effects at early time discussed in the previous case are also seen here. The oil rate from the SAM is too high up to the time of water breakthrough. The difference is caused by an error in the water saturation in the water zone. The water saturation calculated by the SAM is too high, resulting in a higher oil production rate. The water breakthrough time matches well, as does the oil production rate after water breakthrough.

The water production rate graph for Case 101 is shown in Figure 4.18. Good agreement is obtained. The water breakthrough time matches well. The water production rate calculated by the SAM immediately after water breakthrough is initially too low and then later too high, just as in Case 083 (Figure 4.9). The difference is caused by the changing water saturation in the water zone after water breakthrough. Immediately after water breakthrough, the saturation is changing too rapidly, and at late time it is changing too slowly.

The variable distribution graph for Case 101 at two years is shown in Figure 4.19. Good matches were obtained for most variables. The volume of the steam zone calculated by the SAM is too low, and the water zone water saturation is too high. This results in the higher oil production rate seen in Figure 4.18. The locations of the water front and steam front match well, as do the temperature and pressure

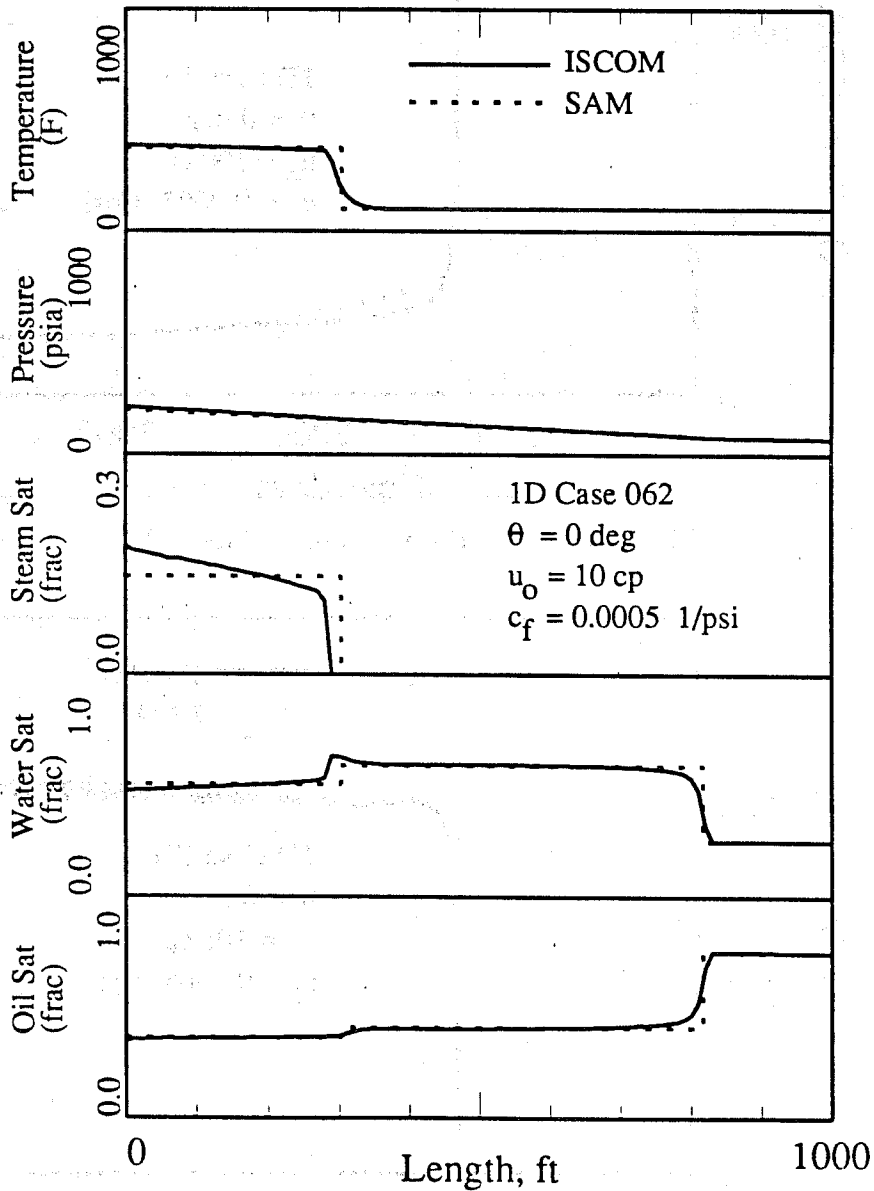


Figure 4.16: Variable Distributions at 4 years, Case 062

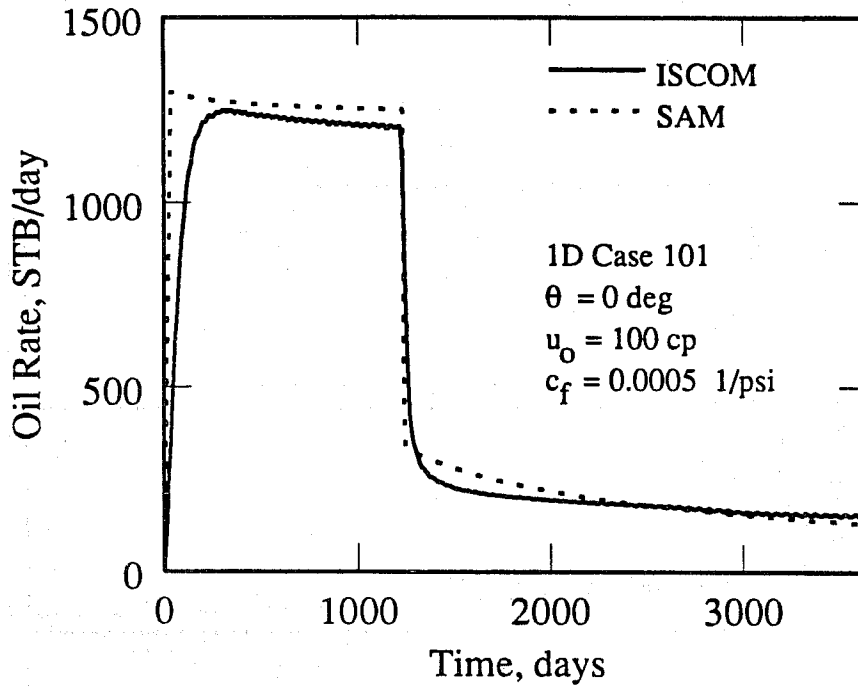


Figure 4.17: Oil Rate vs Time, Case 101

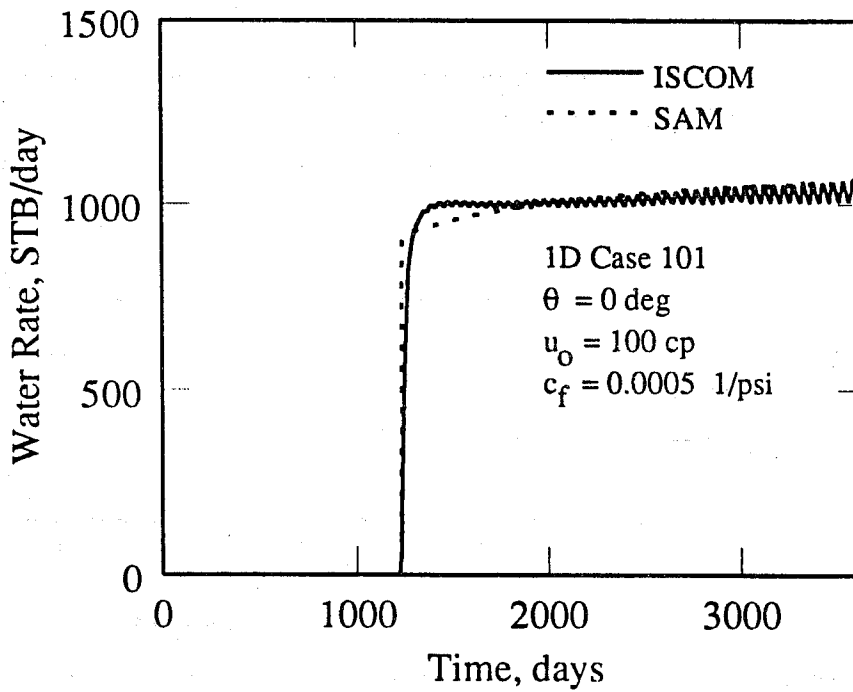


Figure 4.18: Water Rate vs Time, Case 101

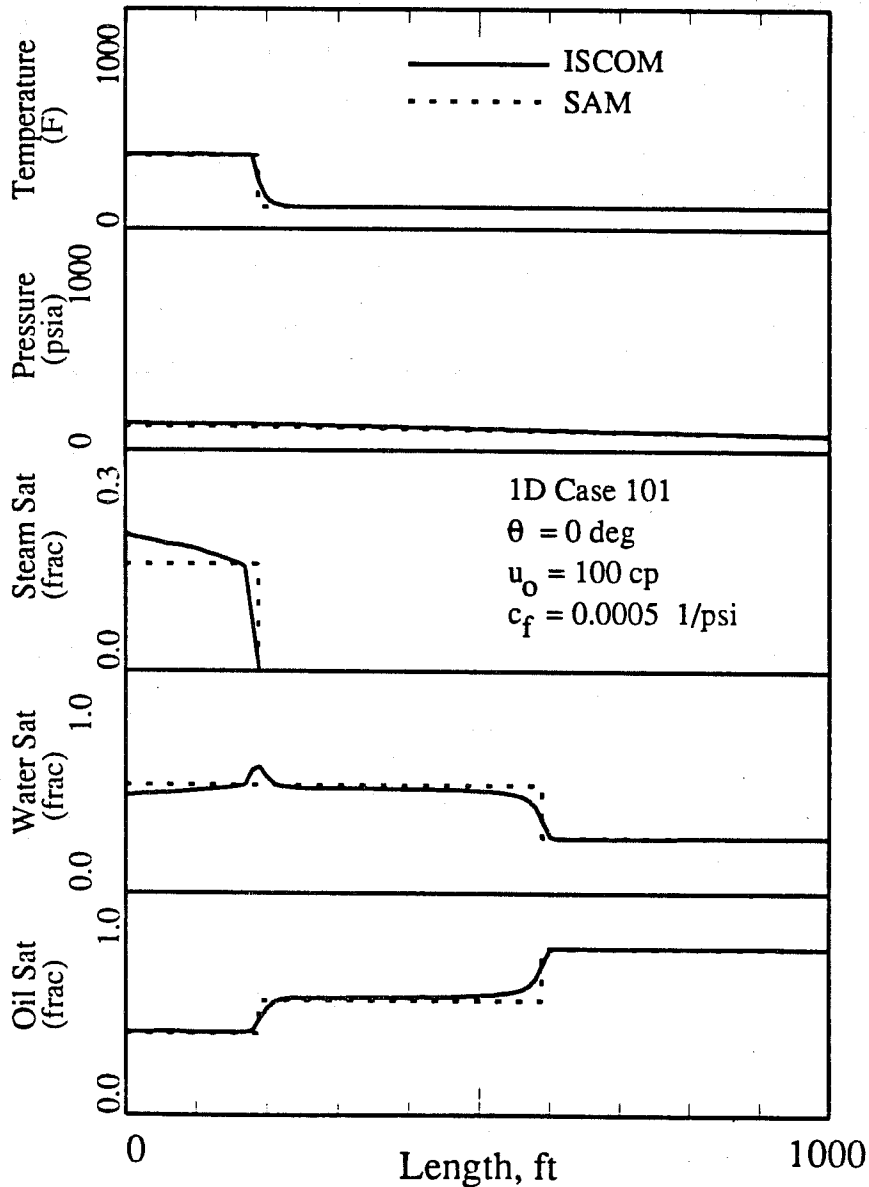


Figure 4.19: Variable Distributions at 2 years, Case 101

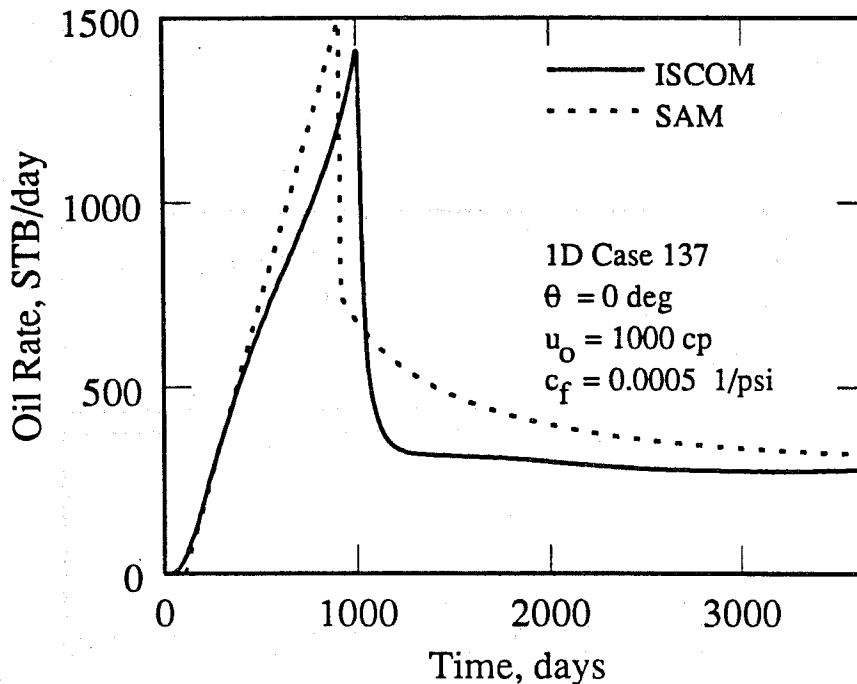


Figure 4.20: Oil Rate vs Time, Case 137

distributions.

The sixth case displayed is Case 137. In this case, the reservoir is horizontal, the formation compressibility is 0.0005 1/psi, and oil viscosity is 1000 cp. Comparison of the oil production rates calculated for Case 137 is shown in Figure 4.20. The quality of the agreement is not as good in this case as in other cases presented. The high pressure drops and the high formation compressibility give rise to large changes in the pore volume of the reservoir. Transient effects are much more pronounced and the SAM does not handle them as well as the thermal simulator. The increasing oil production rate up to the time of water breakthrough is caused by pressure decreases in the system, just as in Case 119 (Figure 4.11). The higher oil rate calculated by the SAM after water breakthrough is caused by differences in the reservoir pore volume caused by pressure errors.

Comparison of the water production rates for Case 137 is shown in Figure 4.21. Just as in the oil production rates, there are differences in the curves. The error in water breakthrough time is caused by differences in pore volume and to pressure

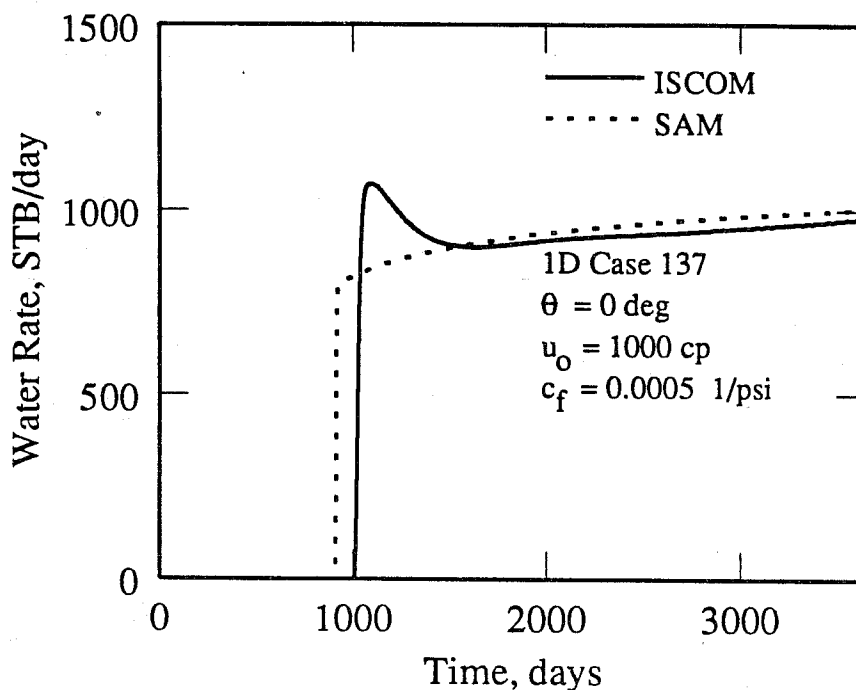


Figure 4.21: Water Rate vs Time, Case 137

effects, as discussed in the previous paragraph. The hump in the simulator water rate shortly after water breakthrough is caused by the rapidly changing system pressure. The pressure decrease after breakthrough results in a pore volume decrease, and as a result water is forced out of the system at a high rate.

The variable distribution graph for Case 137 at one year is shown in Figure 4.22. There is some difference in the pressure curves. The higher system pressure of the SAM results in a lower steam zone volume. The water zone and steam zone water saturations of the SAM are both too high, resulting in a higher oil production rate.

The next four cases are for dipping reservoirs. The angle of dip is 60 degrees. In Cases 224, 263, and 299, steam is injected in the updip portion of the reservoir and fluids are produced downdip. The gravity effects cause the steam to remain closer to the injection well than for the horizontal reservoir cases. Case 263d is for downdip steam injection. This case is identical to Case 263 except that the formation is dipping in the opposite direction.

The seventh case displayed is Case 224. In this case, the reservoir is dipping at

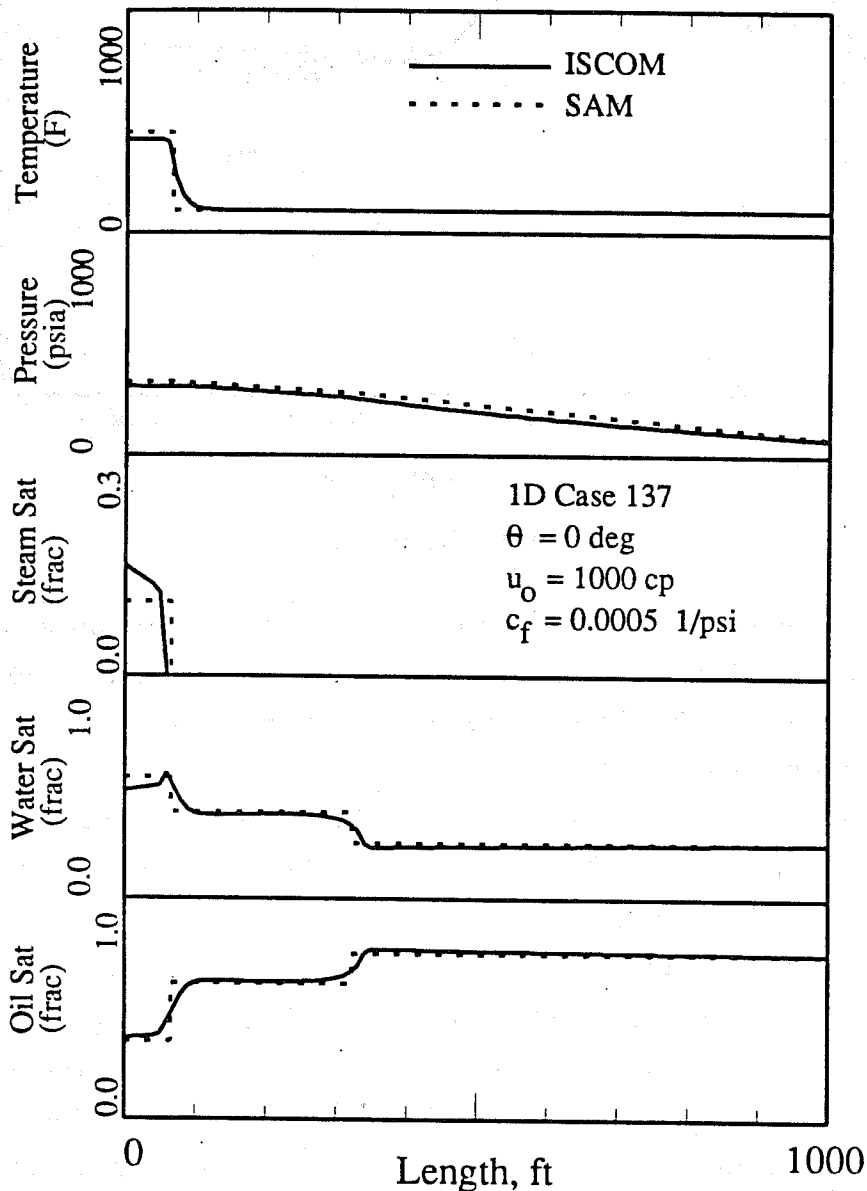


Figure 4.22: Variable Distributions at 1 year, Case 137

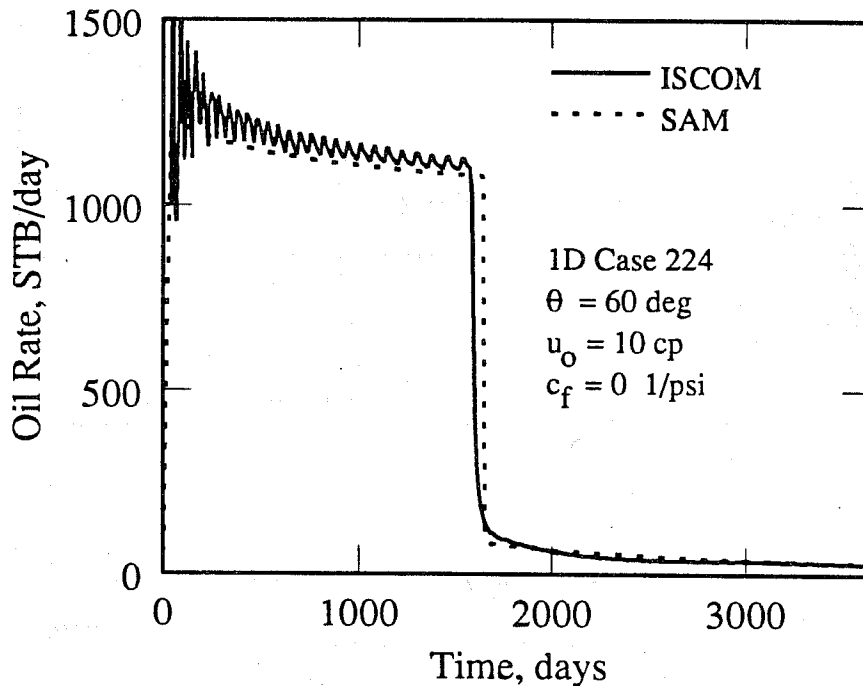


Figure 4.23: Oil Rate vs Time, Case 224

60 degrees, the formation compressibility is zero, and oil viscosity is 10 cp. The oil production rate comparison for Case 224 is shown in Figure 4.23. There is good agreement between the numerical results and the SAM results. The oil production rate before water breakthrough is too low. This difference is caused by a steam zone steam saturation that is too low. Therefore, the steam zone volume is too small, resulting in a lower oil production rate. As a result, the time to water breakthrough is too long.

The water production rate comparison for Case 224 is shown in Figure 4.24. The delay in water breakthrough is caused by the lower steam zone volume, as explained above. The water production rate after water breakthrough is too low. This is also caused by a lower steam zone steam saturation, resulting in more water required to fill the system and less water available to be produced.

The variable distribution graph for Case 224 is shown at four years in Figure 4.25. The steam zone steam saturation is too low, resulting in the lower steam zone volume mentioned earlier. This error also results in a less advanced water front, causing

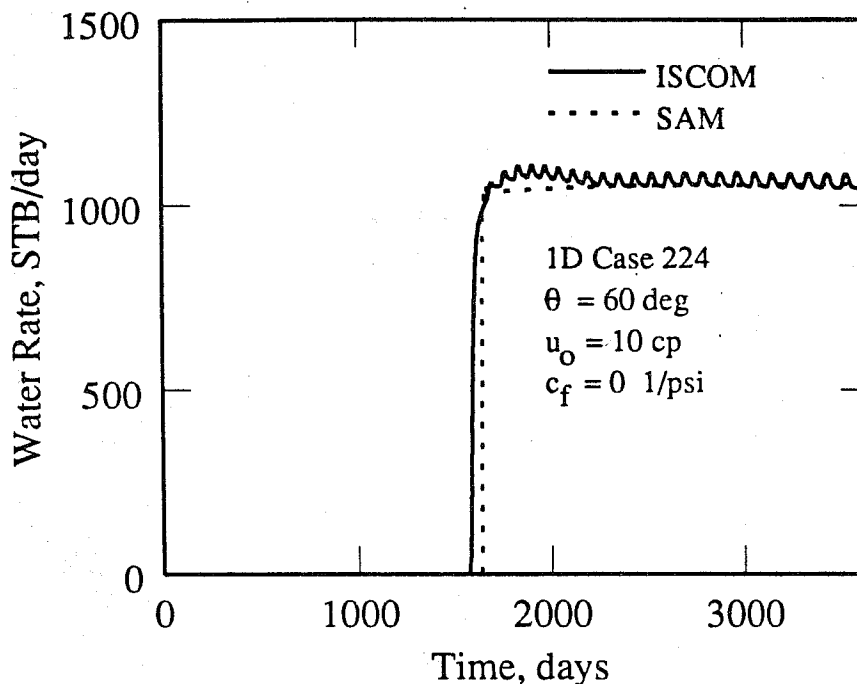


Figure 4.24: Water Rate vs Time, Case 224

a delay in water breakthrough time and a lower oil production rate, as mentioned already.

The eighth case displayed is Case 263. In this case, the reservoir is dipping at 60 degrees, the formation compressibility is zero, and oil viscosity is 100 cp. The oil production rate comparison for Case 263 is shown in Figure 4.26. There is good agreement between the numerical results and the SAM results. The oil production rate for the SAM both before and after water breakthrough is too high, and water breakthrough is too early. The early water breakthrough, like the high oil rate, is caused by a steam zone volume that is too large. The early water breakthrough explains the higher oil rate before breakthrough.

The water production rate graph for Case 263 is shown in Figure 4.27. The earlier water breakthrough is caused by the higher steam zone volume as discussed above. The higher water production rate after water breakthrough is also caused by the higher rate of steam zone growth.

The variable distribution graph for Case 263 at two years is shown in Figure 4.28.

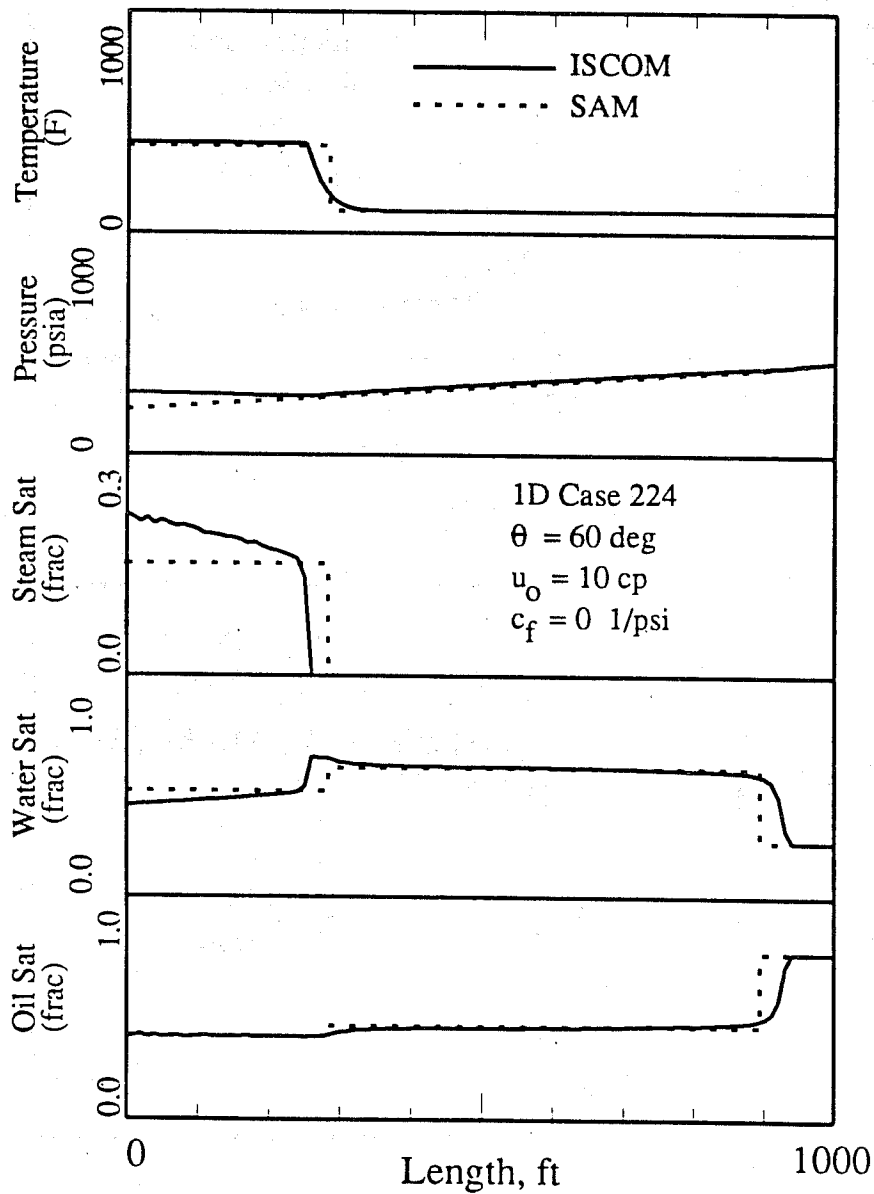


Figure 4.25: Variable Distributions at 4 years, Case 224

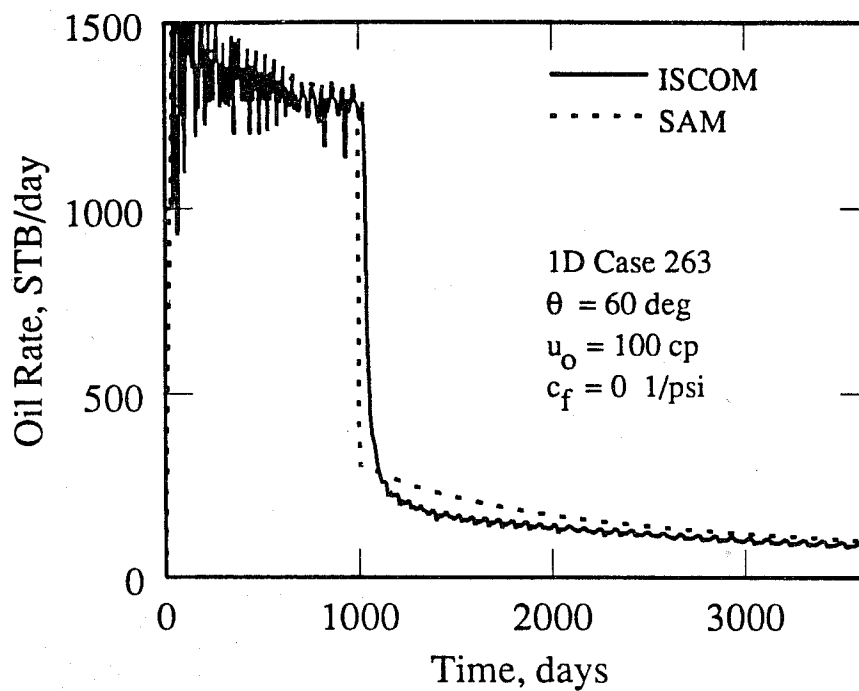


Figure 4.26: Oil Rate vs Time, Case 263

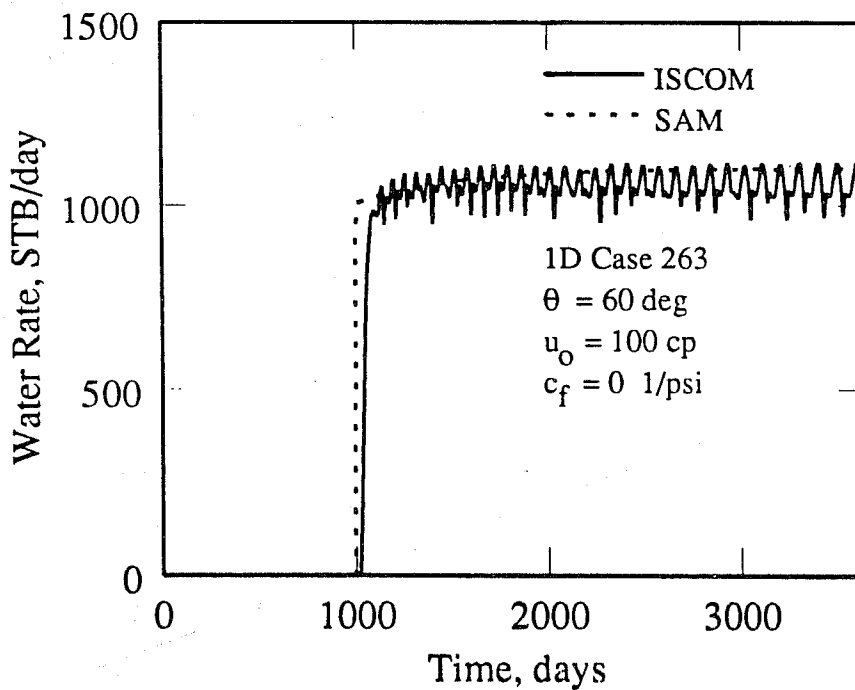


Figure 4.27: Water Rate vs Time, Case 263

Good agreement is observed for most variables. The calculated steam front using the SAM is too far advanced, causing a similar advance in the water front. This difference is partially due to the lower steam zone pressure in the SAM. This error results in higher oil and water production rates. The saturation profiles match well. Comparison of Figure 4.28 with Figure 4.10 from Case 083 illustrates the effect of a dipping reservoir. The most obvious difference is the steam zone steam saturation. The value is much higher for the dipping case. The increased steam saturation is caused by the effect of gravity on the steam displacement. The steam is less dense than the oil and water so it tends to rise to the top of the reservoir, which for updip steam injection is near the injection well. Since the volume of the steam zone is larger because of its lower pressure, the water front propagates farther for the dipping case, giving earlier water breakthrough.

The ninth case displayed is Case 263d. In this case, the reservoir is dipping at 60 degrees, but steam is injected at the downdip well. The formation compressibility is zero and the oil viscosity is 100 cp. This case is the same as Case 263 except that the reservoir dips in the opposite direction. The oil production rate comparison for Case 263 is shown in Figure 4.29. There is good agreement in the water breakthrough time. The oil production rate is too low before water breakthrough, and too high after water breakthrough. The difference is caused by a water zone water saturation that is too low, causing less oil to be displaced and a lower oil production rate. After breakthrough, there is more oil left in the reservoir, resulting in a higher oil production rate. Comparison with Figure 4.26 from Case 263 shows the effect of steam injector location on oil production rate. With updip steam injection, water breakthrough time is earlier and the oil production rate before water breakthrough is higher.

The water production rate comparison for Case 263d is shown in Figure 4.30. The water breakthrough time matches well. The water production rate is too low after water breakthrough. As explained above, the water zone saturation is too low. Comparison with Figure 4.27 from Case 263 shows that with updip steam injection, water breakthrough time is earlier and water production rates are higher than with downdip steam injection.

The variable distribution graph for Case 263d at two years is shown in Figure 4.31.

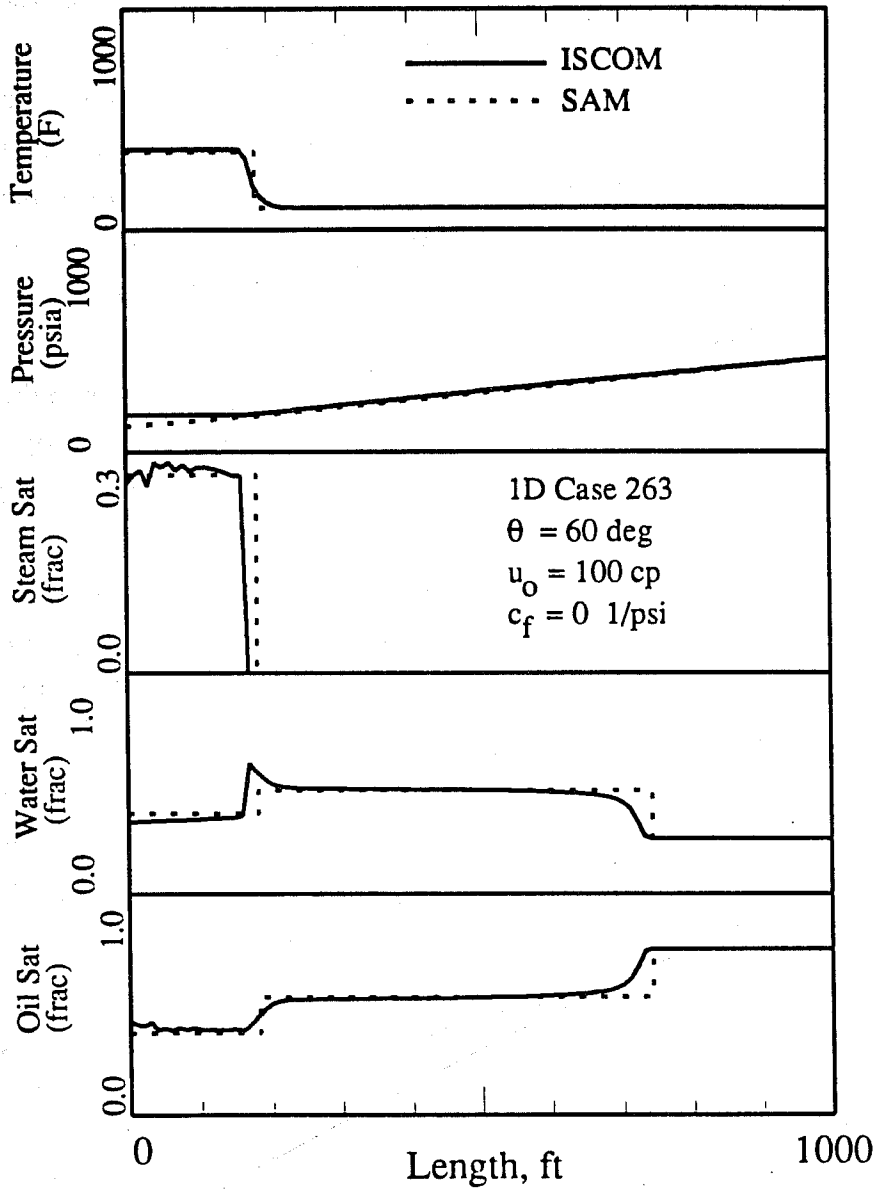


Figure 4.28: Variable Distributions at 2 years, Case 263

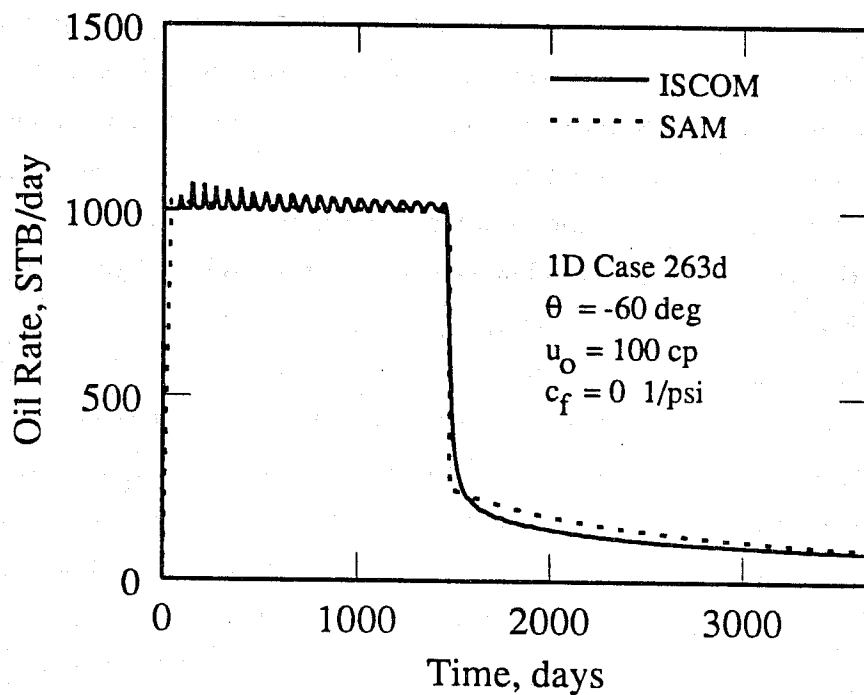


Figure 4.29: Oil Rate vs Time, Case 263d

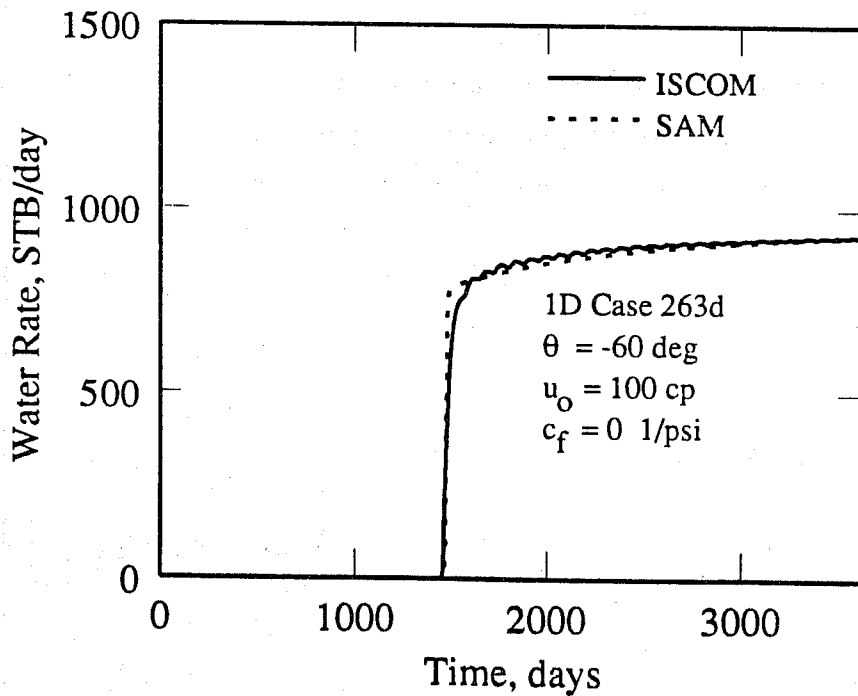


Figure 4.30: Water Rate vs Time, Case 263d

Good agreement is observed for most variables. The steam front is more advanced. The water front location matches well, as do temperature, pressure, and saturation profiles. The steam zone steam saturation in this case is only a few percent. When steam is injected downdip, the fractional flow calculation gives a lower steam saturation and smaller steam zone volume than for updip injection, as is seen in the results. As a result, the water front is less advanced than in the updip steam injection case.

The tenth case displayed is Case 299. In this case, the reservoir is dipping at 60 degree, the formation compressibility is zero, and oil viscosity is 1000 cp. This case is the same as Cases 224 and 263 except for the increased viscosity of the oil. The oil production rate comparison for Case 299 is shown in Figure 4.32. There is good agreement in the water breakthrough time. The oil production rate is too low before water breakthrough, and too high after water breakthrough. These differences are caused by a water zone water saturation that is too low, causing less oil to be displaced and a lower oil production rate. After breakthrough, since there is more oil left in the reservoir, the oil production rate is higher.

The water production rate comparison for Case 299 is shown in Figure 4.33. The water breakthrough time matches well. The water production rate is too low after water breakthrough, but is too high at late time, as in Case 119 and 137. The error, as in the other cases, is caused by a difference in the water zone water saturation.

The variable distribution graph for Case 299 at one year is shown in Figure 4.34. Good agreement is observed for most variables. The steam zone volume is too large, and the water zone water saturation is low compared to the simulator results. Front locations exhibit good matches.

4.3 Concluding Remarks

Comparing the results of the 360 one-dimensional cases showed that the SAM does a good job in reproducing the results of the thermal simulator. This is to be expected because the fundamental equations are the same. The equations are solved differently, but results are consistent. The SAM uses one-dimensional analytical work in an

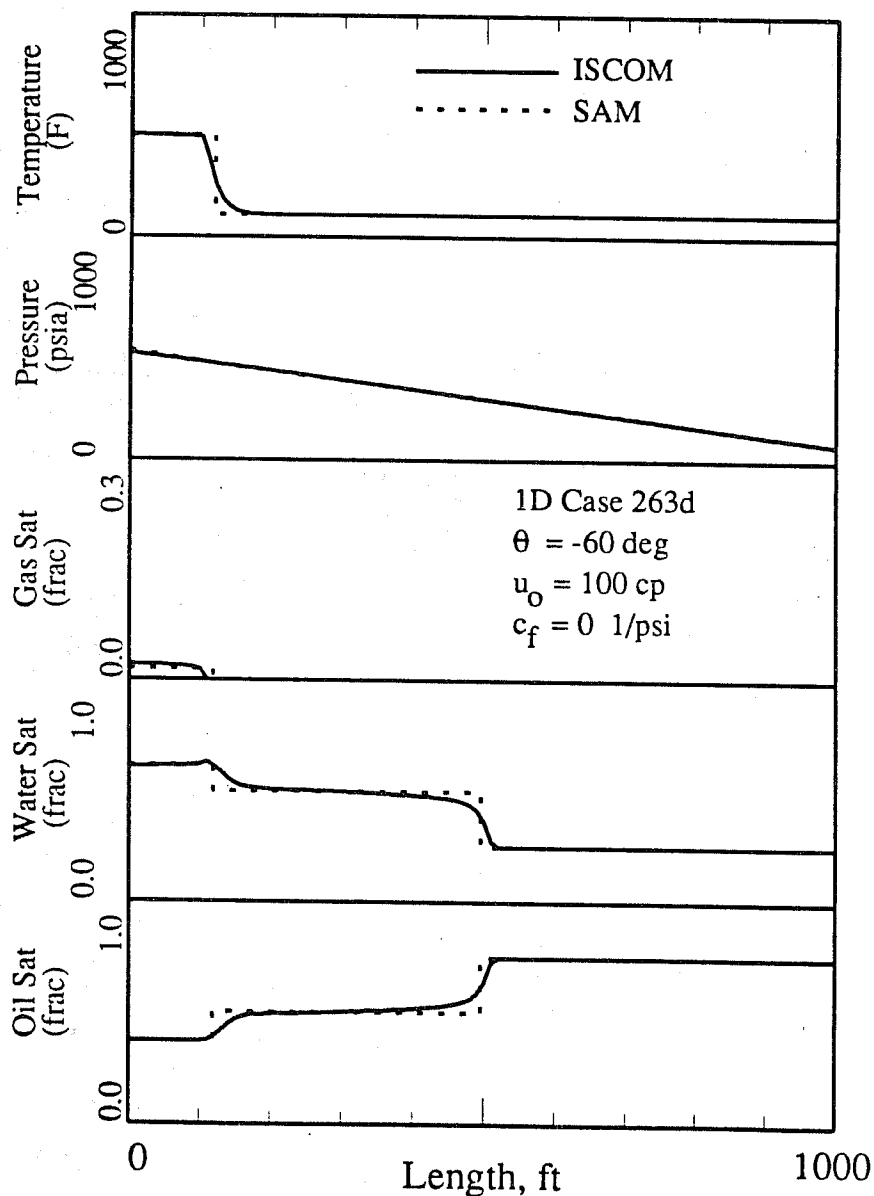


Figure 4.31: Variable Distributions at 2 years, Case 263d

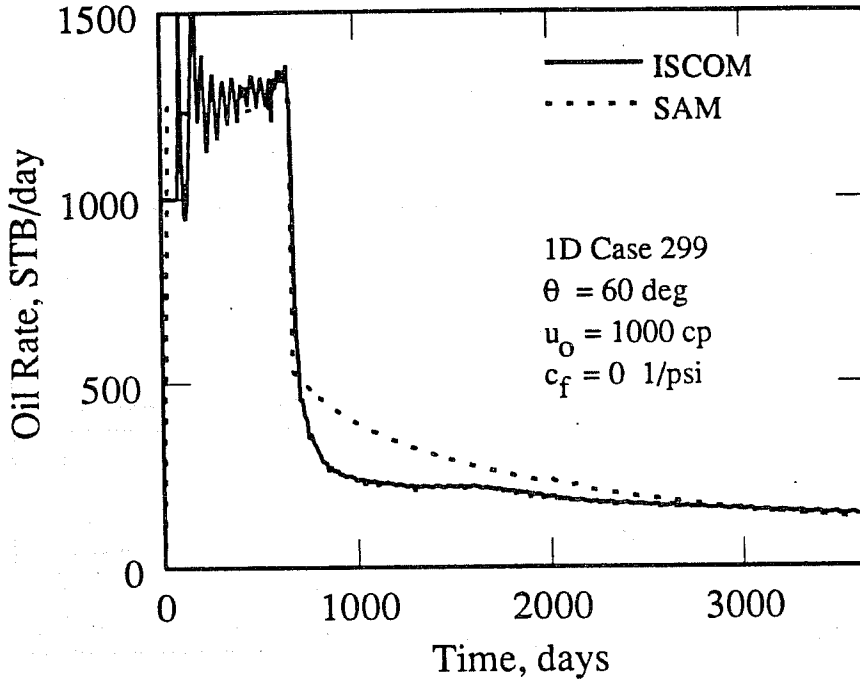


Figure 4.32: Oil Rate vs Time, Case 299

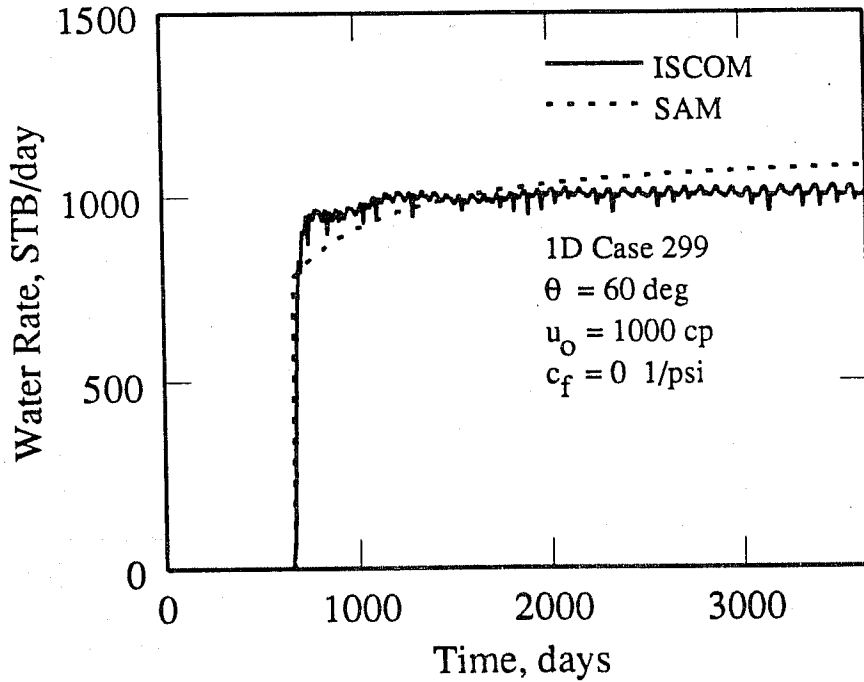


Figure 4.33: Water Rate vs Time, Case 299

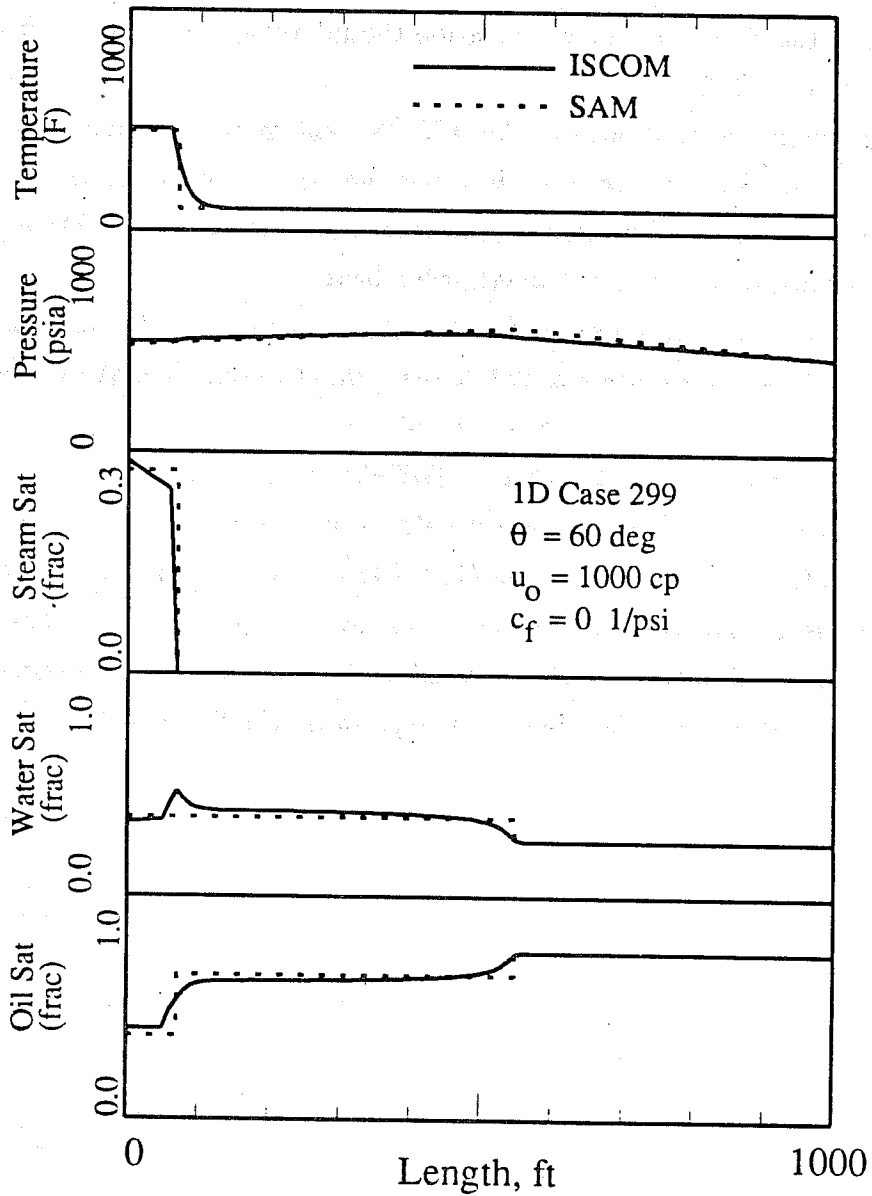


Figure 4.34: Variable Distributions at 1 year, Case 299

iterative method to obtain the solution, while the thermal simulator used a finite-difference numerical method.

A few general trends were seen when comparing the SAM and ISCOM results. Steam front locations were slightly advanced in the SAM compared to ISCOM. The method used for calculating the location of the steam front gave an upper bound for this location, so the SAM steam front location should always be slightly ahead of the location predicted by ISCOM.

The steam zone steam saturation for ISCOM was generally higher than in the SAM, but, since the SAM steam front was more advanced, the volumes of the steam zones are about the same. The steam zone steam saturation in ISCOM was always decreasing with distance because of overburden heat losses.

The water production rate graphs for the SAM show a sharp breakthrough while the ISCOM graphs show a more gradual increase due to numerical dispersion. Water production calculated by the SAM was generally low immediately after water breakthrough but then higher than ISCOM at late times. High oil viscosities gave low water sweep efficiencies and early water breakthrough for both models.

The amplitude of the oscillations seen in ISCOM was higher for high viscosity oils because the pressure changes affect the rate more for high viscosity oils. These are the major trends observed in the one-dimensional SAM. Since the one-dimensional SAM results appeared valid, work then began on expanding the SAM to two dimensions.

Chapter 5

Two-Dimensional Model

The one-dimensional semianalytical model (SAM) closely matched the thermal simulator ISCOM. The next step was to develop a two-dimensional cross-sectional model. This chapter presents the modifications required to convert the one-dimensional model to two dimensions. First, the two-dimensional system is described, and the zones and fronts are defined for the two-dimensional system. Sections are included which deal with the shape of the steam front, how the hot water zone is considered, and how the water front location is calculated. A section comparing different viscous to gravity force ratios and a section explaining the modifications to the pressure drop calculations complete the chapter.

The differences between the one-dimensional and two-dimensional models are greatest for a horizontal system. As the dip of the system increases, the solutions become similar. At the limit, a vertical system would give the same results for either case because all fronts would be normal to the flow direction in the reservoir.

Solving the steam drive problem in two dimensions is more difficult than the one dimensional problem. The two-dimensional system considers gravity override of the steam, resulting in a non-vertical steam front shape. Furthermore, there is a hot water zone of significant size and it must be included. Many of the two-dimensional calculations are the same as the corresponding one-dimensional calculations. All calculation methods are identical except for the ones discussed in this chapter.

The two-dimensional model that is discussed in this chapter is based on either the

assumption of a horizontal reservoir or a reservoir in which steam is injected updip. The model does not consider downdip steam injection because the methods used to determine the shape of the steam front and the location of the water front would not work for updip steam injection.

5.1 Definition of Two-Dimensional

The two-dimensional system considered in this work is an x - z cross-section of the reservoir in Cartesian coordinates. In both horizontal and dipping systems, the x -direction is defined as the direction parallel to the bedding plane of the reservoir, and the z -direction is perpendicular to the bedding plane. The system is two-dimensional in the sense that all variables that are a function of position are a function of x and z only. All calculations are made on a "per unit width" basis so the y -direction does not come into play, and the model is truly two-dimensional. Consider a line in the y -direction that intersects the reservoir at right angles. The pressures, temperatures, and saturations on this line are uniform.

Wells parallel to the z -direction penetrate the reservoir at each end. One of these wells is a steam injection well, the other is a production well. Treatment of wells in two-dimensions is similar to treatment of wells in one dimension, as discussed in Section 3.1.

5.2 Zone Definitions

Figure 5.1 shows the zones used in the two-dimensional model. The steam zone has a different shape than in one dimension. In one dimension, the steam zone shape was normal to the flow direction in the reservoir. In two dimensions, the steam rises to the top of the reservoir and gravity override occurs. The finite-difference grid used in the thermal simulator causes the steam front to have a "stairstep" shape. Just as in the one-dimensional system, the temperature of the steam zone is high and all three phases are mobile. The water zone from the one-dimensional system is called the cold water zone in two dimensions. This is to distinguish it from the hot water

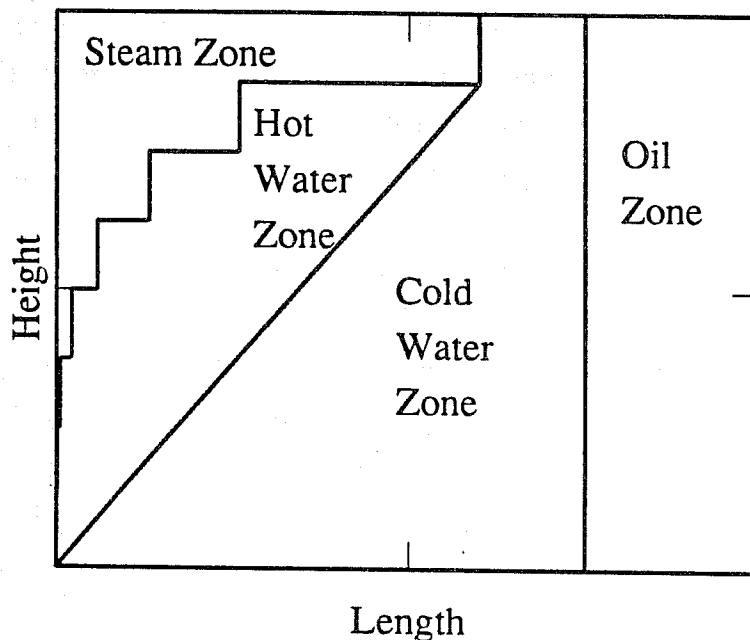


Figure 5.1: Two-Dimensional Zone Definition

zone. The hot water zone could be ignored in the one-dimensional system because it was so small, but it must be considered in two dimensions. Although a temperature gradient exists in the water zone, a good approximation to the shape of the hot water front is to use a straight line to connect the end of the steam zone at the top of the reservoir to the injection well at the bottom of the reservoir. The temperature used for calculation purposes in the hot water zone is the arithmetic average of the steam zone temperature and the initial formation temperature. The temperature in the cold water zone is the initial formation temperature. In both water zones, both the oil and water phases are mobile. The oil zone, as in the one-dimensional system, is at initial reservoir conditions.

5.3 Steam Zone Size and Shape

Several models for defining the shape of the steam front were discussed in the literature survey. Analytical models require an assumption about the shape of the steam

zone. All of the methods discussed in the literature survey have problems of one kind or another. No reasonable analytical solution was found for the two-dimensional problem. The literature search did not identify one, nor were personal efforts successful in generating one. Since a rigorous analytical solution is not available, empirical methods were investigated for determining the shape of the steam front in two dimensions.

A simple equation was needed that would describe the shape of the steam front accurately. The equation must produce both concave upwards and concave downwards steam front shapes, depending on the variables used in the equation. The family of exponential equations where the independent variable ranges from zero to one will give these required shapes, depending on the value of the exponent used in the equation. The equation

$$z_D = (x_D)^n \quad (5.1)$$

with

$$z_D = \frac{z}{H} \quad 0 \leq z \leq H \quad (5.2)$$

$$x_D = \frac{x}{L_{st}} \quad 0 \leq x \leq L_{st} \quad (5.3)$$

was selected because, depending on the value of the exponent, n , a wide variety of physically reasonable steam front shapes can be represented. If the value of the exponent is greater than one, a curve that is concave upward will result. This would resemble the shape of a steam front in which viscous effects are dominant. On the other hand, if the value of the exponent is less than one, the generated curve will be concave downward, resembling the shape of a front where gravity forces are dominant.

It appears that the value of the exponent should depend on the ratio of the viscous forces to the gravity forces. A viscous to gravity force ratio was derived by calculating the velocities, v_x and v_z , of a particle in the steam zone in the x and z directions. For a horizontal reservoir

$$v_x = \frac{k_x k_{rg} \Delta p}{\mu_g L} \quad (5.4)$$

A datum is defined at $H=0$ and the pressure at this datum is p_{datum} . For the oil phase

$$p_o - p_{datum} = -\rho_o \frac{g}{g_c} H \quad (5.5)$$

For the gas phase

$$p_g - p_{datum} = -\rho_g \frac{g}{g_c} H \quad (5.6)$$

Subtracting the two previous equations gives

$$p_o - p_g = \Delta p = -\Delta\rho \frac{g}{g_c} H \quad (5.7)$$

where

$$\Delta\rho = \rho_o - \rho_g \quad (5.8)$$

Furthermore, for the gas phase,

$$v_z = \frac{k_z k_{rg} \Delta p}{\mu_g H} \quad (5.9)$$

Substituting Eq. 5.7 gives

$$v_z = \frac{k_z k_{rg} \Delta\rho \frac{g}{g_c}}{\mu_g H} \quad (5.10)$$

Taking the ratio of the two gas velocities gives the viscous to gravity velocity ratio (VGR)

$$VGR = \frac{v_x}{v_z} = \frac{k_x \Delta p \frac{g_c}{g}}{k_z L \Delta\rho \frac{g}{g_c}} \quad (5.11)$$

The square root of this ratio is the exponent that was found to fit best in Eq. 5.1. Several functional relationships for the exponent were tried, and the results were compared to the steam front shapes provided by the thermal simulator. Matching the shape of the steam front is an ill-defined process. Physically, the steam front shape should be smooth. However, in a finite-difference model, the shape is more of a "stairstep" shape. Furthermore, the boundary between the steam and water zones is not well defined. Saturation gradients exist in both directions and the magnitude of the gradient varies within the reservoir. An "eyeball" fit was used to determine what function for the exponent gave the best results. The square root relationship gave the best overall match of the steam front shape, so it is used in the model. The resulting equation is

$$z_D = x_D^{\sqrt{VGR}} \quad (5.12)$$

The effect, from Eq. 5.12, of the viscous to gravity ratio on the calculated shape of the steam front is shown in Figure 5.2.

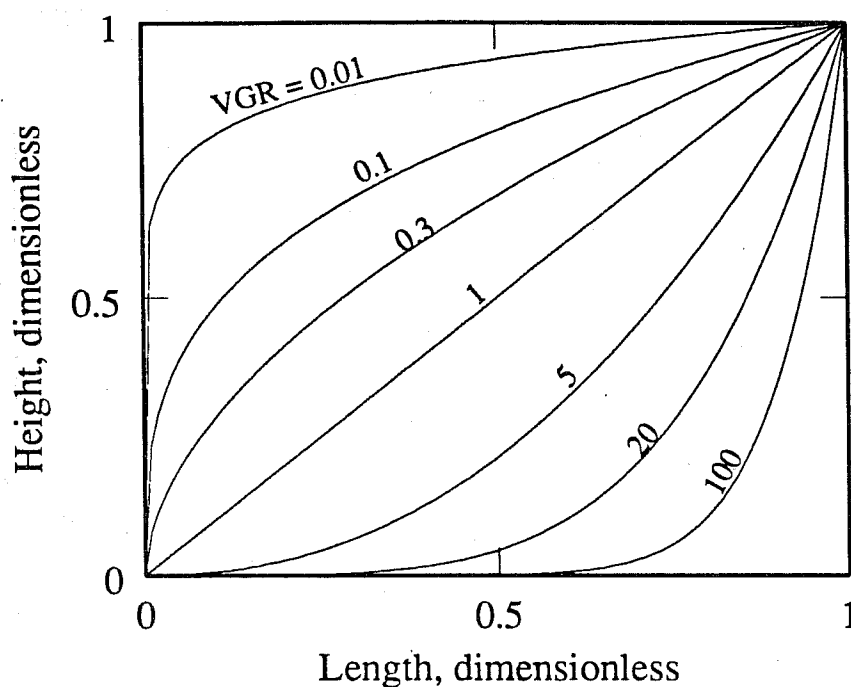


Figure 5.2: Effect of Viscous/Gravity Force Ratio on Steam Front Shape

The two-dimensional SAM uses several layers similar to the layering system in a two-dimensional simulator. To calculate the length of the steam zone in each layer, the length of the steam zone is integrated over the layer and an average steam zone length is calculated in that layer. The same process is used in each layer. This process is shown schematically in Figure 5.3 for a system with four layers.

5.4 Hot Water Zone

A hot water zone was seen in every two-dimensional case run. The high-temperature steam zone that forms near the top of the reservoir gives up heat not only to the formation above but also to the water zone directly below the steam zone, resulting in a hot water zone. The water zone beneath the steam zone moves slowly and there is an accumulation of heat directly below the steam zone. The shape of the hot water zone was fairly uniform from one case to another. The interface between the steam zone and the hot water zone is defined by the shape of the steam front. The interface

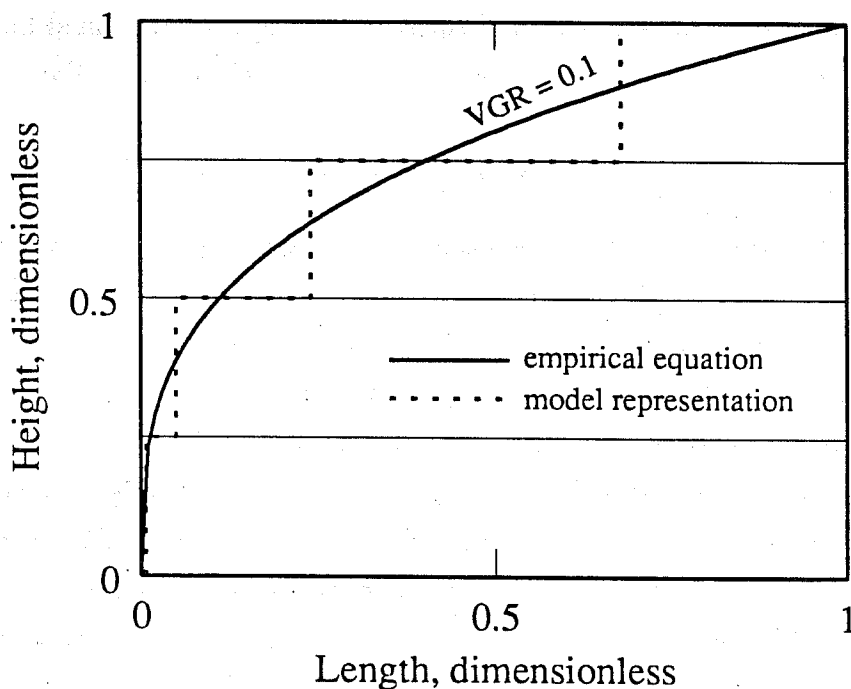


Figure 5.3: Discretization of Steam Zone for a Four Layer Case

between the cold water zone and the hot water zone was nearly linear in the simulated cases, so a straight line was used to define this boundary (see Figure 5.1).

If a line is drawn from the end of the steam zone at the top layer of the reservoir to the base of the steam zone at the bottom, the line forms a boundary between the hot and cold water zones that is reasonably close to that seen in the simulation runs. The temperature of the hot water zone is taken as the arithmetic average of the temperatures in the steam zone and cold water zone. The higher temperature of the hot water zone is reflected in the density and viscosity calculations. The hot water zone is used only to make volumetric calculations when determining production rates. Thus, it is not necessary to have a precise definition of the hot water zone.

5.5 Water Front

In the one-dimensional model presented in Chapter 3, the distance to the water front was calculated from fractional flow theory. The two-dimensional model uses a material

balance similar to the one-dimensional equation, but a new term must be included to determine the volumetric sweep efficiency at water breakthrough. The time to water breakthrough is

$$t_{bt} = \frac{\Delta S_w E_v}{PVI/day} \quad (5.13)$$

where E_v is the volumetric sweep efficiency of the water and PVI is the number of pore volumes injected. A sweep efficiency of unity would give the same answer as the one-dimensional case. Lower sweep efficiency values give earlier water breakthrough times because less of the reservoir is swept by the water. A correlation was developed to determine the water sweep efficiency at water breakthrough.

For the case of a waterflood without steam, a correlation was presented by Craig *et al.* [9] for linear uniform two-dimensional horizontal systems. This correlation was based on experiments with scaled physical two-dimensional models. The volumetric sweep efficiency at breakthrough was graphed as a function of the mobility ratio, M , and the product of two dimensionless groups. The two dimensionless groups are

$$R_1 = \frac{L}{H} \sqrt{\frac{k_z}{k_x}} \quad (5.14)$$

and

$$R_2 = \frac{q_w \mu_o}{\sqrt{k_x k_z} \Delta \rho} \quad (5.15)$$

The product of these two groups is the ratio of horizontal to vertical pressure drop, and in field units it becomes

$$\frac{\Delta p_h}{\Delta p_v} = 127,758 \frac{q_w \mu_o L}{k_x A \Delta \rho H} \quad (5.16)$$

This term will be referred to as the Craig ratio in the remainder of the dissertation.

The Craig ratio is for a horizontal system. The horizontal pressure drop divided by the vertical pressure drop can also be presented as a ratio of viscous to gravity forces. For horizontal systems, the viscous forces act in the horizontal direction (x) and the gravity forces act only in the vertical direction (z). An attempt was made to derive a more general ratio that would apply to dipping as well as horizontal systems. The viscous forces in a dipping system can be represented using Darcy's law expressed

in flow potential instead of pressure. The resulting flow equation in the x -direction is

$$q = \frac{-kA}{\mu} \left(\frac{\partial p}{\partial x} + \rho \frac{g}{g_c} \sin \theta \right) \quad (5.17)$$

after integrating

$$q = \frac{-kA}{\mu} \left(\frac{\Delta p_x}{L} + \rho \frac{g}{g_c} \sin \theta \right) \quad (5.18)$$

solving for the pressure drop in the x -direction gives

$$\Delta p_x = \left(\frac{-q\mu}{kA} - \rho \frac{g}{g_c} \sin \theta \right) L \quad (5.19)$$

The pressure drop in the z -direction is related to the fluid density. The pressure at the datum $H=0$ is defined as p_{datum} . For oil, the equation is

$$p_o - p_{datum} = -\rho_o \frac{g}{g_c} H \cos \theta \quad (5.20)$$

For water, the equation is

$$p_w - p_{datum} = -\rho_w \frac{g}{g_c} H \cos \theta \quad (5.21)$$

The tendency for fluids to segregate is related to the difference in the densities of the two fluids. The pressure drop between the two fluids is obtained by subtracting Eq. 5.15 from 5.16 and is

$$p_w - p_o = \Delta p_z = -\Delta \rho \frac{g}{g_c} H \cos \theta \quad (5.22)$$

where

$$\Delta \rho = \rho_w - \rho_o \quad (5.23)$$

Taking the ratio of the viscous to gravity forces gives

$$\frac{\Delta p_x}{\Delta p_z} = \frac{\left(\frac{q\mu}{kA} + \rho \frac{g}{g_c} \sin \theta \right) L}{\Delta \rho \frac{g}{g_c} H \cos \theta} \quad (5.24)$$

The gravity term represents the tendency for the less dense fluid to segregate upward, and the more dense fluid downward. The difference between the densities of the fluids is used to quantify this effect [21]. Rearranging and using field units, the equation becomes

$$\frac{\Delta p_x}{\Delta p_z} = \left(\frac{127,758 q \mu g_c}{k A \Delta \rho g \cos \theta} + \tan \theta \right) \frac{L}{H} \quad (5.25)$$

This group will be referred to as the modified Craig ratio (MCR) in the remainder of the dissertation. At $\theta=0$, the MCR simplifies to the Craig ratio which is for a horizontal reservoir. At $\theta=90$ degrees, the MCR becomes infinite. Infinite values give a sweep efficiency of unity, which makes physical sense for a vertical reservoir with steam injected at the top. In vertical reservoirs, the front shapes would be expected to be horizontal, that is, perpendicular to the bedding plane of the reservoir, thereby sweeping the entire reservoir at water breakthrough.

The modification of the Craig ratio for reservoir dip results in a horizontal shift in the function on the abscissa. The shift is controlled by two terms, the term with $\cos \theta$ in the denominator, and $\tan \theta$. For high Craig ratios and moderately dipping reservoirs, the $\tan \theta$ term is small in comparison with the $\cos \theta$ term, and the shift is minor and does not have much effect on the sweep efficiency determination. However, for low Craig ratios, the $\tan \theta$ term dominates, and the shift can be several log cycles, thus having a large effect on the sweep efficiency.

Extending Craig's waterflood work to steamflooding was done with the use of a heat function. The heat function, F , is defined as it was in Section 3.4, Eq. 3.10, as the ratio of latent heat to total heat injected into the reservoir. Expressed mathematically, the ratio is

$$F = \frac{1}{1 + \frac{C_w \Delta T}{f_s L_v}} \quad (5.26)$$

The ratio in the denominator of the heat function has been called the modified Jacob number [44]. The heat function has been used in other work, and in practice usually ranges from 0.3 to 0.7 [33, 54]. The temperature change and latent heat value in Eq. 5.26 are pressure dependent, so the heat function is a strong function of quality and a weak function of pressure, as shown in Figure 5.4. The temperature difference in Eq. 5.26 is based on the initial temperature of the reservoir, and a value of 100 degrees F was used to generate Figure 5.4. The steam quality at the injection well is used in Eq. 5.26. The heat function should be evaluated at the pressure in the steam zone because condensation occurs in the steam zone. A waterflood with no steam present has a heat function of zero.

Many ISCOM runs were made for the steamflood problem. Several graphs were constructed using the MCR. Graphs for five different mobility ratios are given in

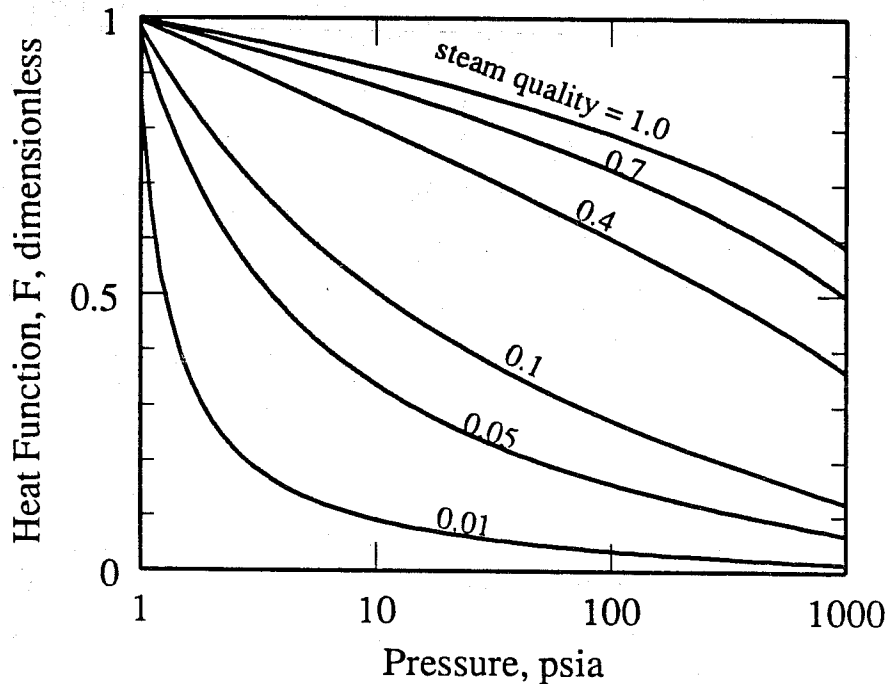


Figure 5.4: Effect of Pressure and Steam Quality on Heat Function, F

Figures 5.5-5.9. Each graph is for a specific mobility ratio. For a given mobility ratio, the sweep efficiency at water breakthrough is a function of the MCR and the dimensionless heat function, F . Each graph shows a family of curves with F ranging from zero to one. The curve for $F=0$ is heavy, and is drawn with both a solid and a dashed line. The solid part of this curve represents the data published by Craig *et al.* The dashed portion of the curve represents an extension of the Craig *et al.* work based on the results of this work. Curves for $F=0.0, 0.2, 0.4, 0.6, 0.8$ and 1.0 are used to contour the data as a function of F . Two different symbols are used to represent the data, each corresponding to the quality of the injected steam used. For a steam quality of 0.7 , a symbol "o" was used. The heat function for this quality varied from 0.5 to 0.8 . The symbol "x" was used for a steam quality of 0.05 . The heat function for this group of cases ranged from 0.05 to 0.2 .

The volumetric sweep efficiency at breakthrough was always higher for the steamflood cases than for the corresponding waterflood cases at the same MCR. There is a good physical reason for this increased volumetric sweep. In a steamflood, the low

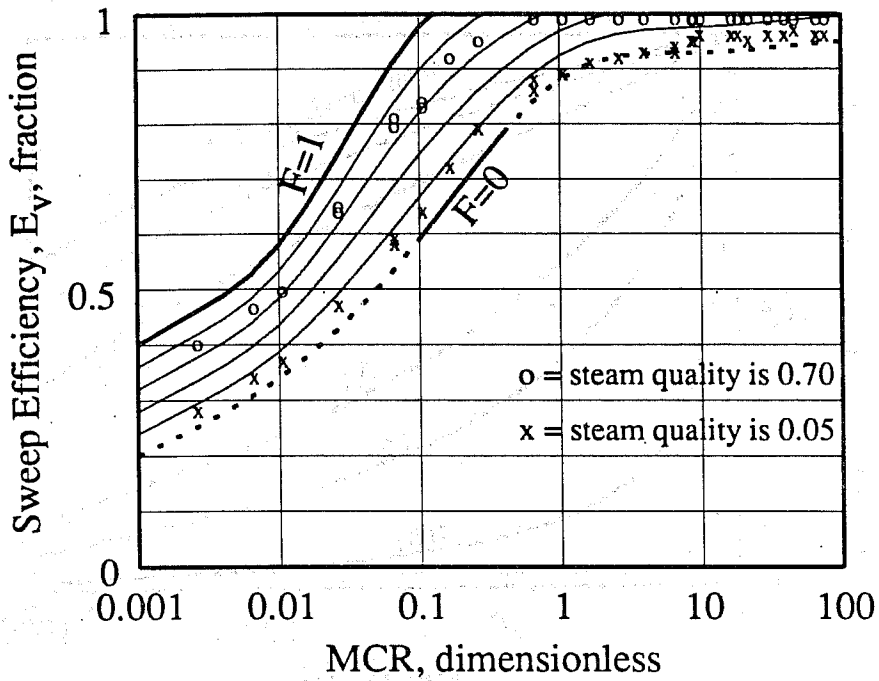


Figure 5.5: Sweep Efficiency at Water Breakthrough, $M=0.039$

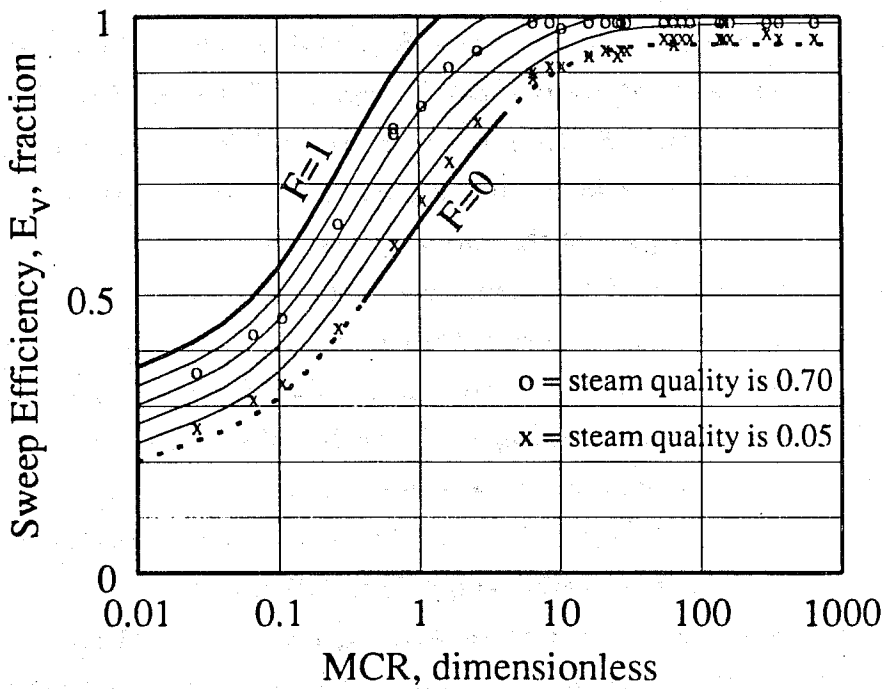


Figure 5.6: Sweep Efficiency at Water Breakthrough, $M=0.319$

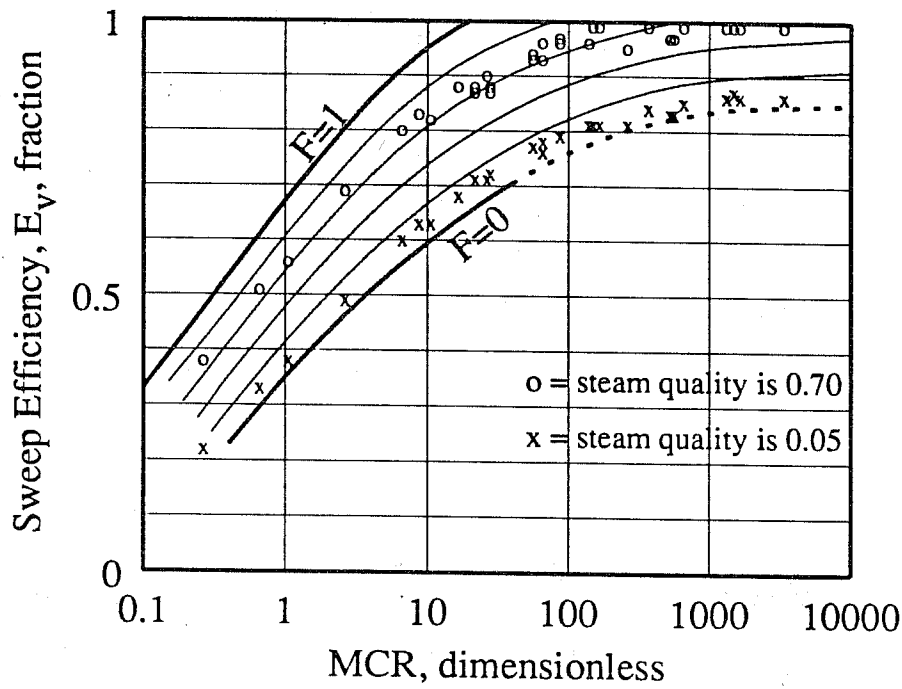


Figure 5.7: Sweep Efficiency at Water Breakthrough, $M=1.44$

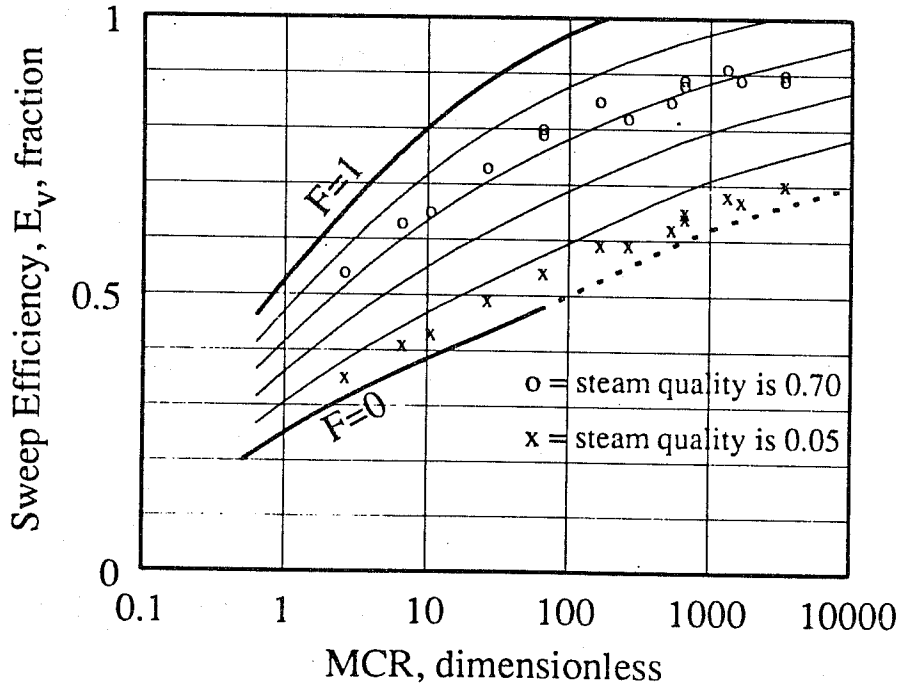


Figure 5.8: Sweep Efficiency at Water Breakthrough, $M=3.25$

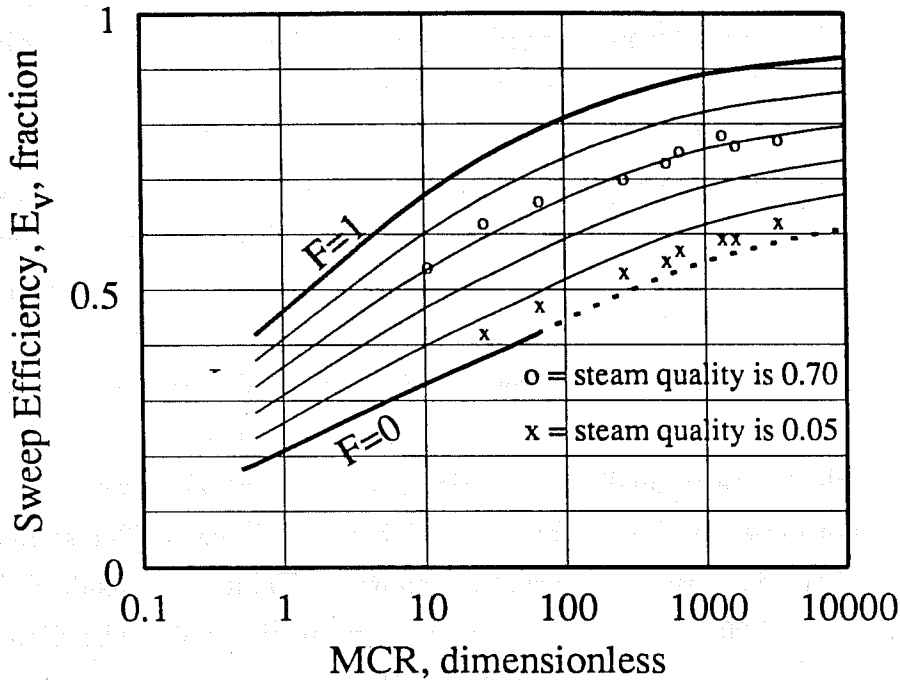


Figure 5.9: Sweep Efficiency at Water Breakthrough, $M=4.80$

density steam tends to rise to the top of the reservoir. It is near the top of the reservoir that most of the steam condenses. Consequently, water is introduced at the top of the reservoir system, aiding in the water sweep of the upper portion of the reservoir. A cold waterflood tends to sweep only the lower portion of the reservoir because the water is usually more dense than the oil it displaces. Therefore, the steam will sweep the top and the condensed water will sweep the bottom of the reservoir, giving an overall higher sweep efficiency than the cold waterflood alone.

An examination of Figures 5.5-5.9 shows different curve shapes for different mobility ratios. For the low mobility ratios, the curves tend to flatten at low MCR. For high mobility ratios, the flattening does not appear in the figures. The reason for the flattening is as follows. As the MCR decreases, the volumetric sweep efficiency also decreases. However, the volumetric sweep efficiency can not become zero because, physically, some finite volume of the reservoir must be swept by water before water breakthrough occurs. The limit must be a value greater than zero. The x -axis for these figures is a logarithmic scale. For small MCR, the lower limit of sweep efficiency

is approached, resulting in the flattening trend observed. This flattening trend may also occur in the graphs for high mobility ratios, but such data was not obtained for the lower portion of the curve. At high mobility ratios, cases that would provide data in the lower ranges of the curves would be physically unrealistic.

Cross plots of some of the data were made to verify Figures 5.5-5.9. The volumetric sweep efficiency, E_v , was plotted on the y -axis while the heat function, F , was plotted on the x -axis. A family of curves was constructed, with each curve representing a different MCR. Cross plots were made for oil viscosities of 10 and 1000 cp. The cross plot for an oil viscosity of 10 cp is shown in Figure 5.10. Curves for MCR's of 0.0665, 0.665, 6.65, and 66.5 are shown. Each letter on the cross plot represents a group of cases for which the steam quality was varied and all other values were held constant. There does not appear to be any bias as variables are changed. The symbols on the cross plot and the data used in the runs are shown in Table 5.1. Standard deviations, which range from 0.0014 to 0.0178, are also shown in the table. The data points on the graph appear to be located slightly below the lines because the graphing software places the top of the letter at the correct location.

The cross plot for an oil viscosity of 1000 cp is shown in Figure 5.11. Curves for MCR's of 2.66, 26.6, 266, and 665 are shown. Again, there does not appear to be any bias as variables are changed. The symbols on the cross plot and the data used in the runs are shown in Table 5.2. Standard deviations, which range from 0.0045 to 0.0128, are also shown in the table. The cross plots show the accuracy of the correlation. The data fall on a linear trend, and lines are graphed through the data. The graphs also show that different combinations of variables that give the same MCR give the same result. Finally, the cross plots can be used to extrapolate to F values of unity.

The length to the water front prior to water breakthrough is given by

$$L_{s+w} = \frac{Q_{res}}{A\phi(\bar{S}_w - S_{wi})E_v} \quad (5.27)$$

This equation is identical to Eq. 3.5 for the one-dimensional model except for the sweep efficiency term in the denominator. The water saturation in the water zone is the average water saturation behind the water front, \bar{S}_w , obtained from the fractional flow curve calculation using initial reservoir temperature. In the SAM, the water front

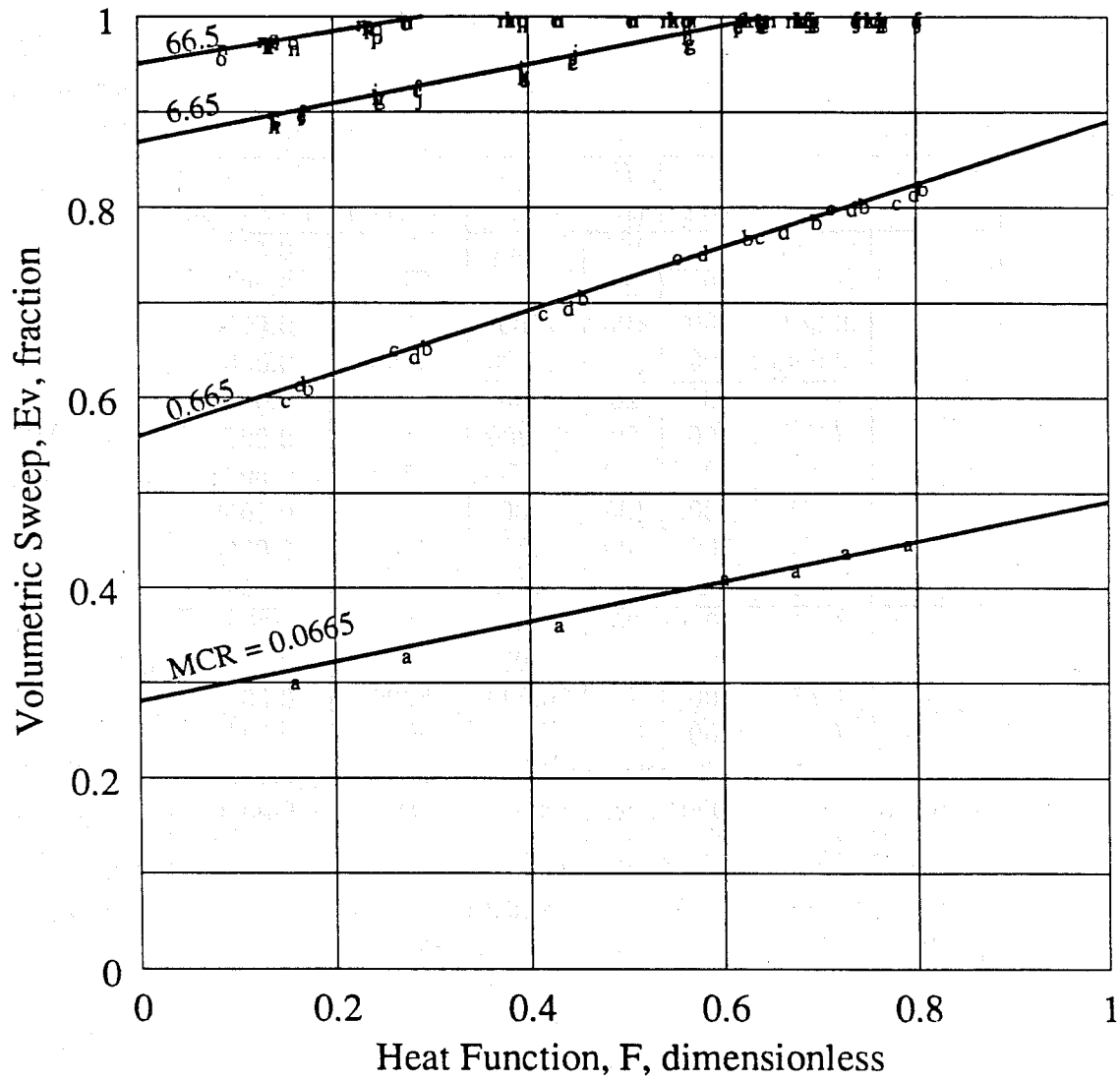


Figure 5.10: Effect of Variables in the MCR on Volumetric Sweep, $\mu_o = 10$ cp

Symbol	MCR	L (ft)	H (ft)	k_x (md)	q_w (bbl/D)	Standard Deviation
a	0.0665	500	100	20,000	50	0.0178
b	0.665	200	20	20,000	50	0.0031
c	0.665	500	100	2000	50	0.0103
d	0.665	500	100	20,000	500	0.0065
e	6.65	200	20	2000	50	0.0025
f	6.65	200	20	20,000	500	0.0025
g	6.65	500	100	200	50	0.0045
h	6.65	500	100	2000	500	0.0055
i	6.65	500	100	20,000	5000	0.0056
j	6.65	2000	20	20,000	50	0.0060
k	66.5	200	20	200	50	0.0014
l	66.5	200	20	2000	500	0.0017
m	66.5	200	20	20,000	5000	0.0064
n	66.5	500	100	200	500	0.0057
o	66.5	500	100	2000	5000	0.0030
p	66.5	2000	20	2000	50	0.0070
q	66.5	2000	20	20,000	500	0.0052

Table 5.1: Symbols and Data for Crossplot of $\mu_o = 10$ cp

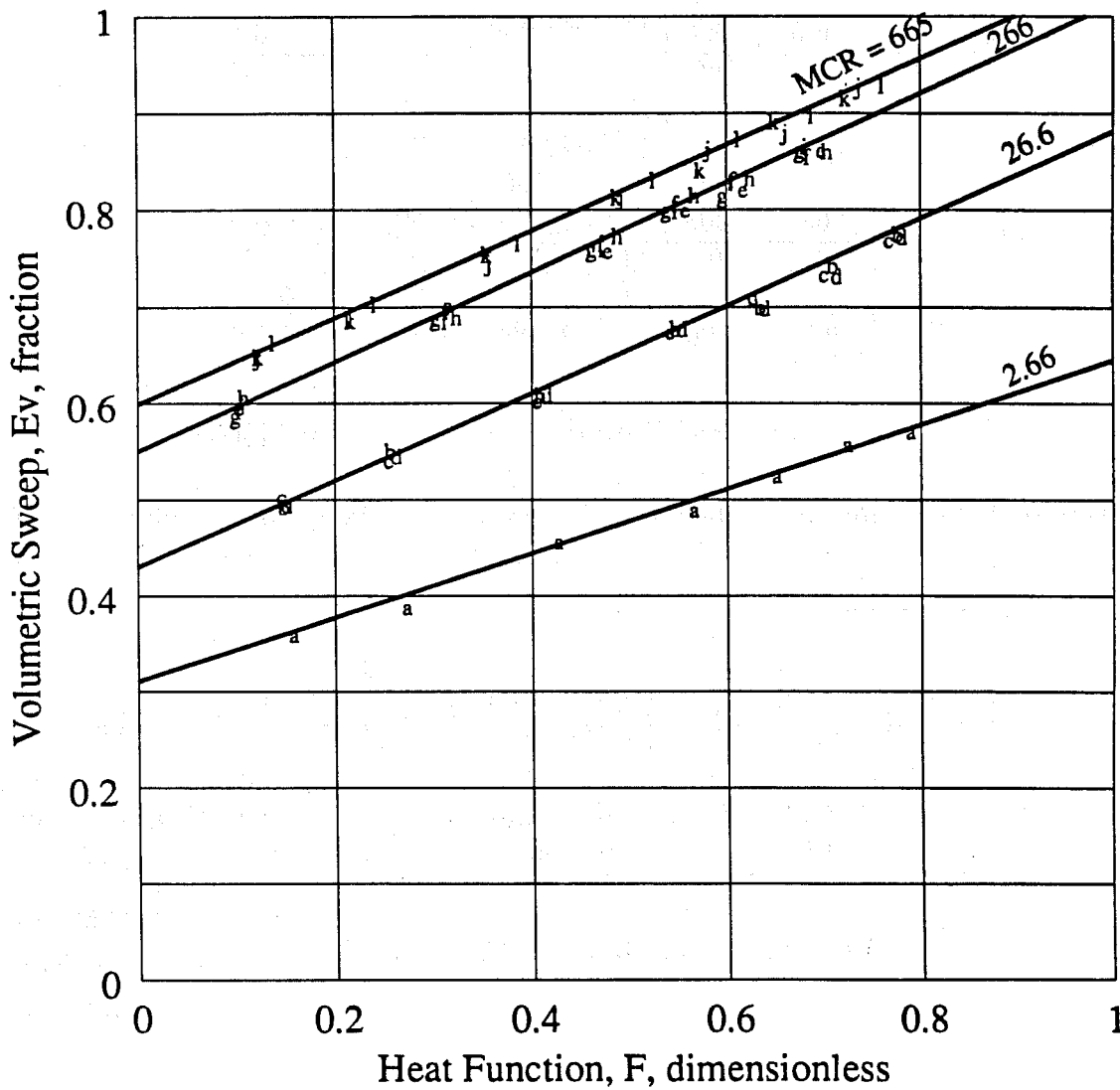


Figure 5.11: Effect of Variables in the MCR on Volumetric Sweep, $\mu_o = 1000$ cp

Symbol	<i>MCR</i>	<i>L</i> (ft)	<i>H</i> (ft)	<i>k_x</i> (md)	<i>q_w</i> (bbl/D)	Standard Deviation
a	2.66	200	100	20,000	50	0.0045
b	26.6	200	100	2000	50	0.0097
c	26.6	200	100	20,000	500	0.0108
d	26.6	2000	100	20,000	50	0.0128
e	266.	200	100	200	50	0.0108
f	266.	200	100	2000	500	0.0062
g	266.	200	100	20,000	5050	0.0057
h	266.	2000	100	2000	50	0.0102
i	266.	2000	100	20,000	500	0.0045
j	665.	200	20	2000	50	0.0072
k	665.	200	20	20,000	500	0.0067
l	665.	2000	20	20,000	50	0.0054

Table 5.2: Symbols and Data for Crossplot of $\mu_o = 1000$ cp

is assumed to be normal to the bedding plane of the reservoir. This combination of front shape and water saturation works well in matching the two-dimensional thermal simulator results.

5.6 Comparison of Viscous to Gravity Ratios

Viscous to gravity force ratios are used to help quantify the degree of override, or underoverride, of one fluid displacing another. The Craig ratio is a viscous to gravity force ratio, as is the VGR used as an exponent in the determination of the shape of the steam front. Another form of a viscous to gravity force ratio was presented by van Lookeren [46]. These three viscous to gravity force ratios will be compared in this section to see how they are related. The Craig ratio is

$$\frac{\Delta p_h}{\Delta p_v} = \frac{q_w \mu_o}{k_x A \Delta \rho} \frac{g_c}{g} \frac{L}{H} \quad (5.28)$$

The van Lookeren ratio is

$$A_{LD} = \frac{w_{st}}{\rho_{st}} \frac{\mu_{st}}{k_{st} A \Delta \rho} \frac{g_c}{g} \quad (5.29)$$

but, by definition,

$$w_{st} = \rho_{st} q_{st} \quad (5.30)$$

Substituting Eq. 5.30 in Eq. 5.29 gives

$$A_{LD} = \frac{q_{st} \mu_{st} g_c}{k_{st} A \Delta \rho} \quad (5.31)$$

The ratio used for the steam zone is

$$VGR = \frac{v_x}{v_z} = \frac{k_x}{k_z} \frac{\Delta p}{L \Delta \rho} \frac{g_c}{g} \quad (5.32)$$

but, from Darcy's law,

$$\frac{\Delta p}{L} = \frac{q_{st} \mu_{st}}{k_{st} A} \quad (5.33)$$

Substituting Eq. 5.33 in Eq. 5.32 gives

$$VGR = \frac{q_{st} \mu_{st} g_c}{k_{st} A \Delta \rho} \frac{k_x}{g k_z} \quad (5.34)$$

A comparison of the three different forms of the viscous to gravity force ratio (Eqs. 5.28, 5.31, and 5.34) shows that all three ratios have the same general form. All three have flow rate, viscosity, and the gravitational constant in the numerator. They all have permeability, cross-sectional area, and density difference in the denominator. van Lookeren's group (Eq. 5.31) is the simplest. The Craig ratio (Eq. 5.28) is similar to the van Lookeren group but is multiplied by a length to height ratio. The steam VGR group (Eq. 5.34) is similar to van Lookeren's group but is multiplied by the x to z permeability ratio. Thus all three groups are similar in nature. The van Lookeren group does not consider anisotropic reservoirs. For the isotropic reservoirs used in this work, the permeability ratio is unity, and the VGR ratio simplifies to A_{LD} , the group introduced by van Lookeren.

5.7 Pressure Drops

The pressure drop calculations for the two-dimensional model are similar in many aspects to the one-dimensional model. The length of the steam zone at the top of the reservoir is used as the length of the steam zone. The reason for this is that the

pressure drop through the steam zone is small because of the high steam mobility. Furthermore, the water zone and steam zone pressures must be the same at the steam front. Using anything other than the steam zone pressure gradient would not honor this constraint. The total length of the water zone and steam zone gives the distance to the water front, so the water zone length is simply the distance to the water front less the length of the steam zone.

The average steam saturation in the steam zone is used for the pressure drop through the steam zone, and the average water zone water saturation, determined from the fractional flow calculation, is used for the water zone pressure drop. The cross-sectional area used in the steam zone calculation is the average cross-sectional area obtained by dividing the volume of the steam zone by its length. For this calculation, the water zone viscosities are evaluated at original reservoir temperature. In short, the top layer of the system is used in calculating zone lengths for pressure drop calculations, and the saturations are evaluated in the same manner as for the one-dimensional problem.

5.8 Concluding Remarks

The modifications that were necessary to transform the one-dimensional model into two dimensions have been presented here. The major modifications were: (1) the empirical method of representing the shape of the steam front, and (2) the extension of the Craig *et al.* work for a horizontal waterflood to consider formation dip and steam drive. Standard deviations were calculated for each line on the cross plots. The standard deviation was low, ranging from 0.14 to 1.78 percent. In the next chapter, results from the two-dimensional SAM will be compared to results from the thermal simulator ISCOM.

Chapter 6

Two-Dimensional Model Results

This chapter shows several comparisons of the two-dimensional semianalytical model (SAM) with the thermal simulator ISCOM. The first section describes the thermal simulation runs, while the second section draws comparisons between the results of six of the 1620 cases run.

6.1 Two-Dimensional Simulator Runs

The thermal simulator was used to make many runs for two-dimensional systems. A two-dimensional data set was assembled that was the same as the one-dimensional set, except that multiple layers were included in the vertical dimension. Steam was injected into the bottom layer of the injection well. When a two-dimensional system is considered, a grid orientation effect is possible. To minimize this effect, a nine-point difference method can be used instead of the usual five-point method. Figure 6.1 compares the results of a two-dimensional case run using five-point and nine-point difference methods. The data set described in Chapter 4 was used. A grid orientation effect appeared to be present. Consequently, a nine-point difference method was used in subsequent runs.

Figures 6.2 and 6.3 present the results from the two-dimensional case used for the grid orientation effect with different gridding systems. The most finely gridded case consisted of 100 grid blocks in the x -direction and eight layers in the z -direction. This

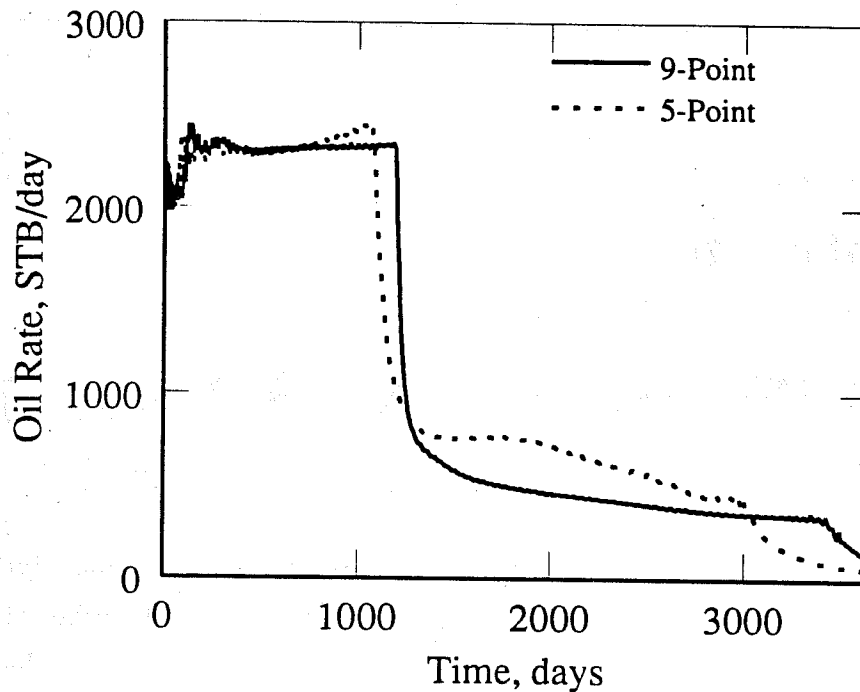


Figure 6.1: Oil Rate vs Time for 5- and 9-Point Difference Method

case is compared to 8×40 , 8×20 , 4×40 , 4×20 , and the one-dimensional 1×100 systems. For the cases with eight layers in Figure 6.2, more grid blocks in the x -direction give later water breakthrough and a lower oil rate after water breakthrough. The declines in production at late time in the eight layer cases are due to steam breakthrough. There is some difference in each of the cases. Both of the cases with four layers match the 8×100 case in terms of water breakthrough time and oil production rate, with the 4×20 system giving the best match. The one-dimensional case gives the worst match. The 4×20 system required much less computer time to solve than the 8×100 system did. Therefore, subsequent two-dimensional runs were made using a 4×20 system.

Inspection of all two-dimensional results, and one-dimensional results, reveals that at early times, the oil production rate is nearly constant, with small oscillations. The oil production rate then increases to a higher value and the amplitude of the oscillations increases for the two-dimensional cases. The cause of this production delay is related to the shape of the steam zone. Steam is injected in the bottom layer of the system. The low density steam rises to the top of the system, condensing

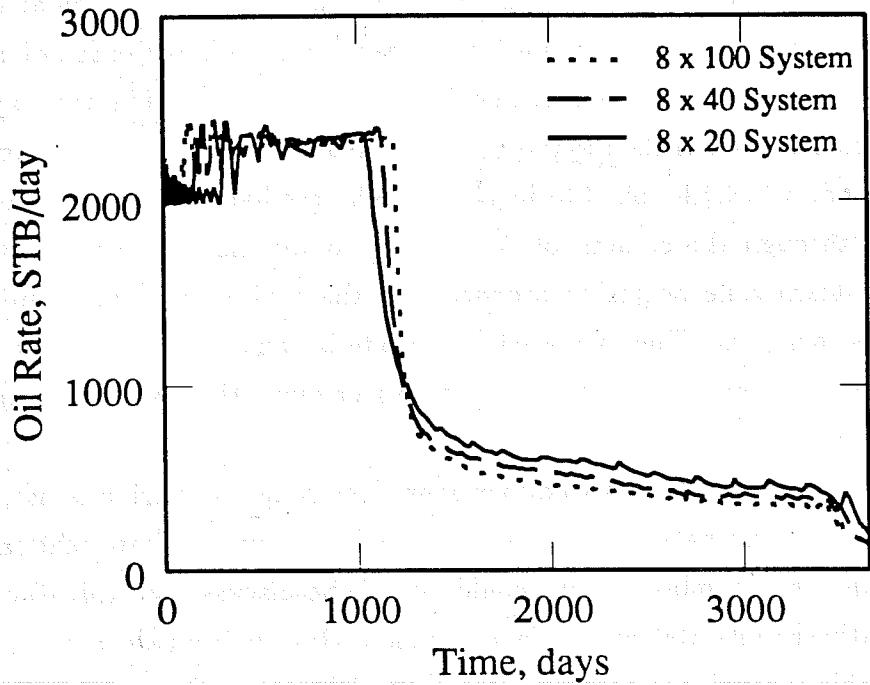


Figure 6.2: Oil Rate vs Time for 8 Layer Grid Systems

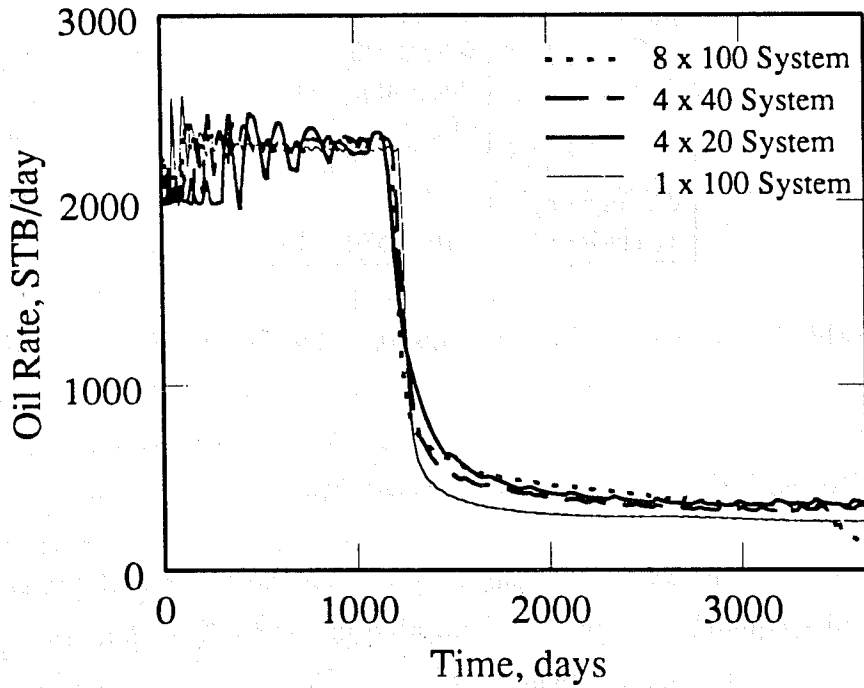


Figure 6.3: Oil Rate vs Time for 1 and 4 Layer Grid Systems

until the injection well grid blocks are heated. The steam saturation at this point is only a few percent, and it is not until the steam zone reaches the top of the reservoir that steam begins to accumulate, and becomes significant. The time at which the steam reaches the top of the reservoir and the steam zone begins to propagate forward is the time at which the oil rate increases. The oscillations are small as the steam zone rises through the column of grid blocks containing the injection well. Then, when the steam zone begins to propagate in the x -direction, the amplitude of the oscillations increases. The increased amplitude is caused by the higher steam zone steam saturation compared to the saturation seen while the steam was rising near the injection well.

Many cases were run for two dimensions. The ranges of variables used are shown in Table 6.1. Combinations of all of the variables required that 1620 cases be run. Clearly this large number of runs could not all be discussed in this dissertation, so representative results were chosen for discussion. Results from all cases are on a floppy disk available through the Stanford University Petroleum Engineering Department.

μ_o (cp)	1, 10, 100, 1000, 10,000
k (Darcy)	0.2, 2, 20
L (ft)	200, 500, 2000
H (ft)	20, 100, 500
q_w (bbl/day)	50, 500, 5000
θ (degrees)	0, 60
f_s (frac)	0.05, 0.70

Table 6.1: Ranges of Variables Used in Two-Dimensional Analysis

6.2 Two-Dimensional Results

Many two-dimensional cases were run on both the thermal simulator and the SAM so that results could be compared. The table in the file 2DCASE on a floppy disk that is available through the Stanford University Petroleum Engineering Department shows the cases run for two dimensions. For each case, the case number, formation

dip, steam quality, oil viscosity, length, height, permeability, and injection rate are given. The table in the file 2DRESULT on the floppy disk shows the results for the two-dimensional cases. For each case, the MCR, volumetric sweep efficiency at water breakthrough, steam zone pressure at breakthrough, and the value of the heat function, F , are displayed. These results are the data points that were used to generate Figures 5.5-5.9. In some of the cases, the injection well pressure exceeded the constraint, and the boundary condition was violated. These cases are denoted by "pres" in the pressure column. The cases were run for a maximum of 50,000 days. If water breakthrough did not occur by this time, the water breakthrough column shows "no bt" as an indication of no water breakthrough.

When graphing the results, there were a few data points that did not fall on the same trend as the rest of the data, but fell well below the curves in Figures 5.5-5.9. Inspection of these cases revealed that, without exception, all of the nonconforming data points came from cases in which the height of the reservoir was greater than or equal to the length of the reservoir. In these cases, the injected water did not sweep much of the reservoir. Since the wet steam is injected at the bottom of the reservoir, more time is required for the steam zone to reach the top of the reservoir when the height is large. While the steam front is ascending, the water front moves toward the production well, and in some cases even breaks through before the steam front propagates past the first column of grid blocks. Obviously, the calculated sweep efficiency should be lower in these cases and this is reflected in the results.

For anisotropic reservoirs, the horizontal to vertical permeability ratio has an effect on how the fronts move relative to each other. The square root of this ratio can be used to transform the anisotropic system to an equivalent isotropic system [16].

When the aspect ratio

$$\frac{H}{L} \sqrt{\frac{k_x}{k_z}} \quad (6.1)$$

is greater than or equal to one, the aspect ratio is too large and the case is flagged by an "a" in the last column (untitled) of the results tables.

Changing the dip of the reservoir changes the results of the fractional flow calculation. For updip water injection the fractional flow of water, f_w , increases as the dip increases, resulting in a lower average water saturation, \bar{S}_w . The mobility ratio

incorporates relative permeability values which are evaluated at \bar{S}_w . Therefore, the mobility ratio is a function of the reservoir dip. The degree to which the mobility ratio is effected by dip depends on the ratio of permeability, cross-sectional area, and density difference to viscosity and flow rate. For most of the cases run in this analysis, the change in the mobility ratio due to dip was not great. However, for some cases, the mobility ratio changed significantly. If the change was more than ten percent, the case is denoted with an "m" in the last column. These cases still fall on the correlations established in Chapter 5.

Comparison of the horizontal and dipping cases allows general observations to be made concerning the effect of reservoir dip. The steam zone did not advance as far in the dipping cases as it did in the horizontal cases. The influence of gravity causes the steam zone to form at the top of the reservoir. For horizontal systems, the top of the reservoir covers the entire length of the system, so the steam zone is thin and long. For a dipping system in which steam is injected upstructure, gravity forces cause the steam to migrate upstructure toward the injection well. This produces a steam front more nearly perpendicular to the bedding planes of the reservoir. The steam saturation in the steam zone is about the same in both cases. Due to gravity forces, water breakthrough occurs earlier in the downward dipping reservoirs, and steam breakthrough occurs later. Consequently, a downward dipping reservoir gives a higher oil production rate before water breakthrough, and a lower oil production rate after water breakthrough.

Table 6.2 presents the range of variables for the six two-dimensional cases for which results are shown and discussed. All of the cases have a permeability of 2 Darcy, length of 500 ft, height of 100 ft, wet steam injection rate of 500 bbl/d, and steam quality of 0.70. Formation dip and oil viscosity are varied in the six cases. Results from the six cases are shown in Figures 6.4-6.27. Comparisons of calculated oil and water production rates are made for each case to illustrate the accuracy of the SAM results. In all of the cases, there is good agreement between the SAM and the thermal simulator.

The first case is for a horizontal reservoir and an oil viscosity of 10 cp. The oil production rate graph for Case 0122 is shown in Figure 6.4. The time to water

Case	θ (degrees)	μ_o (cp)	Figure Number
0122	0	10	6.4-6.5
0203	0	100	6.12-6.13
0287	0	1000	6.14-6.15
1122	60	10	6.22-6.23
1203	60	100	6.24-6.25
1287	60	1000	6.26-6.27

Table 6.2: Two-Dimensional Results Displayed

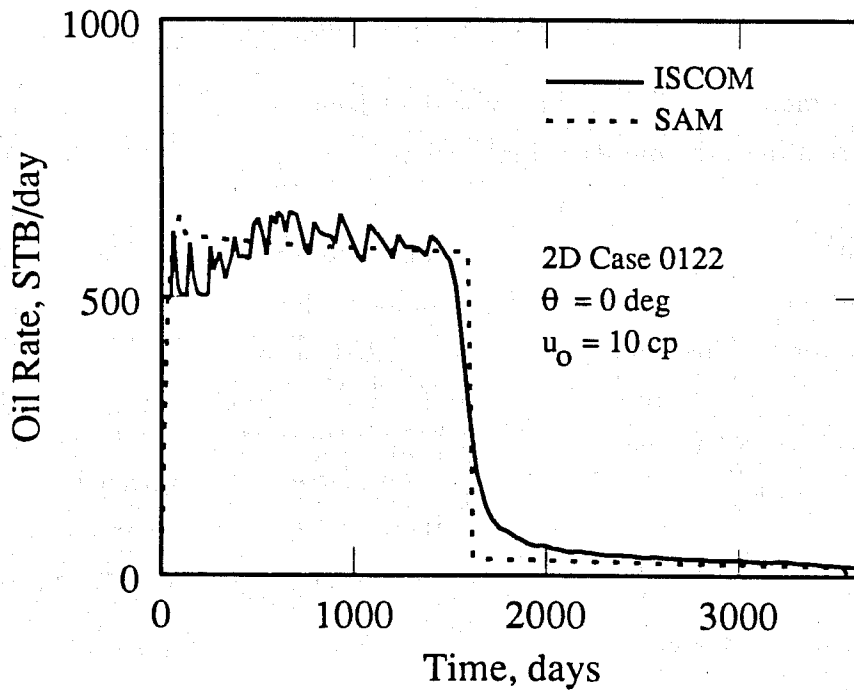


Figure 6.4: Oil Rate vs Time, Case 0122

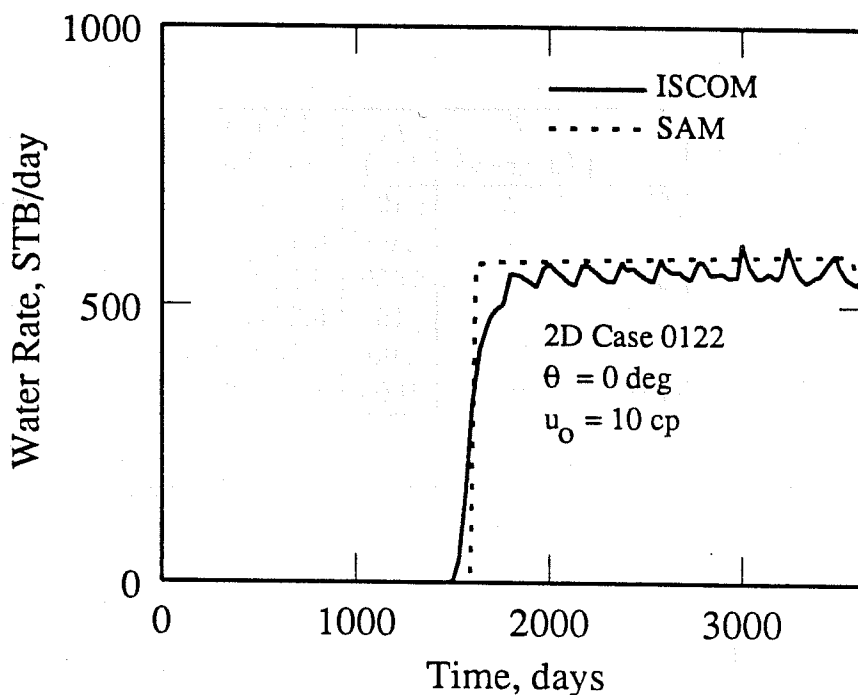


Figure 6.5: Water Rate vs Time, Case 0122

breakthrough matches well, but the immediate decline in oil production rate from the SAM is different from the more gradual decline in rate given by the thermal simulator. The SAM gives an immediate drop because the assumed shape of the water front is normal to the bedding plane of the reservoir. The thermal simulator, on the other hand, computes a non-vertical water front shape with a non-uniform water saturation in the water zone. This behavior results in SAM oil production rates that are too high immediately prior to breakthrough and too low immediately after breakthrough. This also results in SAM water production rates that are lower immediately prior to breakthrough and higher immediately after breakthrough (see Fig. 6.5). The ISCOM results look similar to the effects of numerical dispersion at a front, but the behavior is not due entirely to numerical dispersion. The variability in saturations in the z -direction contributes heavily to this behavior. This general result is seen in all of the two-dimensional cases and will not be discussed further.

The water production rate graph for Case 0122 is shown in Figure 6.5. The match for water breakthrough time is good. The water production rate from the

SAM is higher because the change in the water zone water saturation is too slow. The SAM uses the average water saturation behind the front from the fractional flow calculation for the water zone saturation. The simulator computes water zone saturation for each grid block as a function of both x and z . The different methods of determining the water zone saturation result in the differences between the two curves. The SAM shows a decrease in water rate at late time. This decrease is due to steam breakthrough at the production well. The oscillations in the water rate at late time for ISCOM are caused by the immediate condensation of steam when a new grid block is encountered by the steam zone, like the oscillations in the oil rate.

A few gas and oil saturation distribution graphs are included from Case 0122. Graphs are made at times of 1000, 2000, and 3000 days, and are shown in Figures 6.6-6.11. The figures show a cross-section of the reservoir. The saturations generated by the thermal simulator are displayed for each grid block. The square waves in the gas saturation graphs are the steam front shapes generated by the SAM.

Care must be taken when comparing steam front shapes. The thermal simulator results do not give a sharp interface between the steam zone and the water zone. A saturation gradient exists in both the x - and z -directions, so definition of the steam front is not clear. The SAM uses one average gas saturation for the entire steam zone, whereas the thermal simulator has a saturation gradient within the steam zone. Despite these problems, steam front shapes are compared in these figures. The empirical equation used by the SAM gives good qualitative fits of the front shapes determined by ISCOM. The average gas saturation in the steam zone calculated by the SAM for 1000, 2000, and 3000 days is 26.6, 28.8, and 30.9 percent, respectively. The line in Figure 6.7 is the water front calculated by the SAM.

The second case is for a horizontal reservoir and an oil viscosity of 100 cp. The oil production rate graph for Case 0203 is shown in Figure 6.12. Good agreement is observed for both the water breakthrough time and the oil production rate. The oil production rate after breakthrough is too high because the change in the water zone water saturation is too abrupt in the SAM.

The water production rate graph for Case 0203 is shown in Figure 6.13. The water breakthrough time matches well, and after breakthrough the water production rate

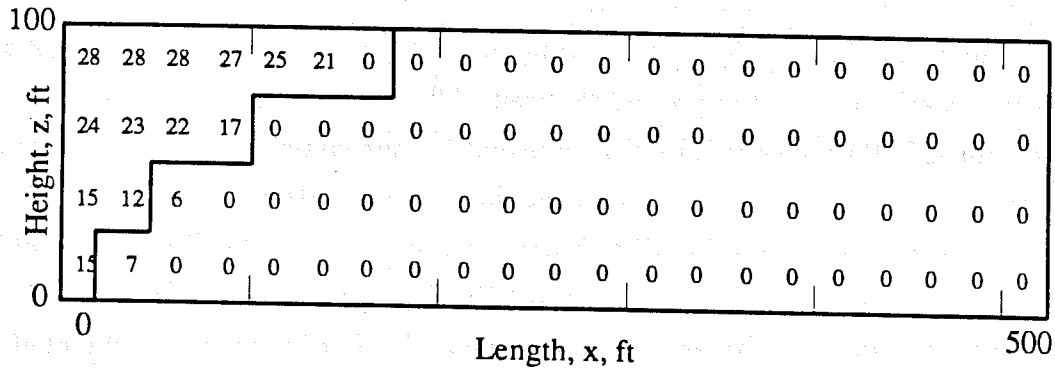


Figure 6.6: Gas Saturation Distribution at 1000 Days, Case 0122

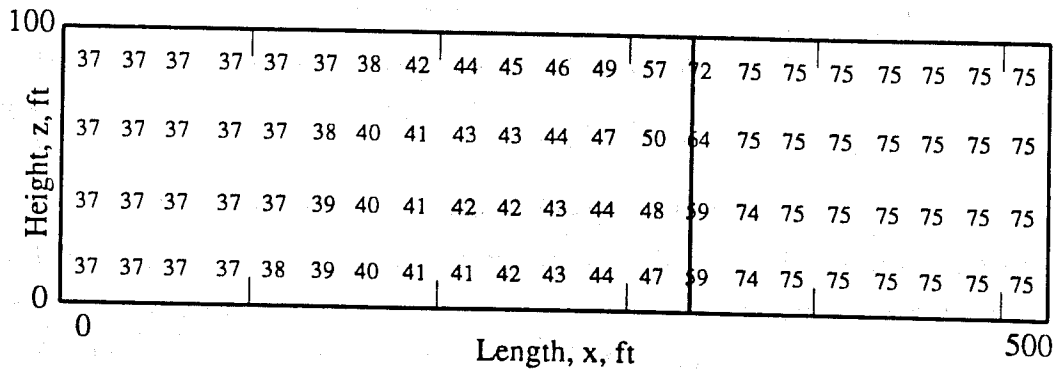


Figure 6.7: Oil Saturation Distribution at 1000 Days, Case 0122

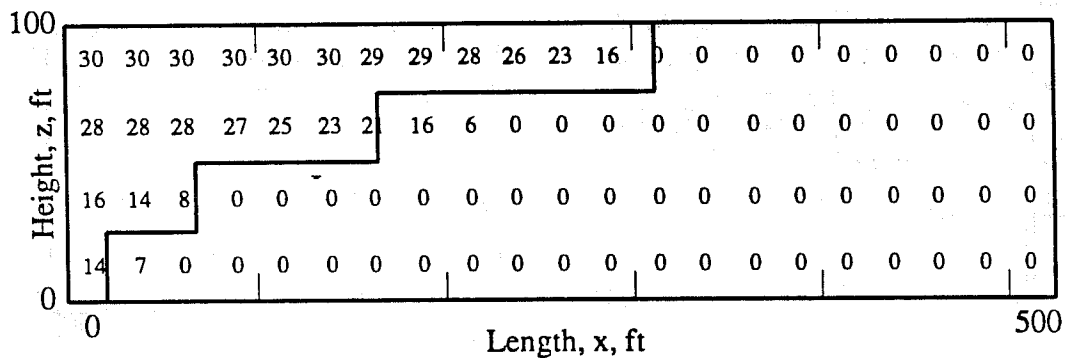


Figure 6.8: Gas Saturation Distribution at 2000 Days, Case 0122

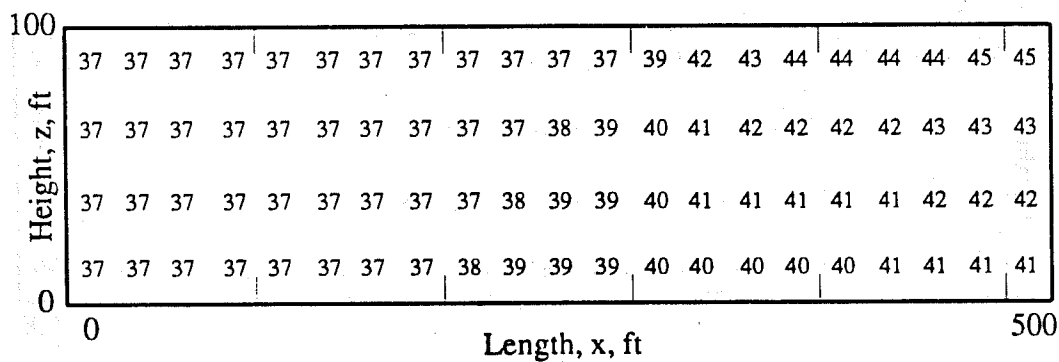


Figure 6.9: Oil Saturation Distribution at 2000 Days, Case 0122

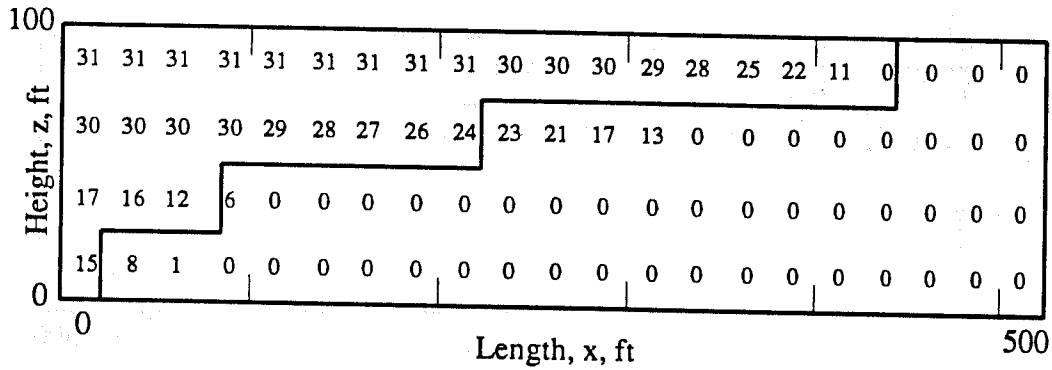


Figure 6.10: Gas Saturation Distribution at 3000 Days, Case 0122

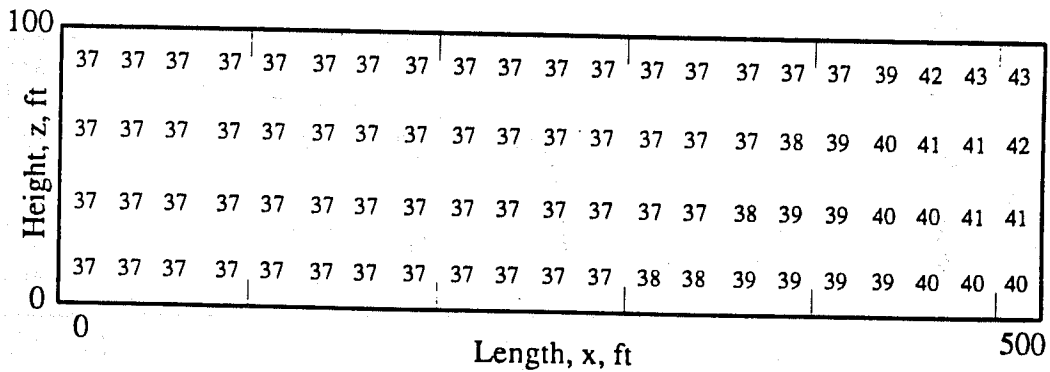


Figure 6.11: Oil Saturation Distribution at 3000 Days, Case 0122

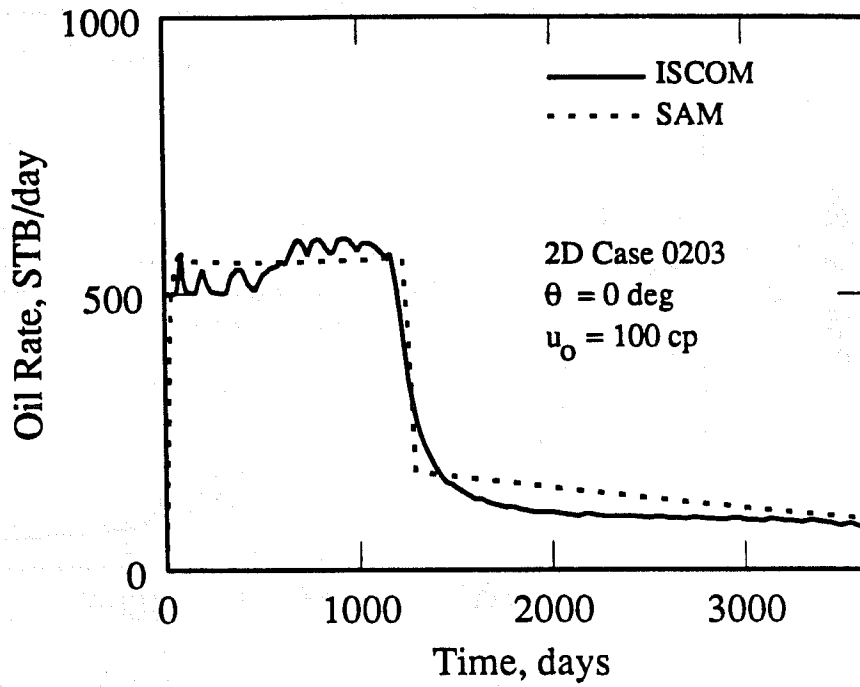


Figure 6.12: Oil Rate vs Time, Case 0203

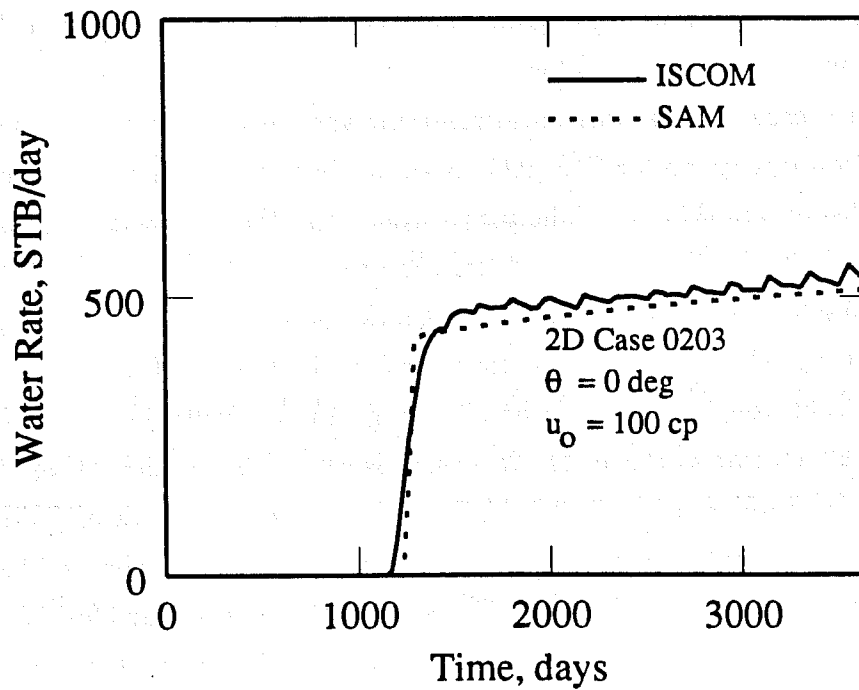


Figure 6.13: Water Rate vs Time, Case 0203

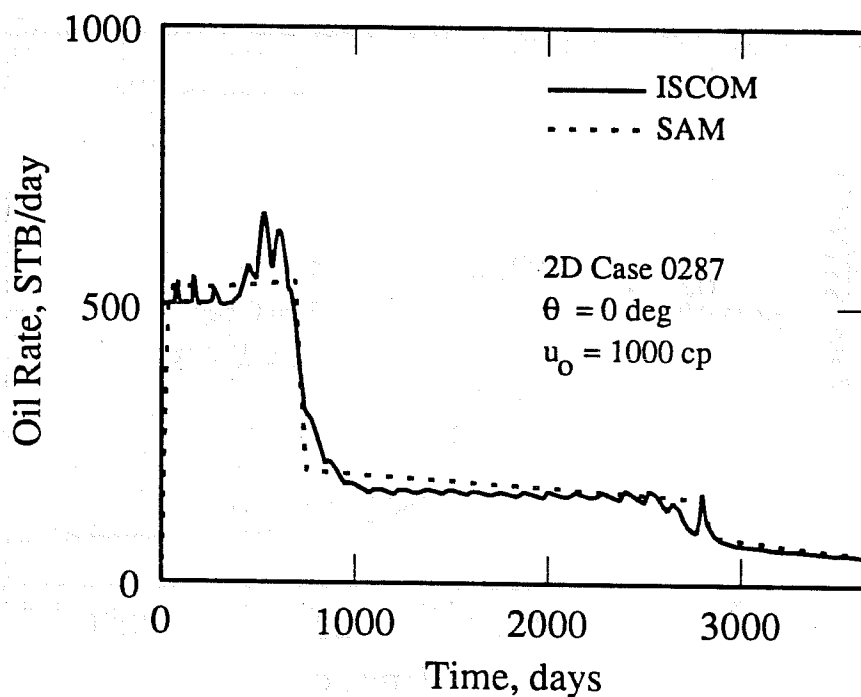


Figure 6.14: Oil Rate vs Time, Case 0287

from the SAM is too low. The same effect that causes the oil rate to be too high causes the water rate to be too low.

The third case is for a horizontal reservoir and an oil viscosity of 1000 cp. The oil production rate graph for Case 0287 is shown in Figure 6.14. Steam breakthrough has been observed in this case. The graph shows that there is good agreement in both the time to water breakthrough and the time to steam breakthrough. Furthermore, the oil production rates match well at all times.

The water production rate graph for Case 0287 is shown in Figure 6.15. The times to water breakthrough and steam breakthrough match well. The large spike in the water production rate at steam breakthrough is caused by condensation of the steam as it enters the production well. The spikes in both the oil and water production rate graphs at steam breakthrough exist for the same reasons that the oscillations exist. The assumption of instantaneous thermal equilibrium causes sharp fluctuations in the production rate graphs as steam rapidly condenses. Water production rates match well at all other times.

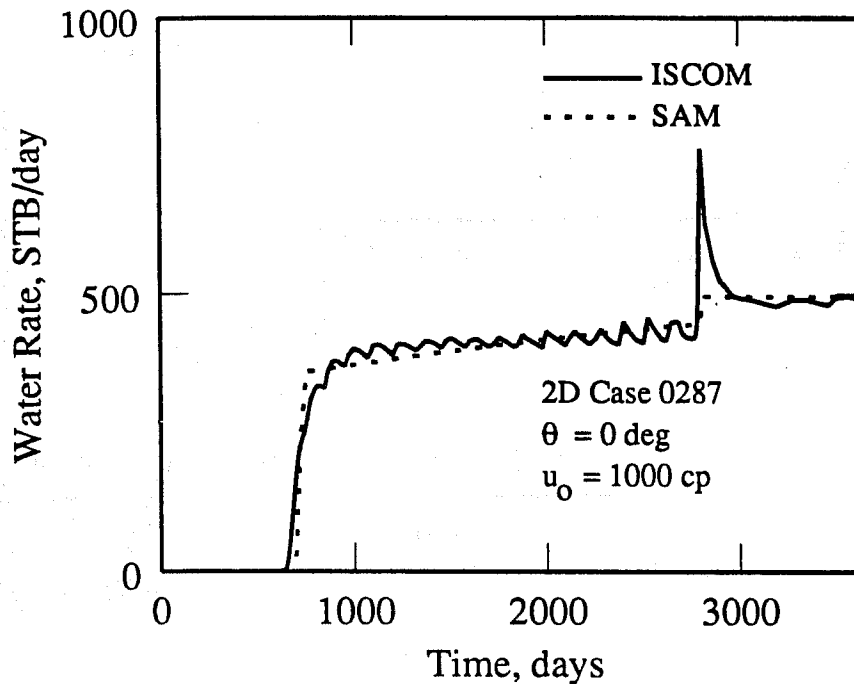


Figure 6.15: Water Rate vs Time, Case 0287

A few gas and oil saturation distribution graphs are included for Case 0287. Graphs are shown for times of 1000, 2000, and 3000 days, in Figures 6.16-6.21. The average gas saturation in the steam zone calculated by the SAM for 1000, 2000, and 3000 days is 27.7, 31.9, and 32.0 percent, respectively. The gravity override is more severe in this case than in Case 0122 because of the higher oil viscosity. As in case 0122, the SAM gives a good fit of the steam front shape.

The fourth case is for a formation dip of 60 degrees and an oil viscosity of 10 cp. The oil production rate graph for Case 1122 is shown in Figure 6.22. The match is a good one. The water breakthrough time and the oil production rates display a close fit. The lower oil production rate after water breakthrough is caused by a rate of steam zone growth that is too low.

The effect of formation dip in two dimensions can be seen by comparing this figure to Figure 6.4 from Case 0122. The only difference between the two cases is the formation dip. Earlier water breakthrough is observed in the dipping case, but the oil production rate is about the same. For a given time, even though more reservoir

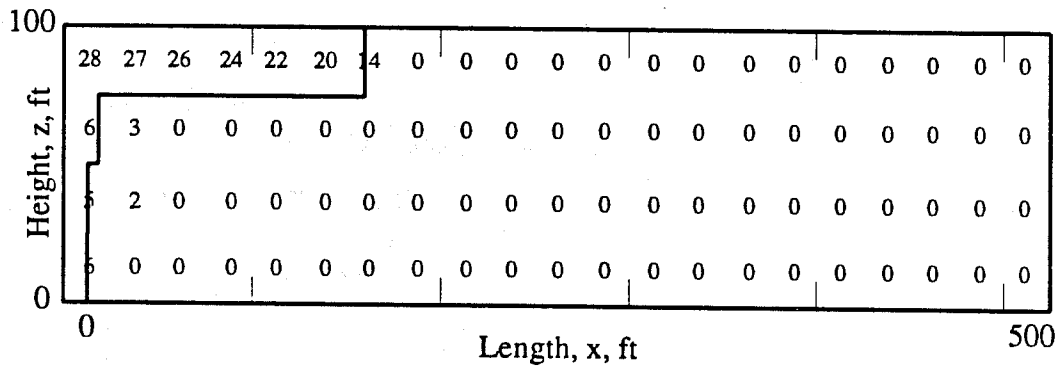


Figure 6.16: Gas Saturation Distribution at 1000 Days, Case 0287

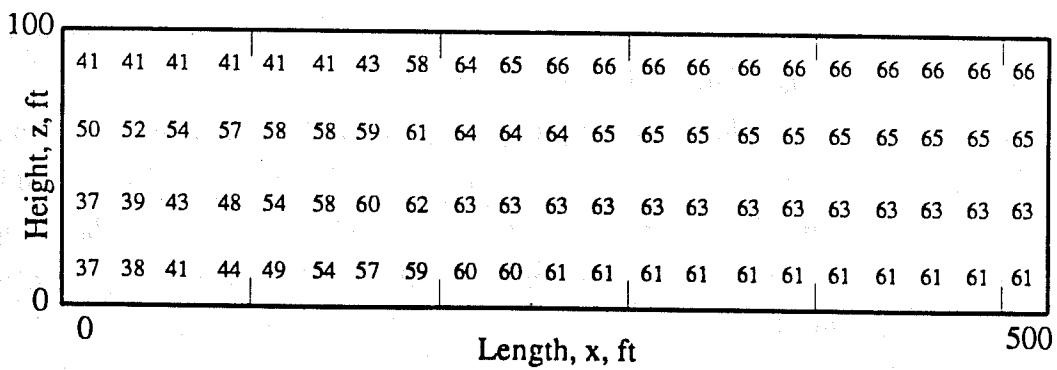


Figure 6.17: Oil Saturation Distribution at 1000 Days, Case 0287

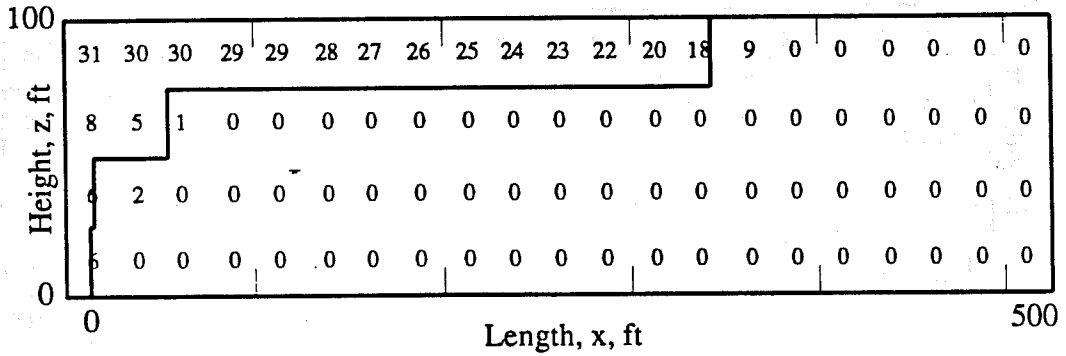


Figure 6.18: Gas Saturation Distribution at 2000 Days, Case 0287

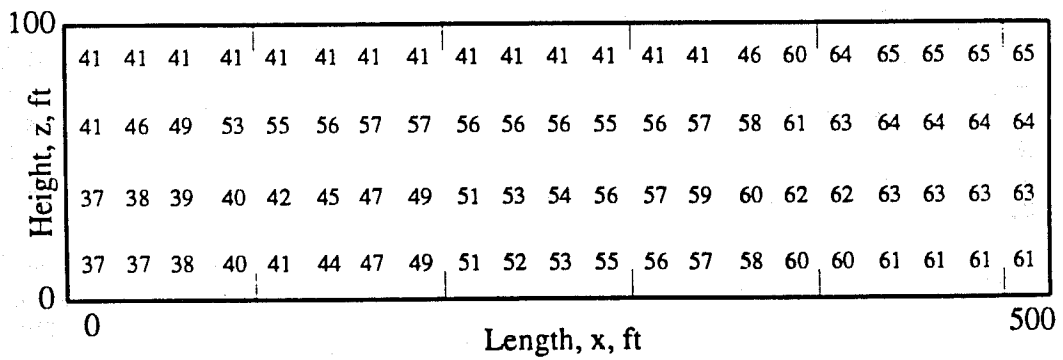


Figure 6.19: Oil Saturation Distribution at 2000 Days, Case 0287

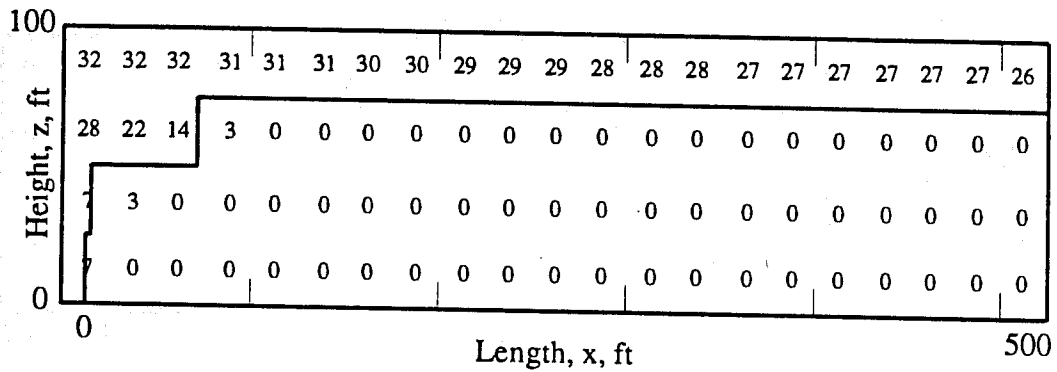


Figure 6.20: Gas Saturation Distribution at 3000 Days, Case 0287

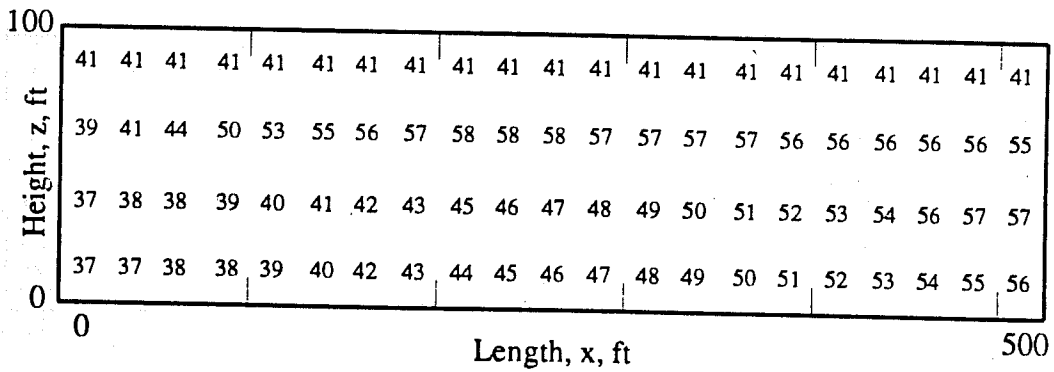


Figure 6.21: Oil Saturation Distribution at 3000 Days, Case 0287

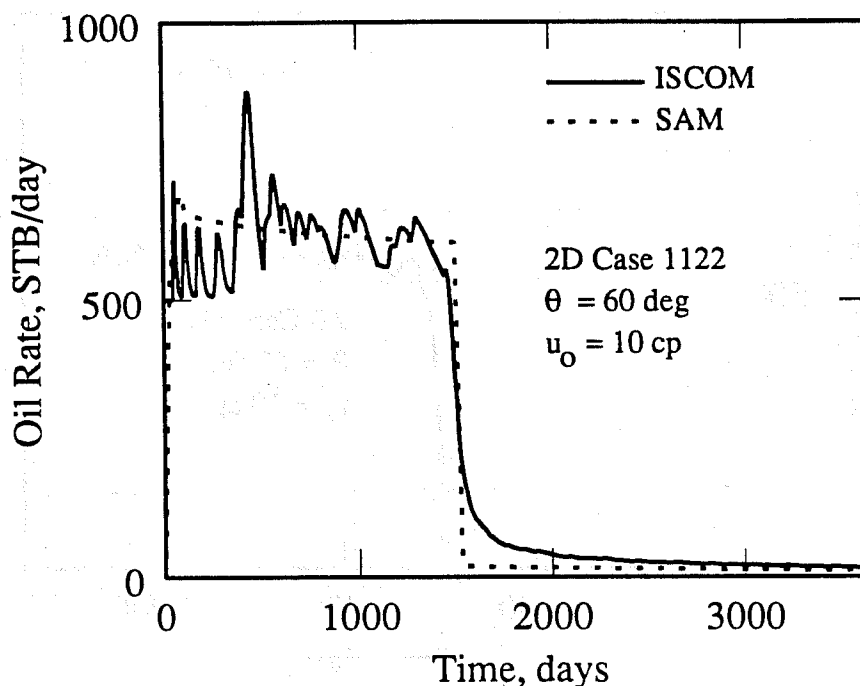


Figure 6.22: Oil Rate vs Time, Case 1122

volume is swept in the dipping case, the oil production rate is not significantly different because of the poorer displacement efficiency associated with the dipping case. For the dipping case, The oil production rate predicted by the SAM at late time is too high.

The water production rate graph for Case 1122 is shown in Figure 6.23. The water breakthrough time is matched correctly, and the water production rate shows little error thereafter.

The fifth case is for a formation dip of 60 degrees and an oil viscosity of 100 cp. The oil production rate graph for Case 1203 is shown in Figure 6.24. There is good agreement observed in terms of water breakthrough time and oil production rate both before and after water breakthrough. The oil production rate predicted by the SAM after breakthrough is too high because of a water zone water saturation that is too high.

The water production rate graph for Case 1203 is shown in Figure 6.25. Again, good agreement is observed. As in the high oil production rate, the water production

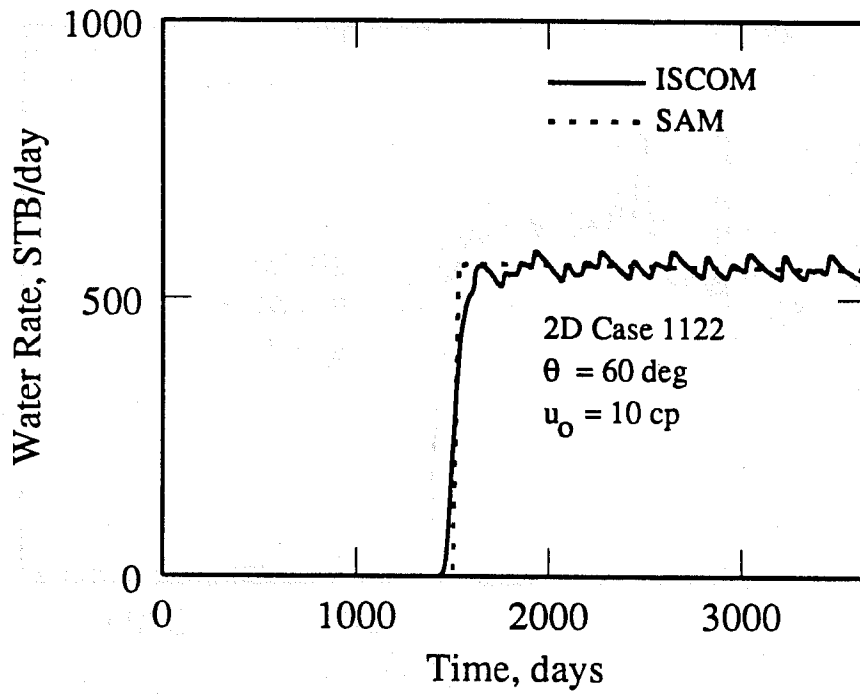


Figure 6.23: Water Rate vs Time, Case 1122

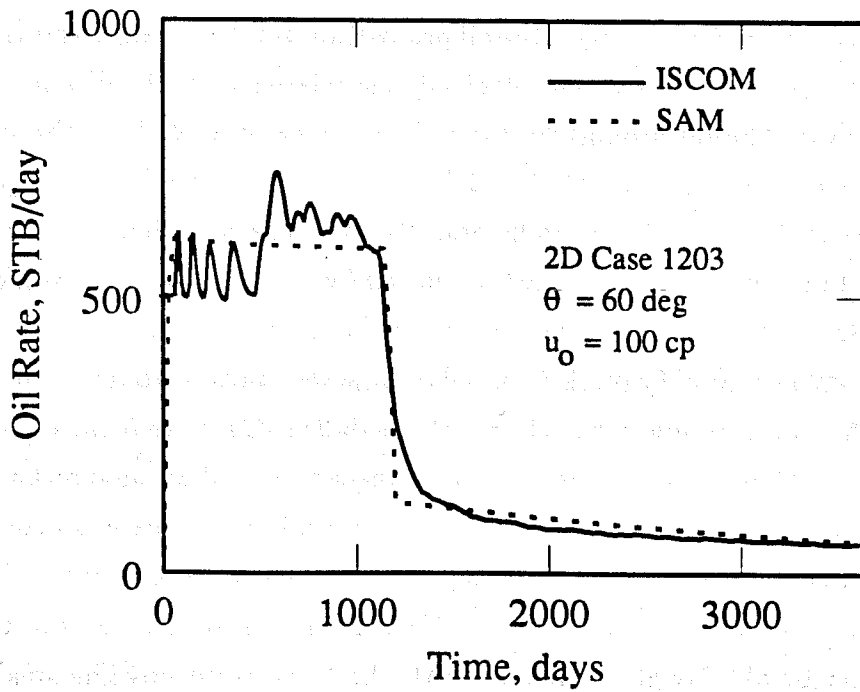


Figure 6.24: Oil Rate vs Time, Case 1203

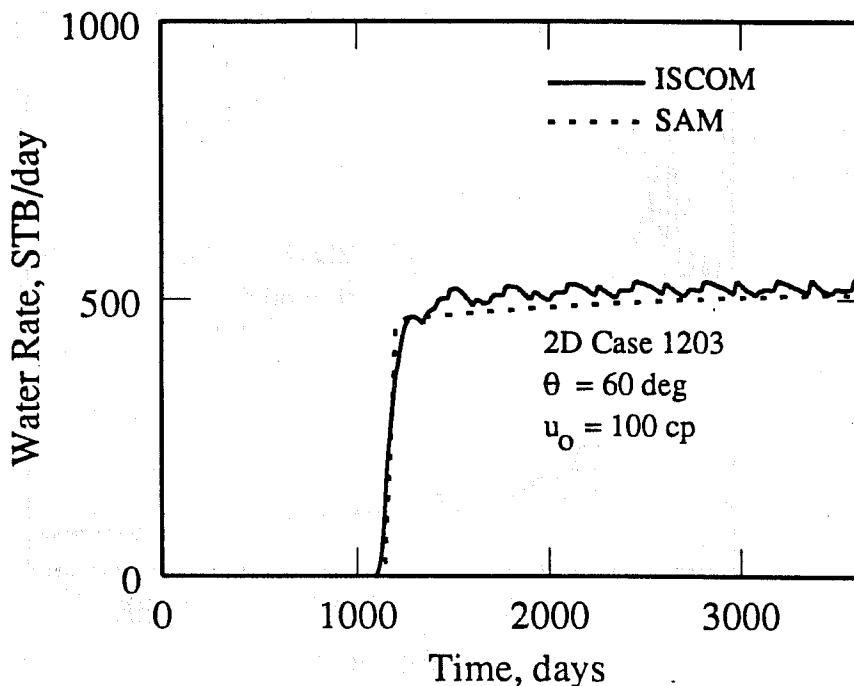


Figure 6.25: Water Rate vs Time, Case 1203

rate predicted by the SAM is too low because of a difference in the water zone saturation.

The sixth case is for a formation dip of 60 degrees and an oil viscosity of 1000 cp. The oil production rate graph for Case 1287 is shown in Figure 6.26. The agreement is good, except for the oil production rate prior to water breakthrough. The oscillations, which are a function of the gridding system and discussed earlier, are more severe here than had been seen earlier. The oil rate is lower in the SAM because the steam zone size is smaller. This results in a delay in water breakthrough, which is more evident on the water production rate graph (Fig. 6.27). Case 0287, the corresponding horizontal case, showed steam breakthrough. Steam breakthrough for Case 1287 is delayed because the steam has a tendency to rise to the top of the reservoir, which is near the injection well for updip steam injection.

The water production rate graph for Case 1287 is shown in Figure 6.27. The delay in water breakthrough predicted by the SAM is caused by the smaller steam zone volume. The water production rate shows a good match, and is lower in the

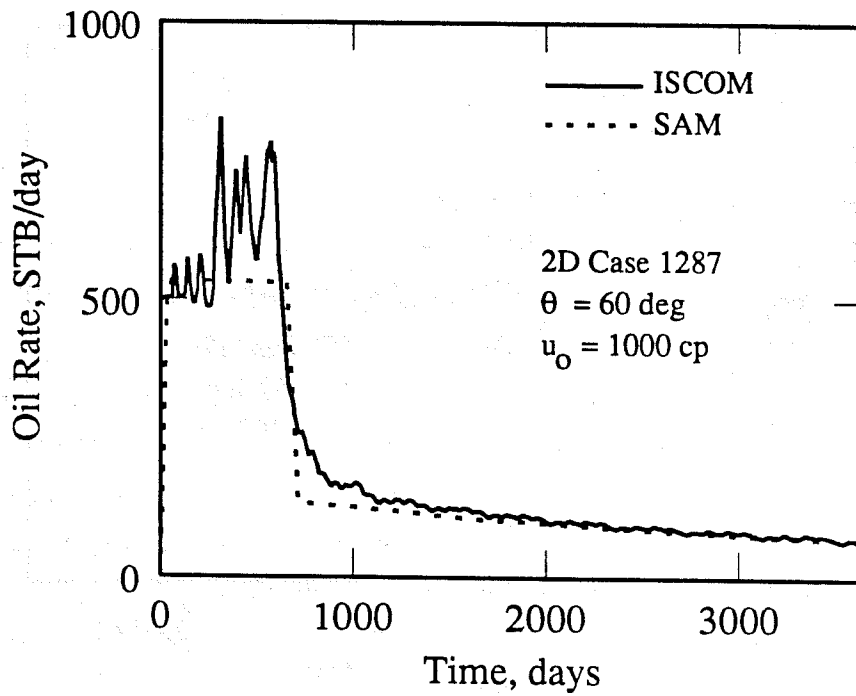


Figure 6.26: Oil Rate vs Time, Case 1287

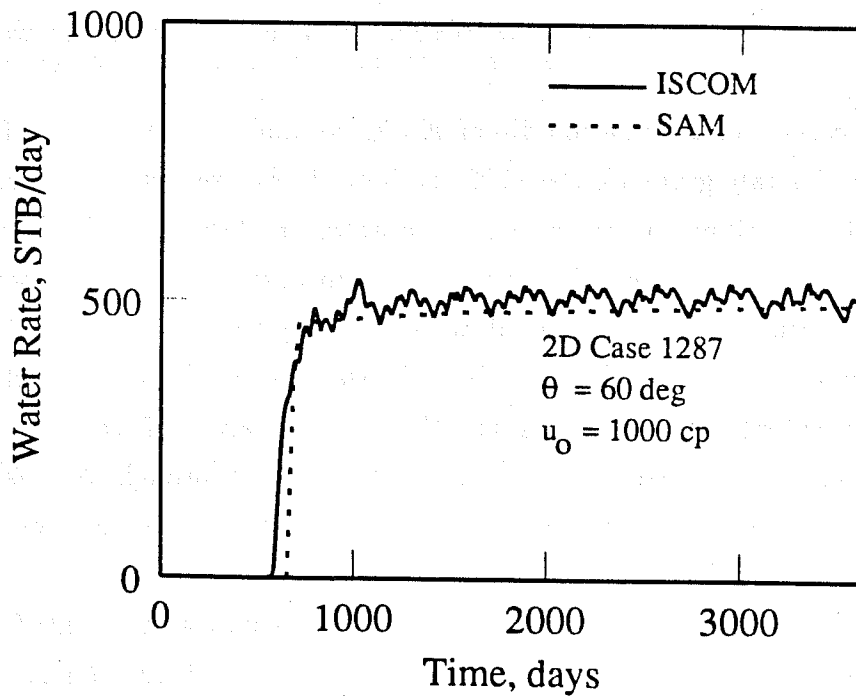


Figure 6.27: Water Rate vs Time, Case 1287

SAM because of the slower advance of the steam zone.

6.3 Concluding Remarks

Comparing results from all of the cases shown in this chapter, as well as the many cases not shown, revealed that the SAM for the two-dimensional system compared well with the thermal simulator ISCOM. A few general trends were noticed when scrutinizing the results. The oil production rate predicted by the SAM just prior to water breakthrough was higher than predicted by ISCOM, and just after breakthrough was lower. The dipping cases run on ISCOM gave oscillations with larger amplitudes and earlier water breakthrough than the horizontal cases. The water production rate predicted by the SAM increased sharply at water breakthrough, while the increase in the ISCOM water production rate was gradual. For both models, high oil viscosities gave early water breakthrough, low oil production rates before water breakthrough, and high oil production rates after water breakthrough.

The SAM considered gravity override of the steam and incomplete volumetric sweep of the reservoir by water and matched the thermal simulator results. This ability to match such results was the objective of this work, and that objective has been achieved.

Chapter 7

Conclusions and Recommendations

Conclusions from the work and recommendations for possible improvements in the model are included in this chapter.

7.1 Conclusions

The results of this study appear to warrant the following conclusions:

1. A semianalytical model (SAM) has been developed for forecasting reservoir response to steam drive for a one-dimensional linear system. Fractional flow theory, energy and mass balances, and an iterative technique are used to forecast reservoir performance. The model estimates pressure, temperature, and fluid saturation distributions, and oil and water production rates as functions of time. The model includes the effects of formation dip, compressibility, thermal expansion, and the water zone. The steam zone steam saturation is calculated, not assumed.
2. The SAM is expanded to forecast reservoir response to steam drive for a two-dimensional x - z cross-sectional system. This model incorporates the features of the one-dimensional model and uses an empirical method for calculating the

shape of the steam front. A new correlation is used to determine the water sweep efficiency at water breakthrough. The standard deviations of the new correlation ranged from 0.14 to 1.78 percent.

3. The SAM results were compared to thermal simulator results. The Computer Modelling Group's general purpose thermal simulator ISCOM was used as a basis for comparison. Results show that the SAM accurately matches pressure, temperature, and phase saturation distributions, as well as oil and water production rates. However, for length to height ratios less than unity, the match was not satisfactory.
4. Computer codes have been written based on the semianalytical models and can be run on a microcomputer. The time required for execution is much less than that for a thermal simulator. Ten year test runs were made on an IBM model 70 personal computer. The one-dimensional cases required about 30 seconds to run, and the two-dimensional cases required about 50 seconds. The ISCOM model often required several hours to run on an Apollo DN10000 system.
5. The one-dimensional model considers both updip and downdip steam injection. The two-dimensional model considers only updip steam injection because of the manner in which the shape of the steam front and the location of the water front is determined. However, updip steam injection is the more common injection method.

7.2 Recommendations

Further work that should be done on this project includes

1. Modify the relative permeability subroutine to handle temperature-dependent relative permeabilities.
2. Place wells at locations other than the end of the reservoir to see how production rates are affected.

3. Expand the model to three dimensions for specific pattern configurations.
4. Modify the boundary conditions to handle variable injection rates.
5. Consider net/gross thickness ratios other than unity.
6. Test the model on layered cases where each layer has a different permeability.
7. Test anisotropic cases in which k_x and k_z are not identical.
8. Attempt to correlate the sweep efficiency curves so that all mobility ratios could be displayed on the same graph.
9. Use Wang's model to calculate the size of the steam zone.

Chapter 8

Nomenclature

<i>a</i>	heat loss parameter	btu/(cu ft-sqrt day)
<i>A</i>	cross-sectional area, or scaling group	sq ft dimensionless
<i>b</i>	steam zone parameter	dimensionless
<i>B</i>	formation volume factor	reservoir volume/standard volume
<i>c</i>	compressibility	1/psi
<i>cc</i>	shape factor	dimensionless
<i>C</i>	specific heat capacity, or correlation coefficient	btu/(lbm-F) unitless
<i>d</i>	thermal expansion coefficient	1/F or 1/F/F
<i>E</i>	efficiency	fraction
<i>f</i>	fractional flow, or steam quality	fraction fraction
<i>F</i>	ratio of latent to total heat injected	dimensionless
<i>g</i>	acceleration due to gravity	ft/sec/sec
<i>h</i>	enthalpy	btu/lbm
<i>H</i>	height	ft
<i>I</i>	injectivity index	bbt/(day-psi)
<i>k</i>	permeability	md

L	length, or latent heat	ft btu/lbm
M	volumetric heat capacity, or mobility ratio	btu/(cu ft-F) dimensionless
MCR	modified Craig ratio	dimensionless
MOV	moveable oil volume	bbls
n	exponent	no units
N	oil produced	bbl
OIP	oil in place	STB
$OOIP$	original oil in place	STB
$OWIP$	original water in place	STB
p	pressure	psia
PVI	pore volumes injected	dimensionless
q	flow rate	STB/day, btu/day
Q	cumulative flow	STB, rbbl, btu
r	radius	ft
R	ratio	dimensionless
s	skin factor	dimensionless
S	saturation	fraction
SAM	semianalytical model	
STP	standard temperature and pressure	
sl	slope	dimensionless
t	time	days
T	temperature	F
v	velocity	ft/day
V	volume	cu ft
w	mass flow rate	lbm/day
W	width, or water injected	ft bbl
WIP	water in place	STB
x	distance along bedding plane	ft

Y	correlation value	varies
z	distance normal to bedding plane	ft
α	thermal diffusivity	sq ft/day
Δ	difference	no unit
θ	angle of formation dip	degrees
λ	thermal conductivity	btu/(ft-day-F)
μ	viscosity	cp
ρ	density	lbm/cu ft
ϕ	porosity	fraction
Φ	flow potential	psi
π	constant=3.14159...	unitless

Subscripts

av	average
b	bottom
bt	breakthrough
c	capillary, constant
con	condensed
D	dimensionless
$datum$	at a datum
end	endpoint
f	formation
g	gas
h	horizontal
i	initial
inj	injection
irr	irreducible
j	phase j
l	liquid
L	linear
$loss$	loss

<i>max</i>	maximum
<i>o</i>	oil
<i>ob</i>	overburden
<i>p</i>	produced
<i>prod</i>	producer
<i>r</i>	relative
<i>ref</i>	reference
<i>res</i>	in the reservoir
<i>R</i>	rock
<i>s</i>	steam
<i>sc</i>	standard conditions
<i>v</i>	vaporization, vertical, volumetric
<i>w</i>	water, wellbore
<i>wf</i>	well flowing
<i>x</i>	x-direction
<i>z</i>	zone, z-direction
1	first coefficient
2	second coefficient

Superscripts

<i>n</i>	time step
*	normalized, or at elevated temperature
	average
-	behind
+	ahead

Bibliography

- [1] Aydelotte, S. Robert and Pope, Gary A.: "A Simplified Predictive Model for Steamdrive Performance," *J. Pet. Tech.* (May 1983) 991-1002.
- [2] Aziz, K. and Settari, A.: *Petroleum Reservoir Simulation*, Elsevier Applied Science Publishers, London (1979) 36.
- [3] Aziz, K., Ramesh, A. B., and Woo, P. T.: "Fourth SPE Comparative Solution Project: Comparison of Steam Injection Simulators," *J. Pet. Tech.* (Dec. 1987) 1576-1584.
- [4] Braden, W. B.: "A Viscosity-Temperature Correlation at Atmospheric Pressure for Gas-Free Oils," *J. Pet. Tech.* (Nov. 1966) 1487-1490; *Trans. AIME*, **237**.
- [5] Buckley, S. E. and Leverett, M. C.: "Mechanism of Fluid Displacement in Sands," *Trans.*, AIME (1942) **146**, 107-116.
- [6] Chu, C. and Trimble, A. E.: "Numerical Simulation of Steam Displacement - Field Performance Applications." *J. Pet. Tech.* (June 1975) 765-776.
- [7] Corey, A. T.: "The Interrelation Between Gas and Oil Relative Permeabilities." *Prod. Monthly*, (Nov. 1954) 38-41.
- [8] Cox, D. O. and Chestnut, D. A.: "Equations For Some Thermodynamic Properties of Saturated Steam," paper SPE 5960 available at SPE, Richardson, Tx.
- [9] Craig, F. F., Jr., Sanderlin, J. L., Moore, D. W. and Geffen, T. M.: "A Laboratory Study of Gravity Segregation in Frontal Drives", *Trans.*, AIME (1957) **210**. 275-282.

- [10] Dake, L. P.: *Fundamentals of Reservoir Engineering*, Elsevier Scientific Publishing Company, New York (1978) 379-390.
- [11] Darcy, H.: "Les Fontaines publiques del la Ville de Dijon, Dalmount, Paris," (1856).
- [12] Dietrich, J. K.: "Three-Phase Relative Permeability Models," paper SPE 6044 presented at the 1976 SPE Annual Technical Conference and Exhibition, New Orleans, Oct. 3-6.
- [13] Dietz, D. N.: "A Theoretical Approach to the Problem of Encroaching and Bypassing Edge Water," *Proc., Kon. Ned. Akad. Wetensch, Amsterdam* (1953) **B56**, 83-92.
- [14] Doscher, Todd M. and Ghassemi, Farhad: "The Influence of Oil Viscosity and Thickness on the Steam Drive," *J. Pet. Tech.* (Feb. 1983) 291-298.
- [15] Dupuit, J.: *Etudes theoriques et pratiques sur le mouvement des eaux*, Dumod, Paris (1863).
- [16] Earlougher, Robert C., Jr.: *Advances in Well Test Analysis*, Monograph Series, SPE, Dallas (1977) **5**, 126-127.
- [17] Ejiogu, G. C. and Fiori, M.: "High-Pressure Saturated-Steam Correlations," *J. Pet. Tech.* (Dec. 1987) 1585-1590.
- [18] Farouq Ali, S. M.: *Oil Recovery by Steam Injection*, Producers Publishing Company, Bradford, Pa. (1970).
- [19] Farouq Ali, S. M. and Abou-Kassem, J.: "Simulation of Thermal Recovery Processes," *The Proceedings of The First and Second International Forum on Reservoir Simulation*, Alpbach, Austria, 1988 and 1989.
- [20] Forsyth, P., Jr., Rubin, B., and Vinsome, P. K. W.: "The Elimination of the Constraint Equation and Modelling of Problems with a Non-Condensable Gas in Steam Simulation." *J. Cdn. Pet. Tech.* (Oct.-Dec. 1981) 63-68.

- [21] Geertsma, J., Croes, G. A., and Schwarz, N.: "Theory of Dimensionally Scaled Models of Petroleum Reservoirs," *Trans.*, AIME (1956) **207**, 118-127.
- [22] Gontijo, J. E. and Aziz, K.: "A Simple Analytical Model for Simulating Heavy Oil Recovery by Cyclic Steam in Pressure-Depleted Reservoirs," paper SPE 13037 presented at the 1984 SPE Annual Technical Conference and Exhibition, Houston, Sep. 16-19.
- [23] Hearn, C. L.: "Effect of Latent Heat Content of Injected Steam in a Steam Drive," *J. Pet. Tech.* (April 1969) 374-375.
- [24] Higgins, R. V. and Leighton, A. J.: "Waterflood Performance in Stratified Reservoirs," RI5618, USBM (1960).
- [25] Hubbert, M. K.: "Darcy's Law and the Field Equations of the Flow of Underground Fluids," *Trans.*, AIME (1956) **207**, 222-239.
- [26] "ISCOM User's Manual," Computer Modelling Group, Calgary (July 1987) 82.
- [27] Jones, J.: "Cyclic Steam Reservoir Model for Viscous Oils, Pressure-Depleted, Gravity Drainage Reservoirs," paper SPE 6544 presented at the 1977 SPE California Regional Meeting, Bakersfield, April 13-15.
- [28] Jones, Jeff: "Steam Drive Model for Hand-Held Programmable Calculators," *J. Pet. Tech.* (Sep. 1981) 1583-1598.
- [29] Lauwerier, H. A.: "The Transport of Heat in an Oil Layer Caused by the Injection of Hot Fluid," *Appl. Sci. Research* (1955) Vol. 5, Nos. 2 and 3.
- [30] Leverett, M. C.: "Capillary Behavior in Porous Solids," *Trans.*, AIME (1941) **142**, 152-169.
- [31] Mandl, G. and Volek, C. W.: "Heat and Mass Transport in Steam-Drive Processes," *Soc. Pet. Eng. J.* (March 1969) 59-79; *Trans.*, AIME, **246**.
- [32] Marx, J. W. and Langenheim, R. H.: "Reservoir Heating by Hot Fluid Injection," *Trans.*, AIME (1959) **216**, 312-315.

- [33] Myhill, N. A. and Stegemeier, G. L.: "Steam-Drive Correlation and Prediction," *J. Pet. Tech.* (Feb. 1978) 173-182.
- [34] Neuman, C. H.: "A Gravity Override Model of Steamdrive," *J. Pet. Tech.* (Jan. 1985) 163-169.
- [35] Palmgren, C. T. S., Bruining, J., and DeHaan, H. J.: "The Effect of Viscous, Gravity and Capillary Forces on the Dynamic Behavior of the Steam Condensation Front," *Proc. Fifth European Symposium on Improved Oil Recovery*, Budapest, April 25-27, 1989.
- [36] Prats, Michael: "The Heat Efficiency of Thermal Recovery Processes," *J. Pet. Tech.* (March 1969) 323-332.
- [37] Prats, Michael: *Thermal Recovery*, Monograph Series, SPE, Dallas (1982) 7, 30-35.
- [38] Ramey, H. J., Jr.: "Discussion on Reservoir Heating by Hot Fluid Injection," *Trans., AIME* (1959) 216, 364-365.
- [39] Ramey, H. J., Jr.: "How to Calculate Heat Transmission by Hot Fluid Injection," *Pet Eng.* (Nov. 1964) 110-120.
- [40] Ramey, H. J., Jr., personal communication, Stanford University, Stanford, California, Sep. 15, 1989.
- [41] Rhee, Shie W. and Doscher, Todd. M.: "A Method for Predicting Oil Recovery by Steamflooding Including the Effects of Distillation and Gravity Override," *Soc. Pet. Eng. J.* (Aug. 1980) 249-266.
- [42] Rubin, B. and Buchanan, W. L.: "A General Purpose Thermal Model," *Soc. Pet. Eng. J.* (April 1985) 202-214.
- [43] Shutler, N. D. and Boberg, T. C.: "A One-Dimensional Analytical Technique for Predicting Oil Recovery by Steamflooding," *Soc. Pet. Eng. J.* (Dec. 1972) 489-498.

- [44] Stegemeier, G. L., Laumbach, D. D., and Volek, C. W.: "Representing Steam Drive Processes With Vacuum Models," *Soc. Pet. Eng. J.* (June 1980) 151-174.
- [45] Stone, H. L.: "Estimation of Three-Phase Relative Permeability and Residual Oil Data," *J. Cdn. Pet. Tech.* (Oct. 1973) **12**, No. 4, 53-61.
- [46] van Lookeren, J.: "Calculation Methods for Linear and Radial Steam Flow in Oil Reservoirs," *Soc. Pet. Eng. J.* (June 1983) 427-439.
- [47] Vogel, J. V.: "Simplified Heat Calculations for Steamfloods," *J. Pet. Tech.* (July 1984) 1127-1136.
- [48] Wang, Fred P. and Brigham, W. E.: "Heat Losses and Frontal Movement During Steam Injection in Porous Media," IEA Cooperative Project on Enhanced Oil Recovery, Hanover and Clausthal, West Germany (Sep. 16-19, 1986).
- [49] Welge, Henry J.: "A Simplified Method for Computing Oil Recoveries by Gas or Water Drive," *Trans., AIME* (1952) **195**, 91-98.
- [50] Whitaker, S.: "The Equations of Motion in Porous Media," *Chem. Eng. Sci.*, **21** (1966) 291-300.
- [51] Whitaker, S.: "Advances in Theory of Fluid Motion in Porous Media," *Ind. and Eng. Chem.*, **61**, No. 12 (1969) 14-28.
- [52] Wingard, J.S. and Orr, F. M.: "An Analytical Solution for Steam/Oil/Water Displacements," SPE paper 19667 presented at the 1989 SPE Annual Technical Conference and Exhibition, San Antonio, (Oct. 8-11).
- [53] Yortsos, Y. C.: "Analytical Modeling Of Oil Recovery By Steam Injection," PhD dissertation, California Institute of Technology, Pasadena, California (1979).
- [54] Yortsos, Y. C. and Gavalas, G. R.: "Analytical Modeling of Oil Recovery by Steam Injection: Part I - Upper Bounds," *Soc. Pet. Eng. J.* (April 1981) 162-178.

- [55] Yortsos, Y. C. and Gavalas, G. R.: "Analytical Modeling of Oil Recovery by Steam Injection: Part 2 - Asymptotic and Approximate Solutions," *Soc. Pet. Eng. J.* (April 1981) 179-190.
- [56] Yortsos, Y. C.: "Distribution of Fluid Phases Within the Steam Zone in Steam-Injection Processes," *Soc. Pet. Eng. J.*, (Aug. 1984) 458-466.

Appendix A

Other Calculations Used in the Model

This appendix deals with several calculations used by the model that are not addressed in the body of the dissertation. The information presented includes the three-phase relative permeability model, the method of smoothing the relative permeability data, and methods of determining porosity, phase densities, phase viscosities, wet steam properties, and oil and water production rates.

A.1 Three-Phase Relative Permeability

The SAM should represent pressure drop for three-phase flow. Pressure drop is represented using Darcy's law for three-phase flow. This calculation requires a relative permeability for each phase. The three-phase relative permeabilities are estimated from two-phase relative permeability data using Stone's second model [45, 12]. This relative permeability model requires as input: (1) the saturation of each phase, (2) the water and oil relative permeabilities at the specified water saturation for an oil-water system, and (3) the gas and liquid relative permeabilities at the specified gas saturation for a gas-liquid system. The three-phase water and gas relative permeabilities are the water and gas relative permeabilities for the respective systems. The oil relative permeability is calculated from a modification of Stone's second model [2].

The equation is

$$k_{ro} = k_{rocw}[(k_{row}/k_{rocw} + k_{rw})(k_{rog}/k_{rocw} + k_{rg}) - (k_{rw} + k_{rg})] \quad (A.1)$$

where

k_{ro} = three-phase relative permeability to oil

k_{row} = relative permeability to oil in an oil-water system evaluated at $1 - S_w$

k_{rw} = relative permeability to water in an oil-water system evaluated at S_w

k_{rog} = relative permeability to oil in a gas-oil system evaluated at $1 - S_g$

k_{rg} = relative permeability to gas in a gas-oil system evaluated at S_g

$k_{rocw} = k_{row}$ at irreducible water saturation

Any three-phase relative permeability model could be used for this calculation. Stone's method was chosen for the SAM because it was also the method chosen in ISCOM.

A.2 Corey Relative Permeability Curves

After water breakthrough, time is determined by constructing a tangent slope to the water fractional flow curve. For increasing time, the slope of the water fractional flow curve must constantly decrease after water breakthrough. To ensure that the slope does decrease, the relative permeability data must be smooth. The method of Corey [7] was used to smooth the relative permeability data, and the equations are:

$$k_{rw} = k_{rw,end}(S_w^*)^{n_w} \quad (A.2)$$

$$k_{row} = (1 - S_w^*)^{n_o} \quad (A.3)$$

$$k_{rog} = (S_l^*)^{n_l} \quad (A.4)$$

$$k_{rg} = k_{rg,end}(1 - S_l^*)^{n_g} \quad (A.5)$$

where n is a correlating exponent and the subscript *end* refers to the endpoint of the relative permeability curve. The exponent values of $n_w=3$, $n_o=2$, $n_l=3$, and $n_g=2$

gave the best fit to the relative permeability data. Saturations were normalized by using the following equations:

$$S_w^* = \frac{S_w - S_{w,irr}}{1 - S_{or} - S_{w,irr}} \quad (A.6)$$

and

$$S_i^* = \frac{S_i - S_{i,irr}}{1 - S_{gr} - S_{i,irr}} \quad (A.7)$$

As with the relative permeability model, any method that gives a smooth fractional flow curve could be used to smooth the relative permeability data.

A.3 Porosity Calculation

The porosity calculation considers changes in pore volume with temperature and pressure. The calculation used is

$$\phi = \phi_{ref}[1 + c_f(p - p_{ref}) - d_f(T - T_{ref})] \quad (A.8)$$

where c_f is the pore volume compressibility of the formation and d_f is the pore volume thermal expansion coefficient of the formation.

A.4 Density Calculation

The density calculation for each liquid phase includes the effects of changes in temperature and pressure. The equation used is the one used by ISCOM [26] and is

$$\rho_j = \frac{\rho_{ref,j}}{[1 - c_j(p - p_{ref})][1 + d_{1j}(T - T_{ref}) + d_{2j}(T - T_{ref})^2]} \quad (A.9)$$

A.5 Liquid Viscosity

The viscosities of oil and water as functions of temperature are determined by interpolating in a table of viscosity values furnished as data. Interpolation is semilogarithmic with oil viscosity on a logarithmic scale and temperature on a linear scale.

Coefficient	Property, Y		
	$p_s^{1/2}(\text{Pa})$	$\rho_w(\text{kg}/\text{m}^3)$	$\ln \rho_s(\text{kg}/\text{m}^3)$
C_0	-175.776	3786.31	-93.7072
C_1	2.29272	-37.2487	0.833941
C_2	-0.0113953	0.196246	-3.20809×10^{-3}
C_3	2.62780×10^{-5}	-5.04708×10^{-4}	6.57652×10^{-6}
C_4	-2.73726×10^{-8}	6.29368×10^{-7}	-6.93747×10^{-9}
C_5	1.13816×10^{-11}	-3.08480×10^{-12}	2.97203×10^{-12}

Table A.1: Correlation Coefficients for Wet Steam Pressure and Density

A.6 Wet Steam Property Correlations

The properties of wet steam are needed for energy and mass balance calculations. Instead of using table look-up methods, correlations were employed because of the savings in computer time. Several published correlations were examined [18, 8, 27, 17]. The correlations of Farouq-Ali and Abou-Kassem [19] were used. Although the rest of this dissertation uses field units, these correlations are presented in SI units because that is how they were published. The equation for each wet steam property, Y , is

$$Y = C_0 + C_1T + C_2T^2 + C_3T^3 + C_4T^4 + C_5T^5 + C_6T^6 \quad (\text{A.10})$$

where temperature, T , is expressed in degrees Kelvin. The coefficients for the necessary wet steam properties are shown in Tables A.1 and A.2. The variable h is enthalpy and L_v is latent heat of vaporization. The equation used for saturation temperature as a function of pressure is

$$T_s = 325.442 - 44.6171 \ln p + 8.93074(\ln p)^2 - 0.626842(\ln p)^3 + 0.0190017(\ln p)^4 \quad (\text{A.11})$$

where pressure is expressed in Pascals. The equation for saturated steam viscosity, μ_g , is

$$\mu_g = 0.00048 (T + 459.6)^{0.593} \quad (\text{A.12})$$

where temperature, T , is in degrees F. The coefficients are part of the data file and may be changed to give the best viscosity match over the pressure interval of interest.

Coefficient	Property, Y		
	$h_w(J/kg)$	$L_v^2(J/kg)$	$h_s(J/kg)$
C_0	23665.2	7184500	-22026.9
C_1	-366.232	11048.6	365.317
C_2	2.26952	-88.4050	-2.25837
C_3	-7.30365×10^{-3}	0.162561	7.37420×10^{-3}
C_4	1.30241×10^{-5}	-1.21377×10^{-4}	-1.33437×10^{-5}
C_5	-1.22103×10^{-8}	0	1.26913×10^{-8}
C_6	4.70878×10^{-12}	0	-4.96880×10^{-12}

Table A.2: Correlation Coefficients for Wet Steam Enthalpy Properties

A.7 Production Rate Calculations

The initial mass of oil and water in place is calculated at the beginning of the program. The density of each phase and the porosity at the initial conditions are calculated. The initial oil and water saturation are specified, so the initial volume of each component in place can be calculated. The original oil in place, $OOIP$, by material balance is

$$OOIP = \frac{LA\phi_i S_{oi}}{5.6146B_{oi}} \quad (A.13)$$

Similarly, the original water in place, $OWIP$, is

$$OWIP = \frac{LA\phi_i S_{wi}}{5.6146B_{wi}} \quad (A.14)$$

In these equation. B is a formation volume factor defined by

$$B_{oi} = \frac{\rho_{o,sc}}{\rho_{oi}} \quad (A.15)$$

and

$$B_{wi} = \frac{\rho_{w,sc}}{\rho_{wi}} \quad (A.16)$$

The average oil and water flow rate for a time step is calculated after the iteration for that time step has converged. At the end of each time step, the locations of the steam and the water fronts, and the phase saturations in each zone are known. The average temperature and pressure in each zone are also known. The porosity and

phase densities in each zone can then be calculated. Thus at any given time, the amount oil and water can be calculated. The oil in place at that time, OIP , is

$$OIP = \sum_{z=o,w,s} \frac{L_z A \phi_z S_{oz} \rho_{oz}}{5.6146 \rho_{o,sc}} \quad (A.17)$$

The water in place at the same time, WIP , is similarly calculated

$$WIP = \sum_{z=o,w,s} \frac{L_z A \phi_z (S_{wz} \rho_{wz} + S_{gz} \rho_{gz})}{5.6146 \rho_{w,sc}} \quad (A.18)$$

The flow rates during a time step are calculated by subtracting the component mass in place at the end of the time step from that at the beginning of the time step and adding the mass of fluid injected. The resulting flow rate equations are

$$q_o = \frac{OIP^{n+1} - OIP^n}{\Delta t} \quad (A.19)$$

and

$$q_w = \frac{WIP^{n+1} - WIP^n}{\Delta t} + q_{w,inj} \quad (A.20)$$

The auxiliary equations that are used to support the SAM have been presented in this appendix. Appendix B deals with assumptions made in the SAM.

Appendix B

SAM Assumptions

This appendix describes the assumptions that are made in the semianalytical model (SAM). Although some of the assumptions appear to be obvious, they are stated anyway for completeness. General assumptions are discussed first, and these are followed by lists of assumptions about phase relationships, energy, initial conditions, and boundary conditions.

B.1 SAM General Assumptions

1. The proposed model uses Cartesian geometry. One-dimensional linear and two-dimensional planar systems are considered. Definitions of these systems are given in Sections 3.1 and 5.1, respectively.
2. Pressure drops across the reservoir system are calculated from Darcy's law.
3. The reservoir is homogeneous and has a constant thickness and cross-sectional area.
4. The thermal properties of the overburden and the underburden are identical and are constant.
5. Capillary pressure is neglected. The heavy oil reservoirs for which this model has been developed typically have permeabilities of one Darcy or more. In

such permeable formations, capillary pressure values are usually only a few psi because of the large pore throats in the rock. Simulation results show that such small capillary pressures have virtually no effect on the results, so the assumption is justified.

6. Instantaneous thermal equilibrium is assumed between the fluids and the rock matrix. The sand grains are small enough, the injection rates low enough, and the thermal conductivities high enough to justify this assumption.
7. Temperature-dependent relative permeability, diffusion, dispersion, fluid adsorption onto the solid surface, chemical reactions, friction, non-Darcy flow, and inertial effects are neglected.
8. The compressibilities of the oil, water, and formation are constant.
9. Viscosities are temperature dependent but independent of pressure.
10. In the one-dimensional model, no gravity override of the steam can occur. An empirical equation is used for steam gravity override in the two-dimensional model.

B.2 Phase Relationships

1. The solid phase does not enter the fluid phases, nor do any of the fluid phases enter the solid phase.
2. Two components are considered, an oil component and a water component. The oil component exists only in the oil phase, and the oil phase is composed entirely of the oil component. The water component can exist in either the water phase or the gas phase, so the gas phase is pure steam and the water phase is made up entirely of the water component. The phase-component relationships are summarized in Table B.1. The oil is a dead oil and nonvolatile, and no solution gas is present in the system. This "dead" oil assumption is not as restrictive as might appear. The heavy oil reservoirs for which this model is intended

Phase	Component	
	Oil	Water
Oil	x	
Water		x
Gas		x

Table B.1: Relationships Between Phases and Components

contain viscous oil. This oil is composed mostly of the heavy hydrocarbons with low volatility. A way to account for distillation without making phase change calculations is to adjust the relative permeability data so that the correct residual oil saturation is obtained [40].

B.3 Energy Assumptions

1. Thermal energy is conserved.
2. Kinetic energy changes are negligible.
3. Mechanical work done by thermal expansion of the reservoir on its surroundings is negligible.

B.4 Initial Conditions

1. The reservoir is uniformly saturated with oil and connate water. The water is at irreducible saturation, so only the oil phase is mobile.
2. The flow potential of oil in the reservoir is uniform and constant. Pressures may vary due to hydrostatic head of the fluids in the reservoir.
3. Reservoir temperature is uniform and constant, and equal to the temperature of the adjacent strata.

B.5 Boundary Conditions

1. The reservoir boundaries are fixed and do not change with time.
2. There is no mass flow between the reservoir and overburden or underburden.
3. Heat flow to the adjacent formations is proportional to the thermal conductivity of the formations and the temperature gradient at the reservoir-formation boundary. Heat is transferred to and in the surroundings by one-dimensional conduction along the coordinate vertical to the bounding surface of the reservoir.
4. The areal perimeter of the reservoir, except for the wells, is a no flow boundary for both mass and heat.
5. There is an injection well at one end of the system and a production well at the other end. The wells penetrate the reservoir at right angles. For dipping reservoirs, the wells are not vertical but perpendicular to the bedding plane of the reservoir. The production well produces at a constant flowing bottomhole pressure. The temperature at the production well is the temperature of the produced fluids. Wet steam is injected at the injection well at a constant rate and enthalpy. The temperature at the injection well is the temperature of the wet steam. The one-dimensional model that was developed considers either updip or downdip steam injection. The two-dimensional model is valid only for updip steam injection because the methods used to determine the shape of the steam front and the location of the water front assume that the steam zone is propagating from an upstructure injection well towards a downdip production well.

The next appendix discusses the structure of the computer program used to solve the model equations.

Appendix C

Program Structure

Computer programs were used to solve the model presented. This appendix describes the structure of the computer programs. Equations that were not mentioned in the body of the dissertation are included here.

The program begins by opening the appropriate data and output files. The data file is opened, as well as files for output of reservoir variables, oil flow rate, cumulative oil production, water flow rate, and cumulative water production. The data is then read from the data file. Several variables are initialized at this point. The initial and surface densities are determined for both phases and used to calculate the original oil and water in place. The water fractional flow curve and tangent construction calculations are then made to determine the average saturation behind the front and the location of the water front for the oil-water system.

The numerical construction of this tangent line requires incrementing water saturation from irreducible to maximum. The increment used in the program is 0.0001. For each increment, the fractional flow of water, f_w is calculated, and the slope from $S_w = S_{wi}$ and $f_w = 0$ to the current values is calculated. The program compares the calculated slope to the maximum slope and if the new slope is greater than the previous maximum, the maximum slope value is updated to the current slope. The water saturation and fractional flow values are also stored. The program also keeps track of the maximum water fraction flow value. This value is at least unity, but may be greater than unity for dipping reservoirs. After the iteration process is complete,

the average water saturation behind the front can be calculated from

$$\bar{S}_w = S_{wbt} + \frac{1 - f_{wbt}}{sl_{max}} \quad (C.1)$$

The maximum slope value, sl_{max} , is used to determine the location of the water front at any time before water breakthrough, and is discussed below.

After water breakthrough, the water fractional flow values are incremented from the value at breakthrough to the maximum water fractional flow value. For each fractional flow value, the corresponding water saturation value is determined from a bisection process. The slope of the tangent line at this point is determined by calculating the fractional flow value at water saturations slightly higher and slightly lower than the current value and taking the difference divided by the difference in water saturation values

$$sl = \frac{f_w^+ - f_w^-}{S_w^+ - S_w^-} \quad (C.2)$$

The number of pore volumes injected is simply the inverse of the tangent slope

$$PVI = \frac{1}{sl} \quad (C.3)$$

The current time is calculated by multiplying the number of pore volumes injected by the pore volume to get volume injected, and dividing by the volume injection rate to get time

$$t = \frac{(PVI)LA\phi}{5.6146q} \quad (C.4)$$

Tangent lines are drawn to the fractional flow curve at fractional flow values greater than the fractional flow at breakthrough. The slopes of these new tangent lines are constantly decreasing. The average water saturation behind the front after water breakthrough is determined by taking the intersection of the new tangent line with the fractional flow value of unity, as shown in Figure C.1

The iterative portion of the program is then executed. The largest loop is the time loop. Time is incremented by the time step specified in the data file. For each time step, the location of the steam and water fronts, the average phase saturation for each zone, and finally the fluids in place must be determined. The determination of these variables requires iteration on pressure. The pressure at the injection well

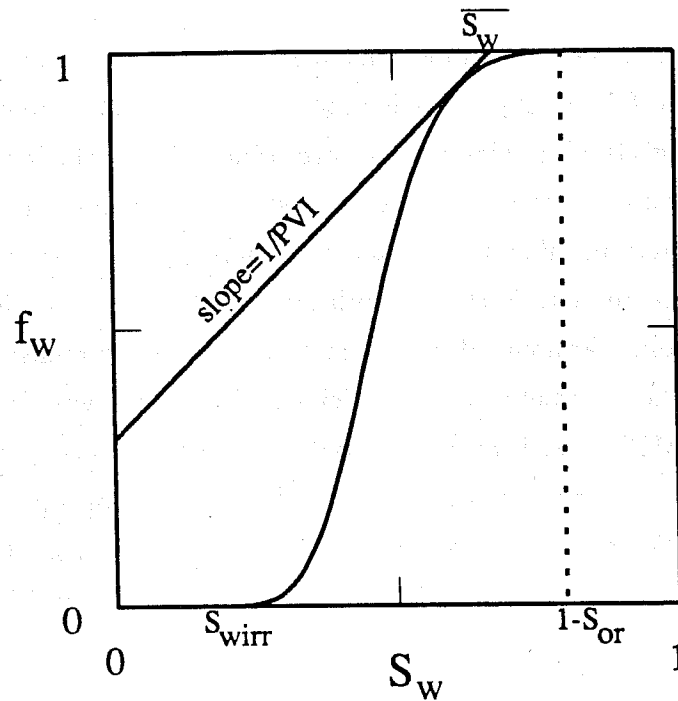


Figure C.1: Fractional Flow Curve Tangent Construction, After Breakthrough

is guessed or estimated, and five pressure drops are calculated. The five calculations consider the pressure drops through the injection well, steam zone, water zone, oil zone, and production well. Thus, a pressure can be calculated for the production well. This calculated production well pressure is compared to the specified flowing bottomhole pressure boundary condition. If the difference between the calculated and specified production well pressure is less than some convergence tolerance, then the local iteration has converged. If convergence is not achieved, the pressure at the injection well is revised and the procedure is repeated until convergence is achieved. After convergence is achieved, the current oil and water in place can be determined and the average rates during the time step calculated. The solution determined is unique because there is only one possible steam front location derived from the energy balance. When this unique steam front location is used to calculate the location of the water front, the mass balance solution provides only one solution for the location of the water front. Therefore the solution is unique. A global iteration to the next time step is then made and the process continues until the stopping time has been

reached.

The difficult part of the program is calculating the pressure drops through each of the three zones. The following process is repeated for each local iteration. First, the pressure drop through the injection well is determined. Next, the length of the steam zone is calculated from an energy balance. The steam saturation in the steam zone is determined from fractional flow theory and the energy balance results. The pressure drop through the steam zone is then calculated. The location of the water front is then determined from fractional flow theory. For the two-dimensional model, this step requires that the volumetric sweep efficiency E_v , be known. For the particular mobility ratio and MCR that is associated with a run, the limits of E_v with the heat function F equal to zero and one are calculated by table look up. This calculation is done only once. For each iteration, E_v is calculated by interpolating between the limits. This procedure saves much computer time. The pressure drop through the water zone is then calculated. Finally, the length of the oil zone is calculated and the pressure drop through this zone determined.

A flow chart summarizing the process is included below. The next appendix discusses the model application and data requirements.

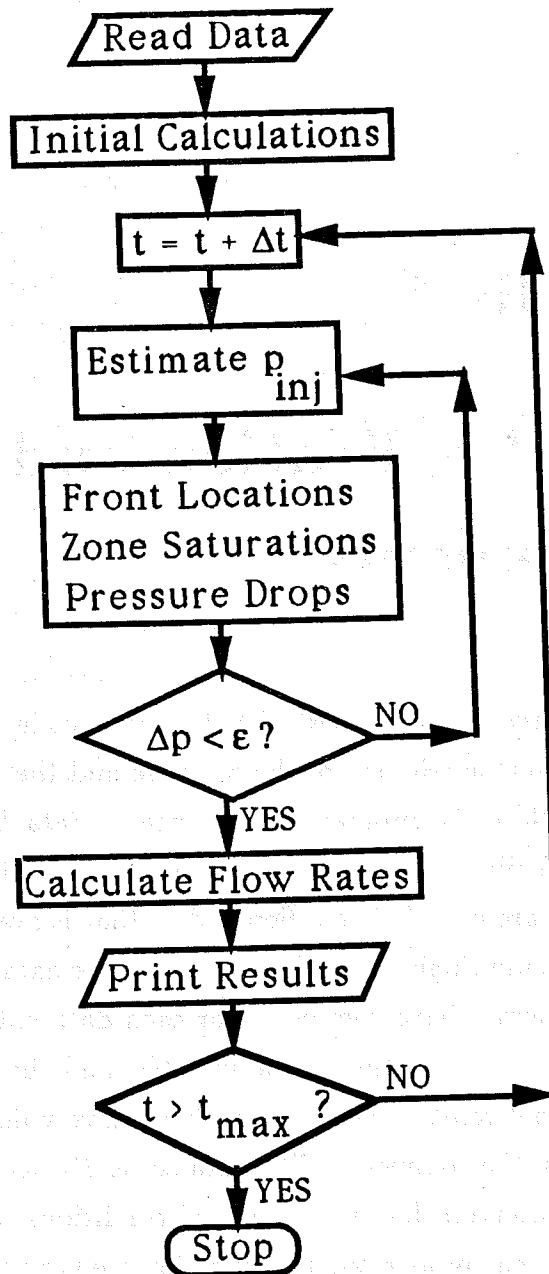


Figure C.2: Flow Chart for Program

Appendix D

Model Application and Data Requirements

The SAM presented in this dissertation has been coded into a computer program. This appendix discusses the use of the program and the data that is required to run the program. Before the program can be run, a data file must be prepared. The name of the data file must be "main.dat" so that it will be read by the program. Sample data files are included on a floppy disk that is available through the Stanford University Petroleum Engineering Department. The data files that are included with the computer program have comments for each data entry. The comments include the variable name, a description of the variable, and the units in which the variable is measured. Do not remove the comment lines! Every line in the data file is read by the program, even the comments. The data set is divided into sections pertaining to general control, reservoir description, initial conditions, PVT relationships, relative permeability, thermal properties, the injection well, and the production well. The appendix ends with a discussion of the output files.

The data set that is read by the model is much like the data set that is used by a thermal simulator. This data set is more detailed than data required by most other analytical models because fewer assumptions have been made. The PVT data section requires most of these extra data. Instead of assuming a constant temperature and pressure, this model considers temperature and pressure changes with time. The

model considers compressibility and thermal expansion of the oil, water, gas, and formation, as well as viscosity changes with temperature for the oil, water and gas. Therefore, data are needed to quantify the effect of these variables. If such data are not available, simple assumptions may be made instead. For example, if data are not available for thermal expansion coefficients or compressibility of the oil, water, or formation, these values may be assumed to be zero. This simplification would reduce the amount of data required, but would result in an incompressible system. Example data sets are included on a floppy disk that is available through the Stanford University Petroleum Engineering Department.

D.1 General Control Section

This section deals with time step control. The time step to be used is read in this section. Unlike simulators, the time step in the analytical model is constant. The solution is determined for each specific point in time. Since the solution does not depend on the solution of the previous time step, any size time increment may be chosen. In the one-dimensional model, the time step after water breakthrough is calculated differently in order to take advantage of the fractional flow analytical method for one-dimensional systems. Time steps are determined by incrementing fractional flow values and determining time from a tangent construction to the fractional flow curve at the specified fractional flow value. The two-dimensional model uses constant time steps at all times. Any size time step can be used, but excessively large time steps result in averaging over long periods of time, and may not supply results in sufficient detail. A time step value of ten to sixty days is recommended. Finally, the time at which the run will terminate is read. When the program increments to a time greater than or equal to this maximum time, the run will terminate after the current time step is completed.

D.2 Reservoir Description Section

The reservoir geometry and rock properties are specified in this section. The dip, length, and width of the reservoir are set. For the one-dimensional model, the height of the reservoir is also set. For two-dimensional runs, the number of layers in the system and the height of each layer must be specified. The grid block size of the production well block is then set. This variable is used to calculate the pressure drop through the production well. The porosity of the reservoir is then set, followed by the x -direction permeability of the reservoir. The x -direction permeability is not the horizontal permeability, but the permeability in the direction of the bedding plane. For a horizontal system, these two values are identical, but for dipping systems they are not. For two-dimensional runs, the x -direction permeability of each layer as well as the z -direction permeability must be specified. For the runs made in this work, the values of the x -direction permeabilities were equal in all layers.

D.3 Initial Conditions Section

This part of the data set deals with the initial condition of the reservoir. The initial pressure for each end of the reservoir is set. For horizontal systems, these two pressures should be identical. For systems with reservoir dip, the downdip pressure should be greater than the updip pressure by a value equal to the hydrostatic head of the reservoir oil, so that the initial flow potential is constant and uniform. The initial oil and water saturations are set next. Since no gas is present at initial conditions, the oil and water saturations should total unity. Furthermore, the water saturation should be the irreducible water saturation, the point at which the relative permeability to water becomes zero for an oil-water system. Finally, the temperature at each end of the reservoir is read. As with initial pressure, the initial temperature of each end of the reservoir should be identical for horizontal reservoirs, and should be different by the amount of the local geothermal gradient for dipping reservoirs. For two-dimensional cases, the pressure and temperature should be for the center of the top grid block of either end of the system.

D.4 PVT Section

This section deals with the pressure, volume, and temperature relationships of the reservoir fluids. A reference pressure and temperature for porosity calculations, density calculations, and the surface pressure and temperature are set. The oil and water phase reference densities at reference conditions are specified. The compressibility and thermal expansion coefficients for the oil and water are also specified in this section. From this data, the oil and water densities can be calculated at any temperature and pressure. Data that would allow density calculations for the steam phase is not necessary because steam densities are determined in another part of the program from steam table data. However, steam viscosity is calculated from a correlation and two coefficients used in this correlation must be specified. Finally, a table of oil and water viscosity as a function of temperature is read, preceded by the number of entries in the table. The maximum number of entries in the table is twenty. Oil viscosities as a function of temperature usually plot as a straight line on ASTM charts [4].

D.5 Relative Permeability Section

Two sets of relative permeability data are needed. This data is used in conjunction with a relative permeability model to determine three-phase relative permeabilities. Both water-oil and gas-liquid data sets are required in order to calculate three-phase values. The model requires that the relative permeability data be smooth, so Corey type relative permeability curves are used. For each system, the saturation-relative permeability endpoints and the exponent for each phase must be specified.

D.6 Thermal Data Section

The formation compressibility and thermal expansion coefficient is set and used to calculate changes in pore volume with temperature and pressure. The density and specific heat of the reservoir rock are specified and used to calculate the amount of energy needed to heat the reservoir. The overburden thermal conductivity and

thermal diffusivity are set and used to calculate heat losses to the overburden.

D.7 Injection Well

The injection boundary condition is specified by the wet steam injection rate at the injection well. The steam quality and the injection temperature are set to calculate the enthalpy injection rate. The water injectivity index is set and used to calculate the pressure drop through the injection well.

D.8 Production Well

The production boundary condition is specified by the constant flowing bottomhole pressure at the production well. The wellbore radius, shape factor, and skin factor at the well are used to calculate the pressure drop into the well.

D.9 Program Files

The executable file TOT.EXE is used to run the program. The source code TOT.FOR was used to compile the executable file. The object code TOT.OBJ was created in the process. D1.COM is the common file. MAIN.DAT is the data file called by the program.

As the program executes, five output files are created. Oil production rate as a function of time is in QO.OUT. Water production rate as a function of time is in QW.OUT. Cumulative oil production as a function of time is in CQO.OUT. Cumulative water production as a function of time is in CQW.OUT. RES.OUT begins with a listing of the data used in the run. Then, for each time step, information is given. This information includes the locations of the steam and water fronts, the average temperature, pressure, and oil, water and gas saturation for each of the three zones, and the pressure at the zone boundaries.